Photoactivation Strategies for Therapeutic Release in Nanodelivery Systems

Seok Ki Choi[*,†,‡]

[†]Michigan Nanotechnology Institute for Medicine and Biological Sciences, [‡]Department of Internal Medicine, University of Michigan Medical School, Ann Arbor, Michigan 48109, United States of America

[*]Corresponding author:

Email: skchoi@umich.edu

ORCID: Seok Ki Choi: 0000-0001-5633-4817

Abstract

Control of therapeutic release constitutes one of most critical aspects considered in the design of nanoscale delivery systems. There are a variety of cellular factors and external stimuli employed for release control. Of these, use of light offers various photoactivation mechanisms that enable to effectively engage in therapeutic release. It also allows a higher degree of spatial and temporal control. Over a recent decade, the application of photoactivation strategies has gained a remarkable growth and made a significant impact on rapid advances in the field of drug delivery. This article aims to review their fundamental concepts and practical applications demonstrated recently in numerous therapeutic areas from cancers to infectious diseases. Its scope is defined with a focus on those photoactivation strategies that occur via either linker cleavage, nanocontainer gating, or disassembly. Each of these is discussed with specific examples and underlying mechanisms that comprise linker photolysis, photoisomerization, photothermal heating, or photodynamic reaction with reactive oxygen species. In summary, this article provides an inclusive summary of new knowledge and insights obtained from recent developments in photoactivation strategies and their applications in therapeutic nanodelivery.

This is the author manuscript accepted for publication and has undergone full peer review but has not been through the copyediting, typesetting, pagination and proofreading process, which may lead to differences between this version and the Version of Record. Please cite this article as doi: 10.1002/adtp.202000117.

1. Introduction

Designing a nanoscale system for effective therapeutic delivery involves considerations in two primary aspects.[1-3] First, it relates to how to incorporate a mechanism of cell targeting. This relies on either passive infiltration (targeting) such as via the enhanced permeation and retention effect in tumors[4] or active targeting by binding to a specific biomarker or receptor.[5, 6] This targeting aspect has been extensively reviewed elsewhere,[3, 5, 7-10] and it is beyond the current scope. Second, it relates to developing a release strategy by which the payload carried in a nanoscale system is released or activated in a precisely controlled manner in the cells or tissues of interest.[11] This involves incorporating a specific mechanism of controlled release or activation for its payload such as a drug molecule, a therapeutic gene or an effector molecule.[11-13] Many existing systems utilize release strategies that are activated conditionally under the influence of cellular factors or in response to pathophysiological stimuli.[11] However, compared to such passive strategies, there are externally stimulated release strategies that are activated in a more controlled manner by applying light irradiation, sonication, or under a magnetic field.[11] Of these, the photoactivation strategy, a term which refers to light-controlled drug activation or release here, has attracted significant attention because of its greater degree of precision in spatial and temporal control.[11, 14-16] It also offers both photophysical and photochemical mechanisms that are highly tunable for various delivery purposes.[11, 14-16] This is evident with an exponential growth of its applications that contributed to advances in the development of nanodelivery systems.

Photoactivation strategies are dividable primarily into three modes, linker cleavage, disassembly and gating, each enabling a payload release. This grouping is arbitrarily made on the basis of their underlying mechanisms that include linker photolysis, photoisomerization, photodynamic reaction or photothermal activation as validated in numerous release systems (**Figure 1**).[11, 16-19] First of all, linker photolysis plays a prominent role in drug release. Its use is also

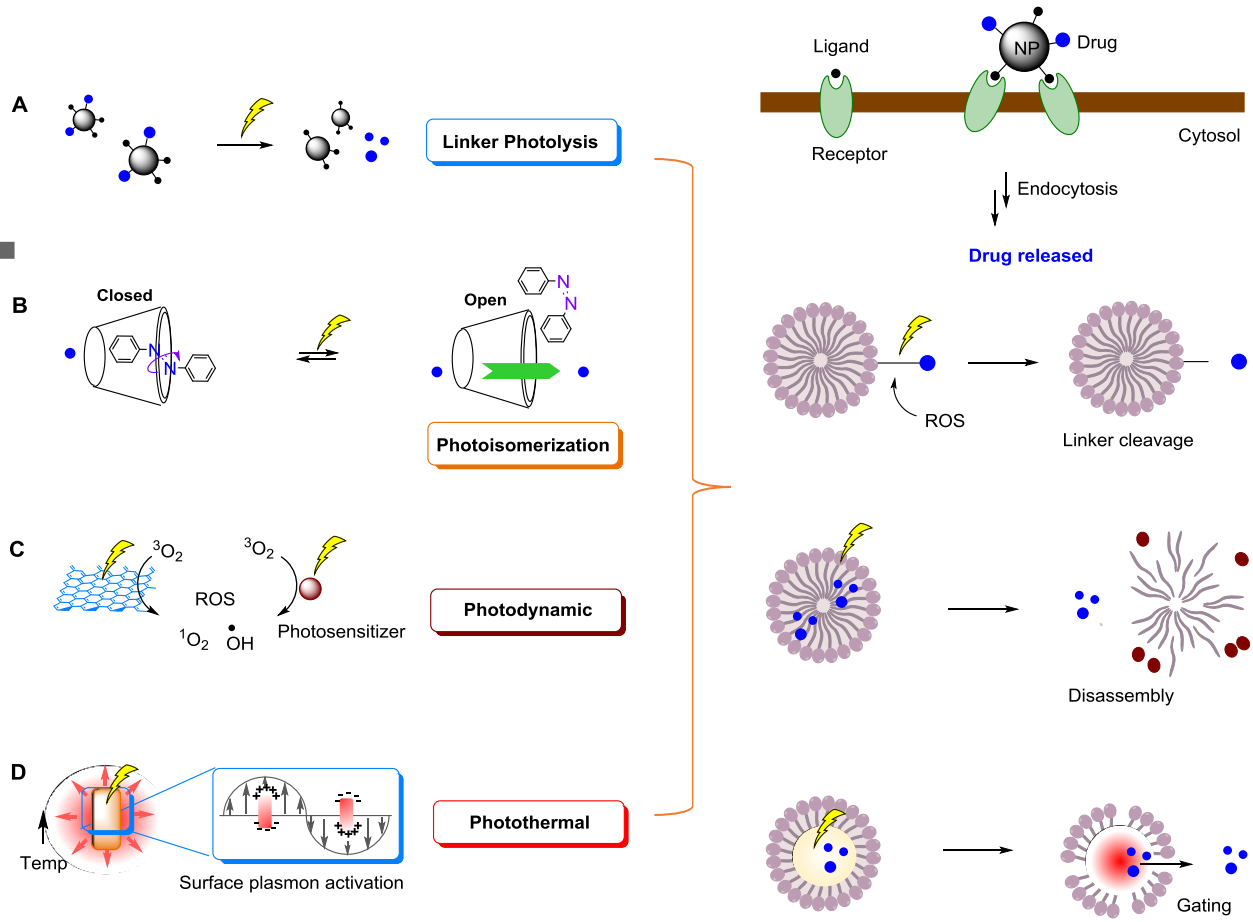

Figure 1. A schematic description for photoactivation strategies applied for payload release in a receptor-targeted nanodelivery system. Each of these strategies (linker cleavage, disassembly, gating; right) is enabled by either linker photolysis (A), photoisomerization (B), photoinduced production of reactive oxygen species (ROS) for ROS-mediated photodynamic effects (C), plasmonic photothermal activation (D), or their combination.

validated in the field of photocaging,[20, 21] a prodrug approach in which a payload molecule is inactivated through its covalent conjugation to a photocleavable linker (photocage).[22] This caged payload remains temporarily inactive until its cage is detached through linker photolysis by light irradiation.[23, 24] Second, photoisomerization refers to a photochemical process in which light triggers a molecular isomerization that can lead to changes in its conformation, shape or even pharmacological activity.[25, 26] This mechanism plays a key role in the control of gating by a drug-loaded nanocontainer through its ability for modulating the gate size and shape.[27] Third, photoactivation involves using a photosensitizer (PS) molecule[28] and photoactive nanomaterial,[29, 30] each having ability to produce reactive oxygen species (ROS)[31] upon light stimulation. Due to its high chemical reactivity, ROS is able to engage in various release mechanisms via either oxidative linker cleavage, nanocontainer fragmentation or disassembly.[32] However, this ROS-mediated release needs to be distinguished from photodynamic therapy (PDT)[19, 33-35] a therapeutic modality based on the induction of cytotoxicity via ROS-specific cellular damages.[31] Lastly, photoactivation is achieved by using a class of photothermal agents that display ability to produce a localized heat through surface plasmon

excitation by light.[36, 37] This light-induced hyperthermia is normally employed in photothermal therapy (PTT), a treatment modality that relies on induction of cytotoxicity by hyperthermia.[18, 36, 38-41] However, heat production occurs strong enough to induce physical alterations as well such as nanocontainer disassembly or pore opening. Thus photothermal activation serves as an important mechanism for release strategies.

Recently, application of photoactivation strategies has played an increasingly crucial role in the development of delivery systems.[11, 13, 42-46] Considering their rapid growth and therapeutic relevance, it would be of significant value to evaluate their contributions made over recent ten years. Here, this review article is therefore interested in compiling their specific examples and discussing their release mechanisms, design concepts, and practical impacts. In its scope, the present article is focused on topics of relevance to release strategies based on linker photolysis, bond isomerization, ROS production, or localized heating. However it excludes applications solely based on PDT[19, 33-35] and PTT[16, 36, 38-40] as these have been extensively reviewed in numerous articles published elsewhere as cited. Instead, it includes release strategies associated with dual mode therapies enabled by PDT or PTT. In its early contents, this article begins with comparing cellular factors vs. non-cellular stimuli involved in release controls, and it provides an overview for photoactivation mechanisms, photoactive nanoparticles (NPs) and photoresponsive linkers. These early contents constitute a fundamental backbone to specific release systems discussed in main topics later. In summary, the present article presents emerging concepts, developments and challenges in the application of photoactivation systems for therapeutic delivery.

2. Control Factors in Therapeutic Release: Cellular vs Light Stimuli

In drug delivery systems, numerous types of chemical, enzymatic or pathophysiological factors play a role in the control of release mechanisms. These involve drug-linker hydrolysis that occurs in subcellular compartments such as acidic endosomes (pH 5.0–6.0)[47] and lysosomes[48, 49] where drug-loaded NPs are temporarily retained after their receptor-mediated endocytosis.[50, 51] Similarly, drug release occurs by linker hydrolysis under specific pathophysiological conditions such as tumor hypoxia (lower oxygen),[52] low pH in extracellular matrices,[53] and enzyme upregulation in tumor-specific matrix metalloproteinase.[54-56] Redox enzymes overexpressed in tumors[50, 57] also contribute to release mechanisms by engaging in reductive cleavage of specialized linkers made of indolequinone[52] and nitroheterocycle.[58] Elevated levels of glutathione and thiols in tumor cells[59] also engage in facilitating the rate of disulfide drug-linker cleavage through thiol-disulfide exchange.[60] Collectively, these cell-based mechanisms occur passively under the condition dictated by certain microenvironmental or pathophysiological factors.

Unlike cellular or physiological stimuli, light application allows an active control in therapeutic release. Its higher degree of spatiotemporal control enables the occurrence of therapeutic activation primarily at or near a targeted tissue within a defined time frame.[11, 29, 61, 62] This can offer a greater resolution than other types of external stimuli investigated as active mechanisms in drug delivery such as ultrasound or magnetic field stimulations.[63, 64] Thus application of photoactivation strategies offers potentially great benefits in delivery systems.[11, 14, 18, 65, 66]

3. Building Blocks in Photoactivation Delivery Systems

A delivery system designed for photoactivation consists of three main elements that include a drug molecule, a linker, and a nanocarrier. The linker plays a role in not only drug attachment but also providing a release mechanism. The nanocarrier provides a physical space and method for drug

loading which occurs through either non-covalent encapsulation or covalent attachment.[11] Additionally, the nanocarrier itself has a photoactive property applicable for photoluminescence, photothermal or photodynamic activation.[16, 19, 29, 34] Several classes of nanomaterials have been identified that provide such photoactive properties.[67, 68]

3.1. Photoactive Nanomaterials

3.1.1. Photothermal Nanomaterials

Photothermal nanomaterials refer to those that are able to produce a localized heat through plasmonic activation.[16, 29, 30, 69-71] These comprise of nano gold (Au) and nano silver (Ag) that exist in various shapes such as spherical gold NP (AuNP),[68, 70, 72, 73] gold nanorod (AuNR),[70] hollow gold nanosphere (HAuNS),[41, 74-77] and porous gold nanocage (AuNC).[69, 78, 79] Their photothermal activation occurs by irradiation at a visible (Vis) and near infrared (NIR) region (500–800 nm). The produced heat rapidly dissipates, causing a localized hyperthermia which is potent enough to kill cells in a close proximity.[80, 81] Besides these functional properties, certain types of nano gold such as HAuNS[41, 74, 75, 77] and AuNC[78, 79, 82] offer unique structural benefits for drug delivery based on tunable cavities for drug loading and large surface areas available for ligand conjugation. This is illustrated with tumor targeted applications using HAuNS conjugated with folic acid,[83, 84] RGD peptide,[41] tumor-specific aptamer,[76] or anti-EGFR antibody,[74] and AuNC conjugated with anti-HER2 antibody.[82] Such PTT application has proven effective for the treatment of tumors[41, 85] and antibacterial infections.[64, 86]

3.1.2. Photodynamic Nanomaterials

Photodynamic nanomaterials[30, 34, 87] refer to those with ability to produce ROS[31] that comprise of singlet oxygen ($^1O_2$), free radicals (·OH, ·OOH, ·NO) and superoxide anion ($\cdot O_2^-$).[88] These include graphene oxide (GO) nanosheet,[89-91] carbon nanotube,[92, 93] TiO_2 nanosphere,[70, 87] and semiconductor quantum dots (QDs).[94] Their mechanism for ROS production involves generation of either photoexcited electrons or electron-deficient holes that engage in an energy transfer reaction with molecular oxygen ($^3O_2$) or water molecules near the surface.[95, 96] ROS production is also catalyzed by NP-loaded PS molecules such as chlorin e6,[97] rose Bengal (RB),[64] and protoporphyrin IX (PPIX).[98] Light activation for ROS production occurs by one-photon absorption of UV[99] and Vis light[95, 96] or two-photon absorption using a focused NIR laser.[96]

3.1.3. Upconversion Luminescent Nanomaterials

Use of NIR-responsive nanomaterials has made a significant impact on expanding the scope of photoactivation strategies.[89, 100-103] These include rare earth element-based upconversion nanocrystals (UCNs) such as $NaYF_4$ doped with lanthanide ions (Yb, Er, Tm).[89, 101, 102, 104-106] UCNs show excitation by NIR irradiation at 980 nm or 808 nm, which is then upconverted for luminescence emission in shorter UV–vis bands.[89, 101, 102, 104, 105] This NIR excitation is of great benefit because it belongs in the first biological window for optical imaging (I-BW), which tends to scatter less and penetrate deeper than UV or Vis light.[107, 108] UCN luminescence at UV–vis bands is highly useful for applications in photoactivation because of its tunability in wavelength (340–360 nm; 450–475; 540–560 nm),[105, 109, 110] and strong intensity enough for triggering linker photolysis, ROS production, or photothermal activation.[104] Besides lanthanide-based UCNs, there are only few other NPs identified for upconversion luminescence that include bismuth ferrite ($BiFeO_3$) and lithium niobate

($LiNbO_3$).[111, 112] Each of these also shows similar NIR excitation at 720–970 nm with luminescence emission at UV–vis bands.[112]

3.2. Photoresponsive Linkers

3.2.1. Linker Types

Photoresponsive linkers refer to those that are able to engage in linker cleavage via either photolysis,[113] oxidative fragmentation by $^1O_2$ reaction,[32, 114-117] photoreduction,[118, 119] or photoisomerization.[25, 120] As summarized in **Figure 2**, these linkers comprise of several types that include *ortho*-nitrobenzene (ONB),[121-125] thioacetal *ortho*-nitrobenzene (TNB),[126] coumarin,[122, 125, 127, 128] $^1O_2$-reactive cyanine,[129, 130] acridine,[131] and photoreducible *N*-methylpyridinium.[118] Linkers that display photoisomerization include azobenzene and coumaric acid. Their activation occurs most optimally in a specific range of wavelength as plotted.[22]

3.2.2. Linker Cleavage

ortho-Nitrobenzene Heterolysis. ONB linkers are most actively used and broadly defined to include *ortho*-nitrophenylethyl (NPE),[132-134] *ortho*-nitrodibenzofuran (NDBF),[124] and *ortho*-nitromandelic acid (NM).[135-137] Their photolysis occurs very effectively by UV absorption,[23, 24, 138-142] or less effectively by visible light absorption via two-photon absorption (710 nm,[124] 750 nm[123, 141]). Their mechanism of photolysis involves C-O bond heterolysis that proceeds through a series of intermediate species that are charged including *aci*-nitro as depicted in **Figure 3A**.[143] Due to such charge generation, the kinetics of ONB photolysis is influenced by media pH conditions,[143, 144] with faster photolysis occurring under basic or acidic pH conditions than physiological pH 7.4.[21, 144, 145] This pH dependency can be beneficial for the drug release in tumor environments where extracellular matrices are maintained slightly acidic (pH 6.2–6.9)[11, 146] and in subcellular endosomes (pH 5.0–6.0)[47] where NPs are taken up and temporarily retained.

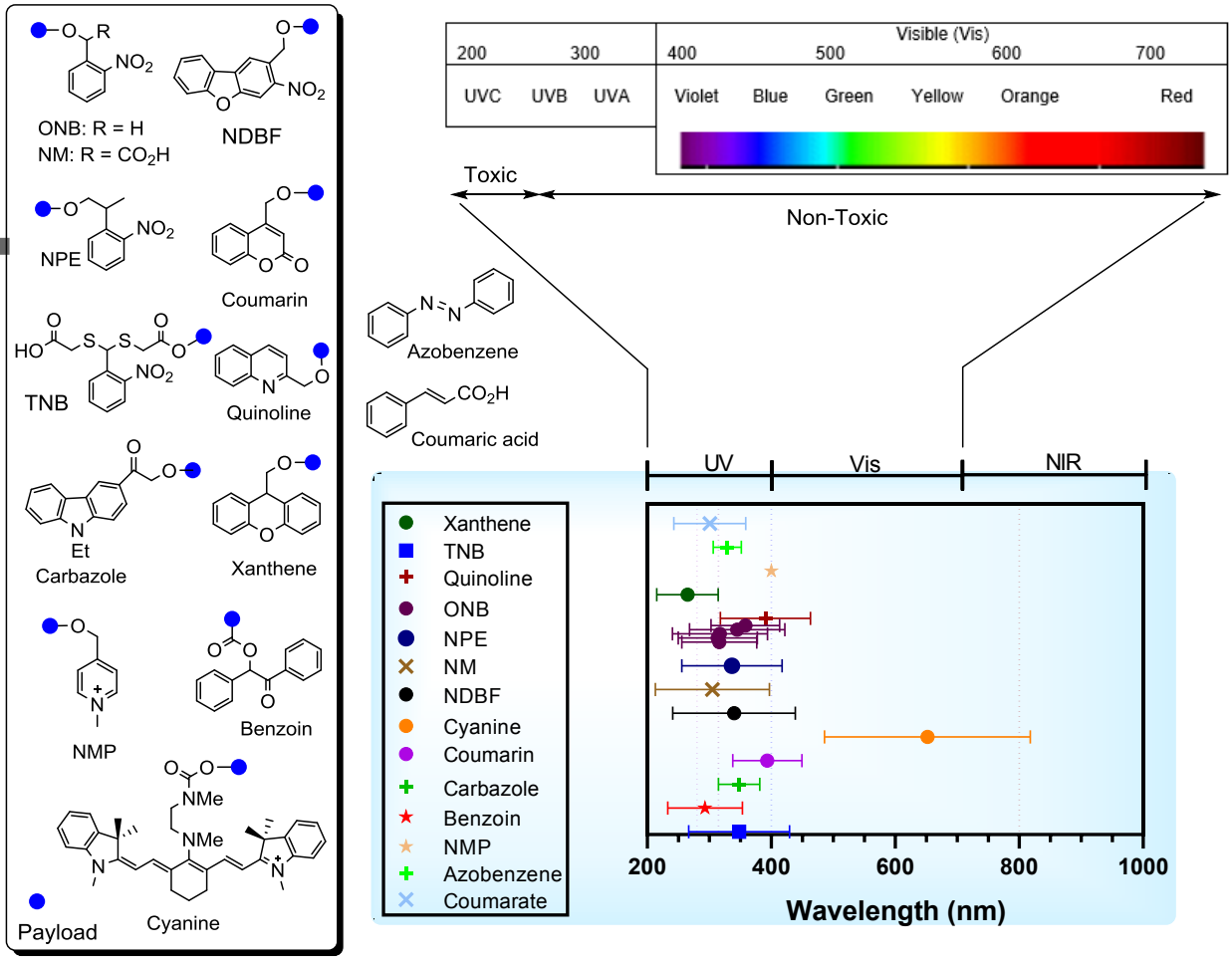

Figure 2. Types of photoresponsive linker used in photoactivation systems that are divided in to photocleavage (box) and photoisomerization (azobenzene, coumarate)

TNB follows a similar mechanism of photolysis like ONB by forming an *aci*-nitro intermediate (**Figure 3B**).[126, 138] It occurs by absorption at long wavelength UV (365 nm) with high quantum efficiency (Φ = 0.19–0.2)[126] comparable to ONB (Φ = 0.01–0.7).[22] However, use of TNB linkers offers practical advantages that include synthetic convenience and a structural symmetry by which two identical arms, each terminated with alcohol or carboxylic acid, are amenable for both drug and NP conjugation as illustrated.

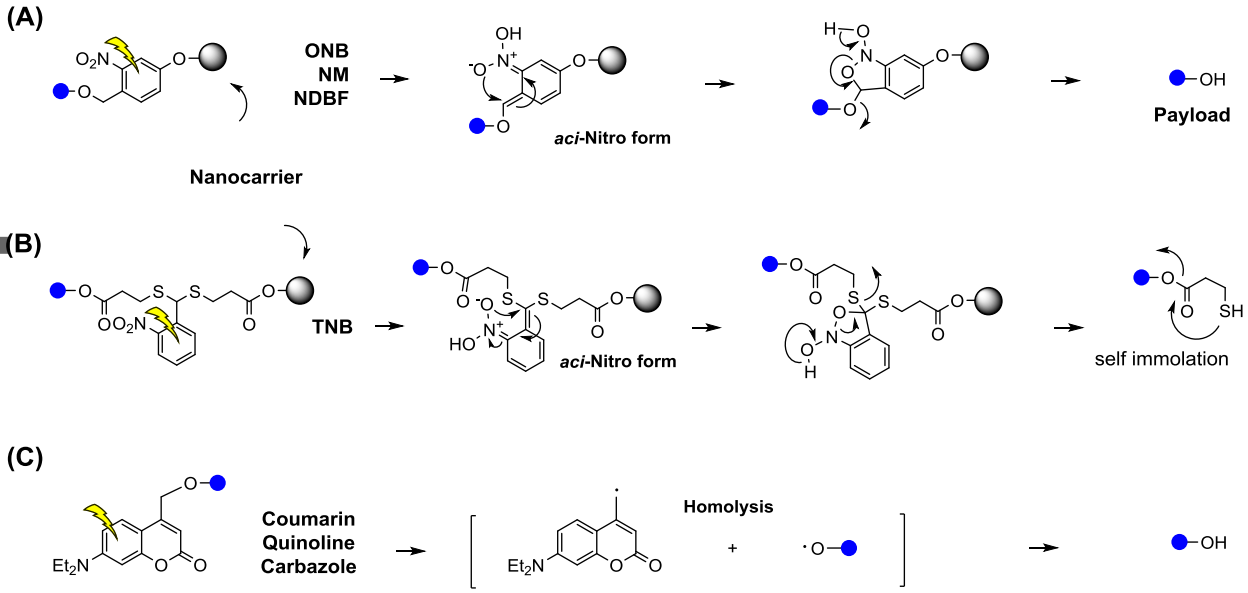

Figure 3. Characteristic mechanisms of linker photolysis. (A) *ortho*-Nitrobenzene (ONB) heterolysis, (B) Thioacetal *ortho*-nitrobenzene (TNB) heterolysis, (C) Coumarin bond homolysis.[22, 147]

*Linker Homolysis***.** A group of linkers undergo homolytic bond dissociation for their photolysis as shown by those derived from coumarin (λ_{max} = 420 nm),[122, 125, 127, 128] quinoline (458 nm),[148-151] and carbazole.[152, 153] This is illustrated with a linker such as coumarin-4-methyl[127] that shows cleavage at its C4 position where its payload is attached (**Figure 3C**).[141] Its photolysis occurs effectively by UV–vis absorption (365 nm,[127, 154] 475 nm[155]) or by two-photon NIR absorption (740 nm,[127, 154] 800 nm[155]).[127] The kinetics of coumarin photolysis is pH dependent like ONB linkers, which occurs faster under an acidic or basic environment than at pH 7.4.[21, 138, 156, 157] This is attributable to its pH-variable absorptivity (ε) and charges generated in the linker and its payload after their dissociation.

*Linker Oxidation and Reduction***.** Linker cleavage is induced indirectly through linker oxidation by reaction with $^1O_2$ produced under the irradiation condition,[114, 115, 129, 130, 158] or reduction via photoelectron transfer.[118] This occurs in a cyanine class of linker which shows an oxidative fragmentation by Vis–NIR irradiation (690 nm, 780 nm) as illustrated in **Figure 4A**.[129, 130, 158] Of interest is its dual function by serving as PS itself that catalyzes $^1O_2$ production,[129, 130] and then participating in [2+2] cycloaddition with $^1O_2$ that results in its dioxetane adducts. Due to their instability, these adducts rapidly undergo a series of self-fragmentations and cellular hydrolysis, leading to its payload release. Linker cleavage via oxidative fragmentation also occurs in other linker types that include alkene,[114] bis(alkylthio)ethene,[115, 159] alkylsulfide,[116] and bis(alkoxy)anthracene[32, 117] (**Figure 4B**). Each cleavage is triggered by $^1O_2$ reaction, but it varies in its fragmentation pattern. In addition to oxidation, photoreduction is applicable for linker cleavage but in fewer linkers such as *N*-methylpyridinyl-4-methyl that occurs via photoelectron transfer (**Figure 4C**)[118] and fluorophore boron-dipyrromethene (BODIPY) (**Figure 4D**).[119]

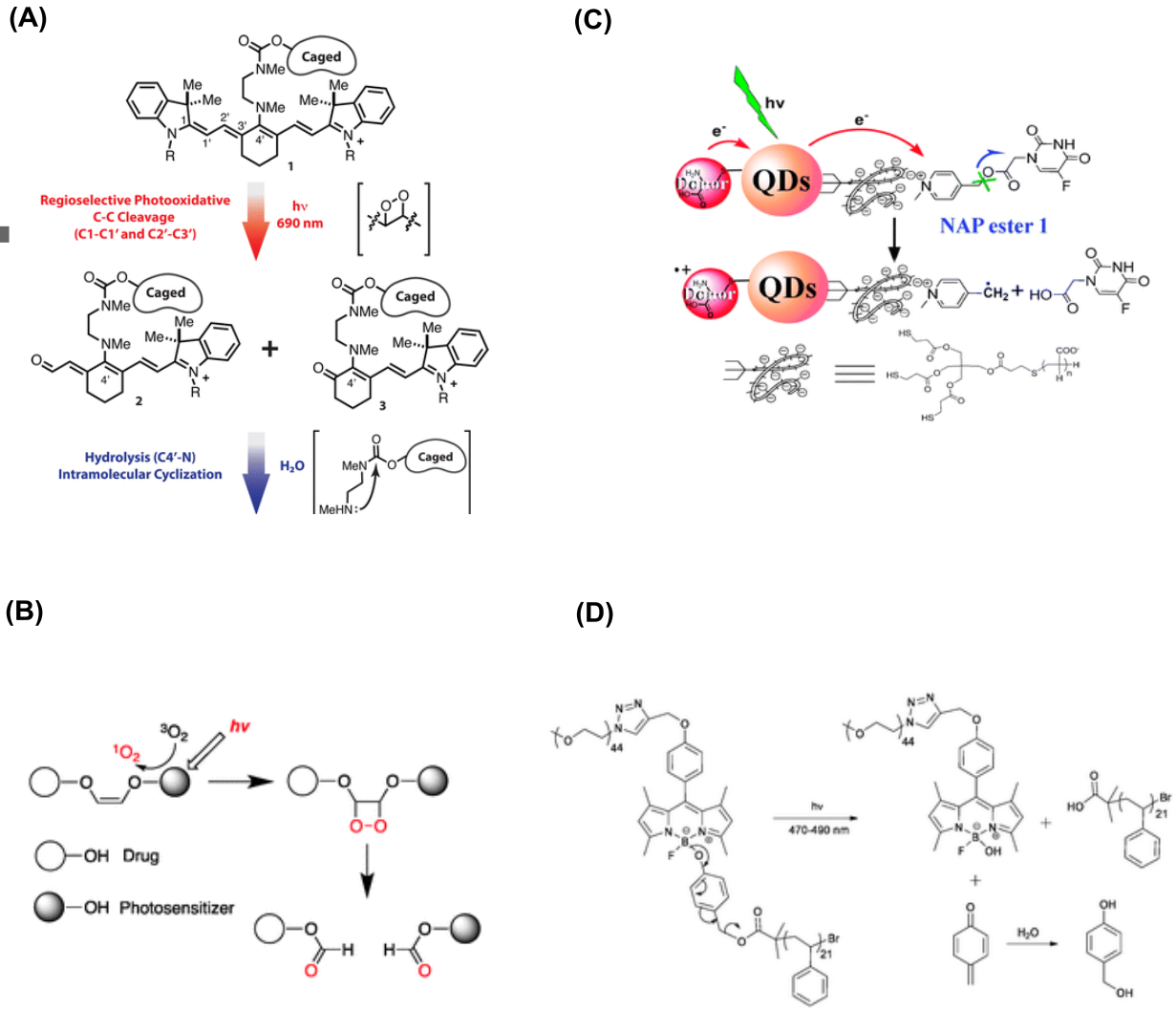

Figure 4. Mechanisms of photooxidation and photoreduction applied in linker cleavage. (A) Oxidative fragmentation of a cyanine linker by [2+2] $^1O_2$ addition.[129] Reproduced with permission, Copyright 2014, American Chemical Society. (B) Oxidative fragmentation of vinyl diether by [2+2] $^1O_2$ addition.[114] Reproduced with permission, Copyright 2012, Royal Society of Chemistry. (C) Reductive cleavage of *N*-methylpyridinyl-4-methyl via electron transfer.[118] Reproduced with permission, Copyright 2011, Royal Society of Chemistry. (D) Reductive cleavage of 4-hydroxybenzyl coordinated to BODIPY.[119] Reproduced with permission, Copyright 2015, Royal Society of Chemistry.

3.2.3. Photoisomerization

Despite lack of linker cleavage, photoisomerization enables a release mechanism by serving as an on-off switch in response to a light stimulus.[120, 160-162] This occurs in double bond-based linkers such as azobenzene, coumarate, and fumarate that have ability for isomerization between two conformational states, trans and cis, each displaying a distinct molecular shape (**Figure 5**). Its on-off

function is based on directing their isomerization at either trans or cis conformation, which is achieved by irradiation at a specific wavelength. This is illustrated by azobenzene that exists as a trans-azo form under a visible condition but isomerizes to a cis-azo form when the light is switched to shorter UV. Use of this isomerization strategy has proven highly effective in the design of gating or disassembly systems.[120, 160-165]

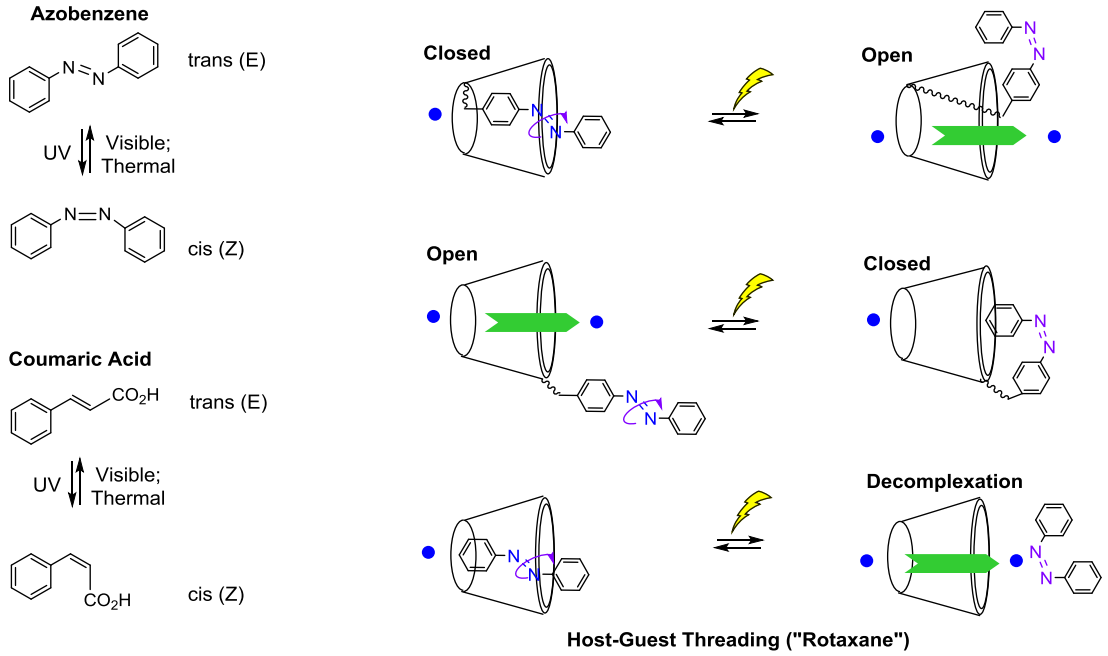

Figure 5. Release systems controlled by photoisomerization via pore gating (upper, middle) or host-guest decomplexation (lower)[120, 160-162]

4. Therapeutic Release via Linker Photolysis

4.1. Cytotoxic Agents

Methotrexate (MTX). MTX is a cytotoxic drug that inhibits dihydrofolate reductase localized in cytosol.[166] Despite its antitumor activity, MTX shows lack of tumor selectivity and dose-limiting toxicity.[167] Its photocontrolled delivery was achieved by MTX conjugation through an ONB linker to a folate receptor (FAR)-targeted poly(amidoamine) (PAMAM) dendrimer.[24, 138] Exposure of this conjugate to medium or long wavelength UV led to rapid MTX release via ONB photolysis.[24, 138] The drug release was verified independently in a cell viability assay performed using FAR(+) KB tumor cells that showed light-dependent induction of potent cytotoxicity.[24]

Doxorubicin (DOX). DOX (adriamycin) is an anticancer agent that blocks DNA replication by inhibiting topoisomerase II.[168] Like most cytotoxic agents, DOX lacks tumor specificity, and it has been frequently applied in drug delivery systems based on dendrimer,[23, 142, 169] brushed polymer[170] and UCN.[142, 171] One such system involves folate (FA)-conjugated PAMAM dendrimer employed for tumor-targeted DOX delivery (**Figure 6A**).[23] DOX was loaded in this dendrimer by its covalent attachment through ONB. Irradiation of the ONB caged DOX[142] or its dendrimer conjugate[23] at 365 nm resulted in rapid DOX release. This was consistent with induction of potent cytotoxicity in FAR(+) KB cells by irradiation *in vitro*. In a follow-up study, Wong et al. studied photolytic DOX

release using TNB-caged DOX which was conjugated to the FA-conjugated PAMAM dendrimer.[169] This conjugate showed light-controlled DOX release, which was similarly verified by the induction of cytotoxicity observed in FAR(+) KB cells. In each of these systems, DOX delivery using the FA-conjugated dendrimer resulted in an FAR-specific cellular uptake and greater cytotoxicity than its non-targeted comparator. This points to an important role of tumor targeting in addition to the precise control of drug release.[108]

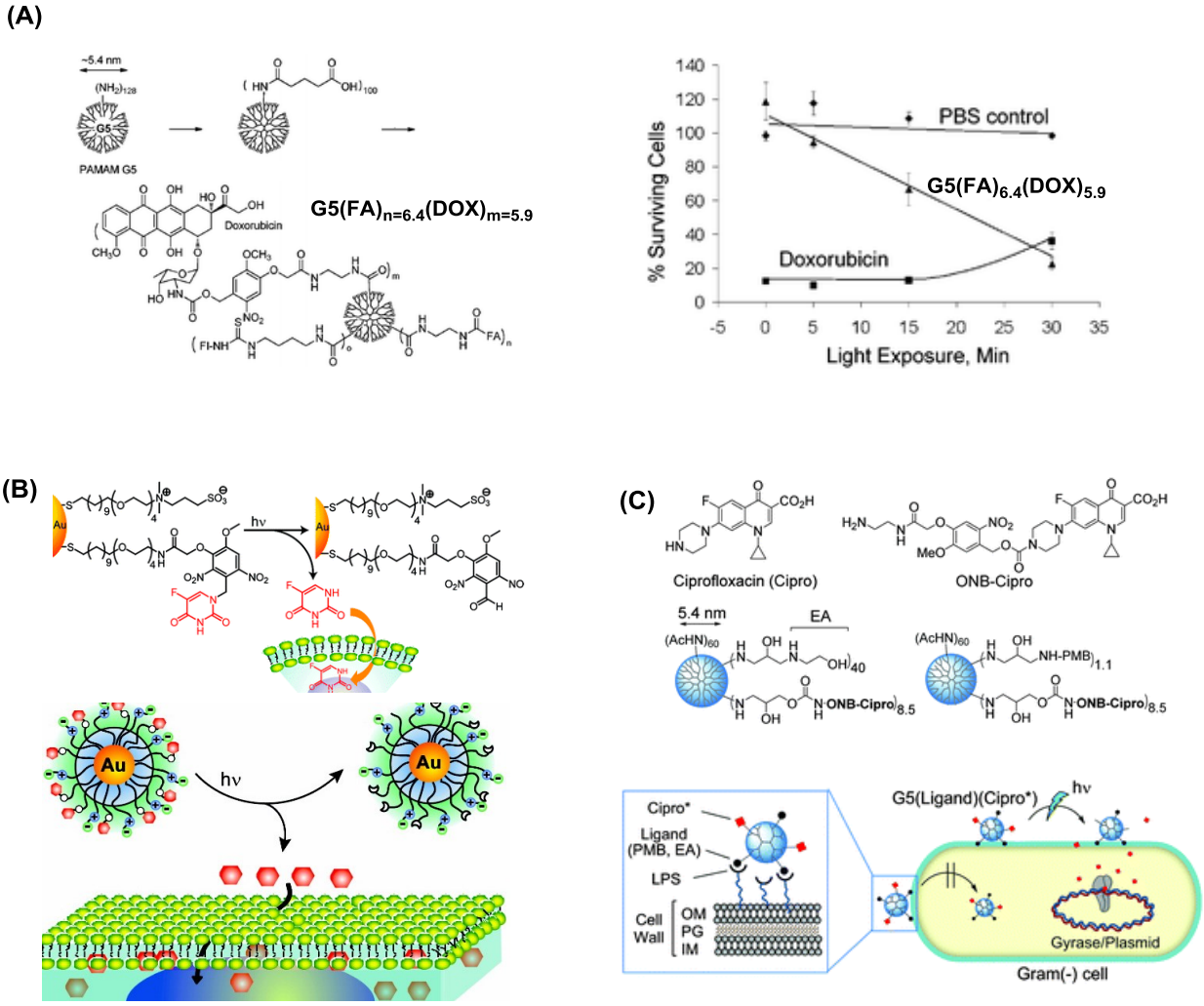

Figure 6. Therapeutic release via linker photolysis at long wavelength UVA. (A) Structure of FA-conjugated generation 5 (G5) PAMAM dendrimer which is attached with ONB-caged DOX, G5(FA)(DOX) (left), and its induction of cytotoxicity in FAR(+) KB cells by irradiation at 365 nm (right).[23] Reproduced with permission, Copyright 2010, Royal Society of Chemistry. (B) AuNP attached with 5-FU on the surface, AuNP@5-FU, for its photochemical delivery to cell.[140] Reproduced with permission, Copyright 2009, American Chemical Society. (C) Polymyxin B-conjugated dendrimer attached with ONB-caged ciprofloxacin, G5(PMB)(Cipro), for light-controlled ciprofloxacin release in bacterial cells.[172] Reproduced with permission, Copyright 2010, Royal Society of Chemistry.

Linker photolysis for DOX release is achievable by NIR irradiation using UV-emitting UCNs.[142, 169, 171] Wong et al. reported such a release system designed with mesoporous silica oxide ($mSiO_2$)-coated UCN (UCN@$mSiO_2$) (**Figure 7A**).[142] Its silica surface was functionalized with FA-conjugated dendrimer for FAR targeting and conjugated with ONB-caged DOX. Its DOX release was demonstrated to occur by irradiation at not only 365 nm but also 980 nm. They verified the effectiveness of tumor-targeted DOX delivery in FAR(+) KB cells *in vitro*, in which cell death occurred selectively only with the cells treated with the drug-loaded UCN and exposed to NIR at 980 nm. In a continued study, Wong et al. applied this UCN nanocomposite for DOX delivery by NIR-controlled TNB photolysis.[169] TNB-caged DOX was attached to the outer surface of UCN coated with a mesoporous silica layer.[98, 169] As anticipated, this drug-loaded nanocomposite showed an FAR-specific uptake as well as induction of cytotoxicity in FAR(+) KB cells in response to irradiation at 980 nm. Other approaches have been also effectively demonstrated for the NIR release of DOX loaded in UCNs. Dcona et al. reported a non-covalent approach based on the electrostatic adhesion of ONB-caged DOX on the UCN surface.[171] Xiang et al. coated a layer of ONB-caged polymer on the UCN surface prior to encapsulation with unmodified DOX.[173] Irradiation at 980 nm led to polymer fragmentation via ONB photolysis, ensuing DOX release.

5-Fluorouracil (5-FU). As an inhibitor of thymidylate synthase, 5-FU has been actively employed in a number of delivery systems. In a first report, Agasti et al. designed AuNP conjugated with 5-FU through an ONB linker,[140] and demonstrated a precise control of its drug release by long wavelength UV (**Figure 6B**). The drug release was consistent with the induction of cytotoxicity in cancer cells *in vitro*. Another system for 5-FU delivery was designed by Liu et al. using semiconductor QD by its tethering through an *N*-methyl-4-picolinium linker.[118] Unlike ONB, this linker cleavage occurs reductively via photoinduced electron transfer from the QD core

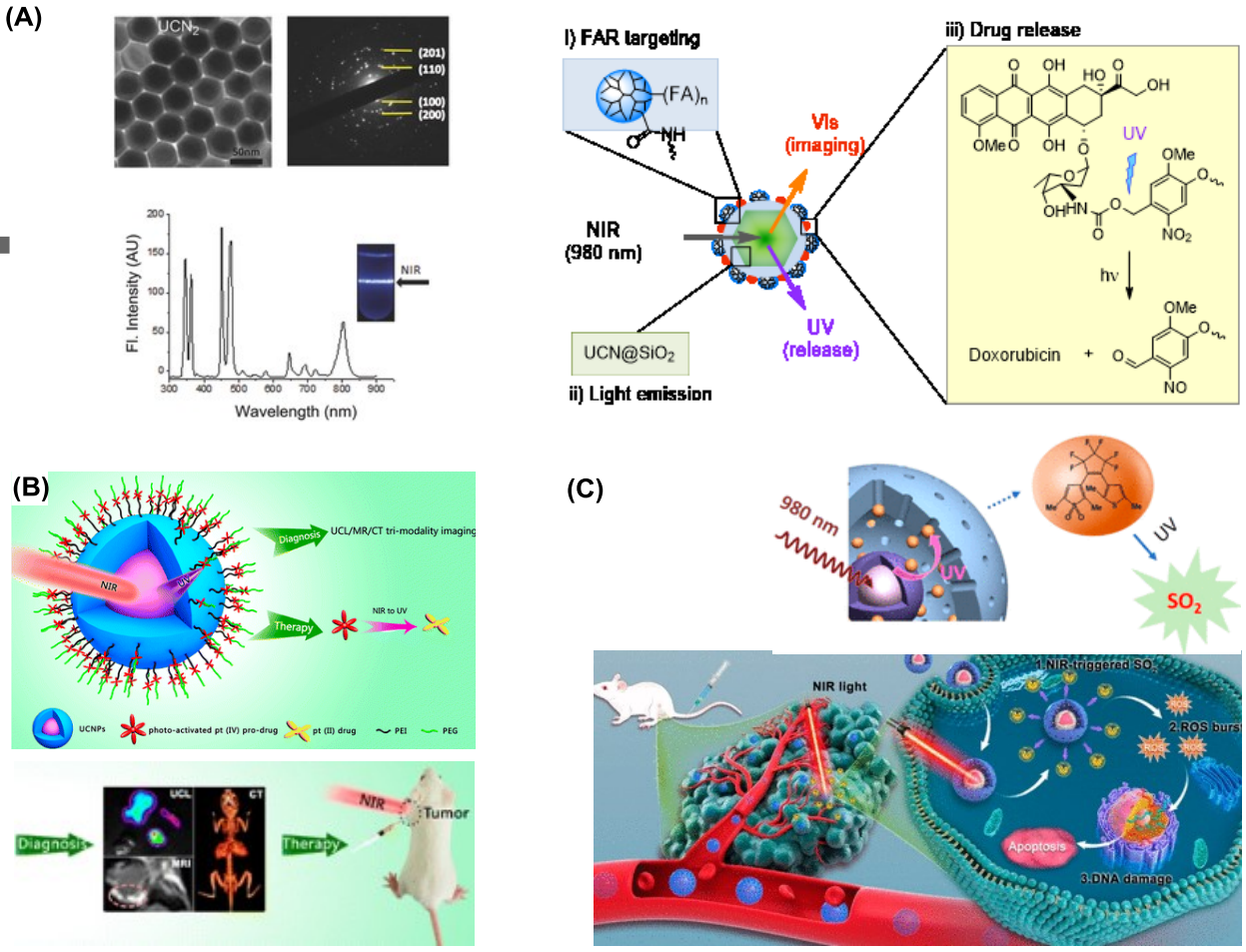

Figure 7. Photolytic release systems based on NIR-responsive upconversion nanocrystal (UCN). (A) Left: Transmission electron microscope image of UCN ($NaYF_4$:25%Yb/0.3% Tm) (upper) and its upconversion luminescence spectrum acquired by continuous wave laser excitation at 980 nm (lower). Right: A modular assembly of UCN by covalent conjugation of G5(FA) dendrimer and ONB-caged DOX on its surface.[142] Reproduced with permission, Copyright 2015, The Wiley & Sons. (B) A schematic illustration for a multifunctional UCN nanocomposite ($NaYF_4$:Yb/Tm) loaded with a platinum(IV) prodrug for NIR-controlled imaging and antitumor therapy *in vivo*.[174] Reproduced with permission, Copyright 2013, American Chemical Society. (C) NIR light-triggered sulfur dioxide (SO_2) generation using SO_2 prodrug-loaded rattle-structured upconversion@silica nanoparticles.[175] Reproduced with permission, Copyright 2019, American Chemical Society.

to the drug-attached picolinium group. Such QD-mediated photolysis occurs by irradiation in a visible region in which most QDs show strong absorption. Another approach for photolytic 5-FU release involves a retro [2+2] dissociation reaction as reported by Jin et al.[176] For this purpose, they prepared

polymer micelles by self-assembly of coumarin ester-appended poly(methacrylate) copolymer. The coumarin ester enabled for drug conjugation via its [2+2] cycloaddition with 5-FU. Micelle photolysis at 254 nm led to 5-FU release, which occurred through linker photolysis via retro [2+2] reaction.

Taxane. Despite numerous reports on photocaged taxane derivatives,[177-180] their application in delivery systems has been rarely studied. Xu et al. reported such a delivery system for paclitaxel using a pyramid-shaped RNA nanocage.[181] The drug was attached through ONB at the end of a RNA branch extended from the main nanocage.[181] Paclitaxel release occurred by UV irradiation, and it was verified by the induction of cytotoxicity in breast cancer cells *in vitro*.

Camptothecin. This anticancer agent blocks DNA replication by inhibiting topoisomerase I. Hu et al. reported a polymer micelle system designed for camptothecin delivery. Its micellar surface was functionalized with FA for tumor targeting,[182] while its hydrophobic core was encapsulated with ONB-caged camptothecin.[182] This micelle showed an FAR-specific uptake in cancer cells, and it released camptothecin via ONB photolysis that resulted in ~10-fold greater cytotoxicity than no irradiation *in vitro*.

Chlorambucil. It is one of alkylation agents that display potent anticancer activities. Yu et al. reported pyrene-caged chlorambucil loaded in polymer NPs prepared by its aggregation with mPEG-block-poly(L-lysine).[183] The drug release was demonstrated by irradiation at 365 nm in a cell-based assay, which led to cancer cell death *in vitro*. Photolytic chlorambucil release is achievable using a visible light-responsive linker as reported by Janett et al.[131] They designed prodrug aggregates made of chlorambucil caged with acridin-9-methanol, which showed the drug release by irradiation at 410 nm. Linker photolysis at other visible wavelengths was achieved using a pair of donor and acceptor dye molecules which served as a UV-emitting transducer. Huang et al. prepared a BODIPY dye-encapsulated mesoporous silica nanocapsule, which was then loaded with coumarin-caged chlorambucil in its shell layer.[184] Linker photolysis occurred by irradiation at 650 nm which resulted in luminescence emission at 432 nm by the BODIPY dye pair. Its drug release was confirmed by tumor cell death observed *in vitro*. Furthermore, long wavelength photolysis was achieved at NIR using lithium niobate ($LiNbO_3$), a photoactive NP that displays two-photon absorption at 790 nm with luminescence emission at UV–vis bands.[111] Its surface was conjugated with coumarin-caged chlorambucil, and its drug release occurred by irradiation at 790 nm via coumarin linker photolysis.

Platinum-based Agents. Linker photolysis is applicable in the release of a platinum anticancer agent using its oxidized prodrug which is released via photoinduced reduction.[185] Li et al. designed human serum albumin carrying a Pt(IV) prodrug linked through amide conjugation. Its irradiation enabled to release a reduced, active Pt(II) species, which was verified by the induction of potent cytotoxicity in cisplatin sensitive as well as resistant cancer cells. Reductive Pt release was also achieved using polymer micelles as reported by Song et al.[186, 187] They designed an azide or pyridine-coordinated Pt(IV) prodrug, which was then encapsulated in the hydrophobic core. Irradiation resulted in the prodrug activation to Pt(II), which rapidly escaped from the hydrophobic core. Using a UCN nanocarrier opens a route for the NIR-activated Pt(II) release. Dai et al. designed a UCN nanocomposite loaded with an azide-coordinated Pt(IV) prodrug on its shell surface (**Figure 7B**).[174] Irradiation at 980 nm enabled Pt(II) release, which was consistent with the inhibition of tumor growth in mice treated with the composite.

4.2. Antibacterial Agent

Ciprofloxacin displays its potent antibacterial activities by inhibiting a bacterial DNA gyrase.[188] Shi et al. reported a PEG-based hydrogel loaded with ciprofloxacin by attachment through an ONB linkage.[189] Irradiation at 365 nm resulted in the drug release as verified by the induction of its potent antimicrobial activity against S. aureus. Its controlled delivery is achievable using a bacteria-targeted system as reported by Wong et al. using PAMAM dendrimer functionalized with PMB, a bacteria-targeting ligand validated for selective binding to lipopolysaccharide present in Gram(−) bacterial cells.[172, 190] Irradiation of this targeted dendrimer co-conjugated with ONB-caged ciprofloxacin resulted in the rapid release of ciprofloxacin (**Figure 6C**).[172] This was also confirmed in a bacterial growth assay, indicating a potent antimicrobial activity induced under the light condition only.

4.3. Nucleotides

Linker photolysis is also applicable for large biomacromolecules. Han et al. applied this approach for DNA delivery using AuNP as a non-viral vector.[191] They fabricated AuNP by surface coating with positively charged, ONB-caged PEG chains prior to loading of dsDNA (37-mer) on this functionalized AuNP via polyplex formation. By irradiation at 350 nm, its PEG surface showed charge neutralization due to ONB detachment, which promoted its dsDNA release through surface charge repulsion. Brown et al. reported a similar approach using AgNP covered with an antisense DNA oligonucleotide which was caged with ONB.[192] This DNA-coated AgNP vector showed photoactivated antisense DNA release, which was verified in a cellular assay by its ability to block the expression of its target gene, intracellular adhesion molecule-1.

Photolysis for nucleotide release is designed using NIR-responsive UCN. Pan et al. applied this approach in CRISPR gene editing for cancer therapeutics.[193] They coated the UCN surface with ONB-caged Cas9-sgRNA, a single guide RNA that targets a tumor gene (polo-like kinase-1). NIR irradiation led to desired gene editing as verified by inhibition of tumor growth *in vivo*.[193] Another example for gene release involved UCN loaded with an ONB-caged morpholino oligonucleotide on the surface.[194] This system enabled NIR-triggered gene escape in endosomes by which gene knockdown occurred more effectively in a melanoma model.

4.4. Gas Molecules of Biological Significance

Application of controlled release for small di or tri-atomic gas molecules is highly challenging due to their lack of functional moiety for temporary inactivation. It requires other strategies such as using its donor or precursor molecules as demonstrated by nitrogen oxide (NO), which has been most actively studied for light controlled release. Fraix et al. identified a nitroaniline-based NO donor with ability for NO release via its photofragmentation.[195] It was loaded in β-CD-based polymer NPs through its host-guest complexation in the β-CD hydrophobic cavity along with zinc-phthalocyanine (ZnPc) co-loaded as PS. Irradiation at 400 nm resulted in NO and $^1O_2$ release, both of which contributed to cell death in melanoma cells *in vitro*. Application of this nitroaniline for NO release was achieved using carbon QD as well,[196] in which the NO release is triggered by photoinduced energy transfer from the QD core to the NO donor localized in the shell. Its release activity was evident with decreased cell viability in HeLa cells *in vitro*, and lowered tumor volume in tumor-grafted mice.

A second approach for NO release relies on using a metal-NO chelate through photoinduced bond dissociation. Xiang et al. loaded a ruthenium nitrosyl (Ru-NO) complex on the surface of FA-conjugated nanoTiO_2 for its targeted delivery in FAR(+) HeLa cells.[197] Visible irradiation above 400 nm resulted in both NO and $^1O_2$ release by TiO_2. This Ru-NO approach was also demonstrated using

graphene QD by its covalent functionalization on the surface.[198] Irradiation at 808 nm resulted in NO release along with hyperthermia induction by the QD. This dual therapy accounted for a potent antitumor efficacy in a tumor model.

Photolytic gas release is broadly applicable to various gas molecules that include carbon monoxide (CO),[199] sulfur dioxide (SO_2)[175] and hydrogen sulfide (H_2S).[200, 201] CO release is achieved using a manganese carbonyl complex with ability to undergo Mn-CO dissociation by irradiation at 365 nm.[199] This Mn-CO complex was used for NIR-responsive CO delivery by its loading in polymer-coated UCN as reported by Pierri et al.[199] Such NIR approach was also applied for SO_2 delivery using UCN@mSiO_2 loaded with thiophene-1,1-dioxide as the SO_2 precursor (**Figure 7C**).[175] H_2S release is achieved in a prodrug approach such as using an ONB-caged precursor.[200] Chen et al. designed PEG-coated UCN for encapsulation of this ONB-caged H_2S precursor in its shell layer,[200] and showed H_2S release by excitation at 980 nm.

In section summary, linker photolysis constitutes a significant fraction of research efforts in the development of photoactivated release systems. As summarized in **Table 1**, its applications are validated in a wide range of therapeutic molecules from antitumor agents[11, 13, 103, 202] (DOX,[23, 203] 5-FU,[140] MTX,[24, 138] paclitaxel,[126, 177] camptothecin[182]), antibacterial agents,[172] gas molecules (NO,[195, 197] CO,[199] H_2S[201]) to nucleotides.[193]

Table 1. Therapeutic release via linker photolysis

Therapeutic Area	Nano Delivery System	Design		Ref
		Payload	Linker (Light, nm)	
Anticancer	G5(FA)(MTX)	MTX	ONB (365)	[24, 138]
	G5(FA)(DOX)	DOX	ONB (365), TNB (365)	[23, 169]
	UCN@G5(FA)-DOX	DOX	TNB (980)	[142]
	UCN@DOX	DOX	ONB (980)	[171]
	AuNP@5-FU	5-FU	ONB (365)	[140]
	QD@5-FU	5-FU	*N*-Methyl-4-picolinium (Vis)	[118]
	Poly(methacrylate) micelle	5-FU	[2+2] Addition (254)	[176]
	RNA nanocage	Paclitaxel	ONB	[181]
	Polymer micelle	Camptothecin	ONB	[182]
	Poly(L-lysine)	Chlorambucil	Pyrene (365)	[183]
	NP aggregate	Chlorambucil	Acridin-9-methanol	[131]

			(410)	
	Mesoporous silica nanocapsule	Chlorambucil	Coumarin (650)	[184]
	$LiNbO_3$	Chlorambucil	Coumarin (790)	[111]
	Human serum albumin	Pt(II)	Pt(IV) azide	[185]
	Polymer micelle	Pt(II)	Pt(IV) azide	[186, 187]
	UCN@Pt(IV)	Pt(II)	Pt(IV) (980)	[174]
Antibacterial	PEG Hydrogel	Ciprofloxacin	ONB (365)	[189]
	G5(PMB)(Cipro)	Ciprofloxacin	ONB (365)	[172]
Nucleotide	AuNP@dsDNA	dsDNA	ONB (350)	[191]
	AgNP@DNA	Antisense DNA	ONB	[192]
	UCN@RNA	Cas9-sgRNA	ONB (980)	[193]
Gas Molecule	β-CD Polymer	NO	Nitroaniline (400)	[195]
	QD@Nitroaniline	NO	Nitroaniline (350, 800)	[196]
	$NanoTiO_2$	NO	Ru-NO (400)	[197]
	Graphene QD	NO	Ru-NO (808)	[198]
	UCN@(Mn-CO)	CO	Mn-CO (980)	[199]
	UCN@Thiophenedioxide	SO_2	Thiophenedioxide (980)	[175]
	UCN@H_2S Precursor	H_2S	ONB (980)	[200]

5. Therapeutic Release via Photolytic Disassembly

5.1. Liposome Disassembly

Photolytic disassembly is defined arbitrarily as a process in which drug molecules loaded in a nanocontainer are released upon its nanocontainer disassembly triggered by photolysis. This is applicable in a liposomal structure made of photocleavable lipids within its bilayer structure. Chandra

et al. reported an ONB-caged liposome that showed disassembly by irradiation at 365 nm. It was successfully used to release 6-carboxyfluorescein loaded internally.[204] This liposomal control was similarly applied in the release of a magnetic resonance imaging (MRI) contrast agent using an ONB-caged Gd(III) complex which was tethered to the water-exposed surface.[205] Its release resulted in a decrease in T_1 relaxivity when the liposome was photolyzed at 400 nm.

5.2. Polymer Micelle Disassembly

Disassembly via UV–vis Photolysis. Polymer micelle disassembly has proven effective in the controlled release of payloads such as dye[119, 206] and drug molecules.[207, 208] It is illustrated with the release of Nile red encapsulated in polymer micelles (polymersomes) made of either ONB-caged block copolymer,[206] or photocleavable BODIPY polymer.[119] These micelles showed degradation upon irradiation at 365 nm (ONB) or 470–490 nm (BODIPY), which was attributed to photolytic degradations at the hydrophobic core. Polymer micelle disassembly is applied in a similar manner for drug delivery as demonstrated by DOX release from micelles prepared with ONB-caged amphiphilic block copolymer[208] or poly(acrylate) ester copolymers.[207]

Micelle disassembly generally occurs regardless of its shape or surface functionalization. Yang et al. reported DOX-loaded cylinder-shaped tubisomes made of cyclic peptide-bridged photocleavable copolymers (**Figure 8A**).[209] The tubisome disassembly occurred rapidly after irradiation at 365 nm, and DOX release that followed was consistent with the induction of cytotoxicity in breast cancer cells. Sun et al. reported CD44-targeted DOX delivery using polymer micelles made of ONB-caged hyaluronic acid (HA). This HA polymer was also used to play a role in tumor targeting[210] because of its affinity to a CD44 biomarker overexpressed in cancer cells. DOX release occurred by UV irradiation, which accounted for potent inhibition of tumor growth in mice. Tumor-targeted DOX delivery was also achieved using a DNA aptamer Sgc8 conjugated to photocleavable polymer micelles as reported by Yang et al (**Figure 8B**).[211] They observed selective micelle binding and uptake by leukemia cells, and the induction of cytotoxicity associated with DOX release by UV irradiation.

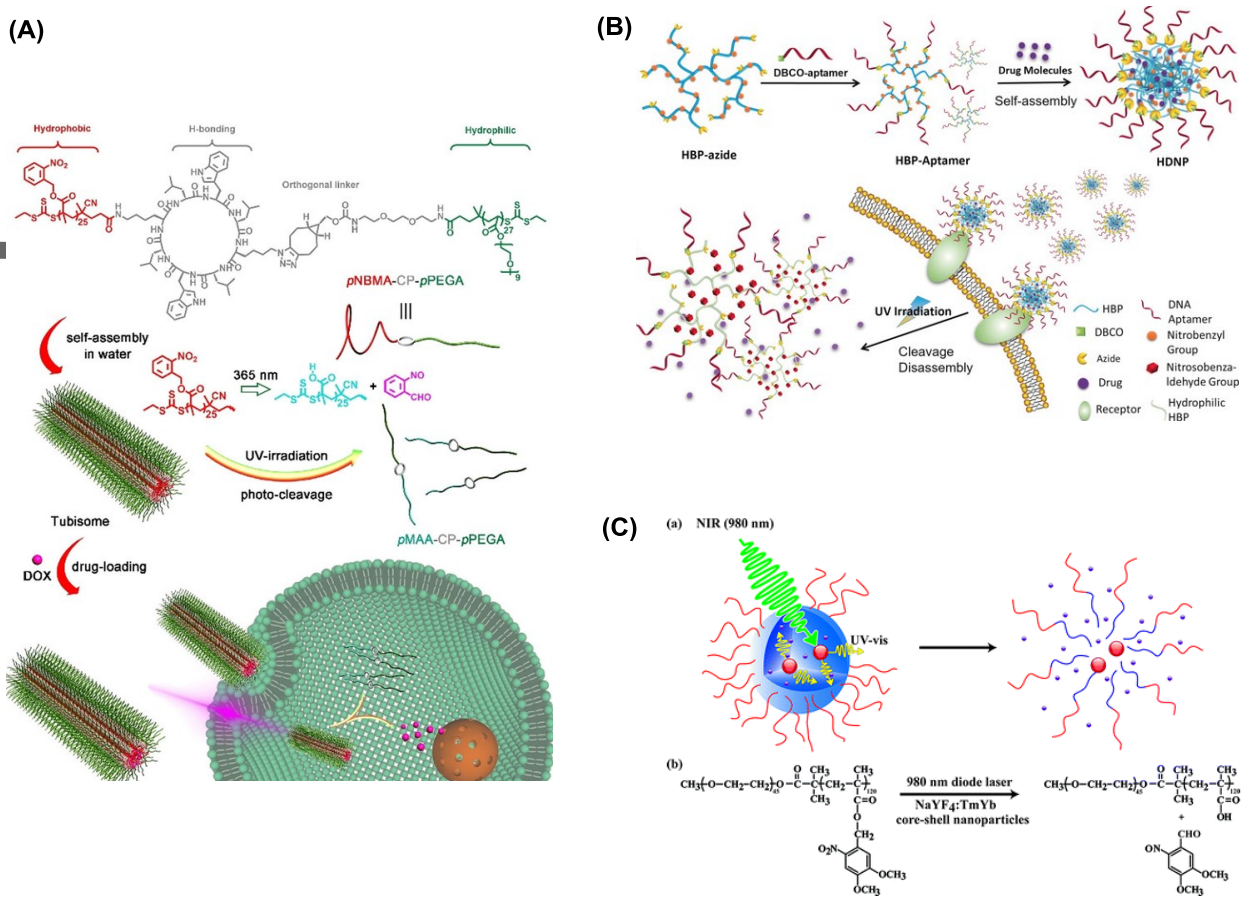

Figure 8. Therapeutic release via polymer disassembly induced by linker photolysis. (A) Phototriggered disassembly for drug release by DOX-loaded tubisomes made of photocleavable copolymers.[209] Reproduced with permission, Copyright 2020, The Wiley & Sons. (B) Aptamer-grafted hyperbranched polymer micelles for controlled release of Dox by UV irradiation.[211] Reproduced with permission, Copyright 2018, The Wiley & Sons. (C) Upconversion luminescence-controlled disassembly of polymer micelles.[212] Reproduced with permission, Copyright 2011, American Chemical Society.

Caging with coumarin and other photolabile linker is also effective in the design of polymer disassembly systems. Sun et al. designed DOX-encapsulated polymersomes composed of di-block copolymers caged with coumarin in the shell layer.[213] Irradiation at 430 nm resulted in coumarin detachment, which triggered DOX release via liposome disassembly. Photolytic disassembly was demonstrated using 2-nitroresorcinol polyacetal as a photolabile polymer as reported by Pasparakis et al.[214] They prepared polyacetal aggregates encapsulated with camptothecin, and showed occurrence of polymer disassembly triggered by irradiation with UV or visible light which was less effective.

Disassembly via NIR Photolysis. It is doable to integrate UCN with polymer micelles for NIR-triggered photolytic disassembly. Yan et al. designed UCN-encapsulated micelles made of ONB-caged poly(methacrylate) copolymers (**Figure 8C**).[212] Irradiation at 980 nm resulted in micelle

disassembly by a mechanism attributed to ONB detachment by UV luminescence emitted from UCN. This approach allowed to release DOX which was co-loaded with UCN within the micelle.[215] The drug release was consistent with the induction of cytotoxicity observed in MCF-7 breast cancer cells under NIR irradiation. This strategy was similarly applied for NIR-induced siRNA delivery.[216] Here, Zhao et al. designed UCN coated with ONB-caged cationic brush polymers in order to load negatively charged siRNA which is encoded to block an intracellular cancer target. By 980 nm irradiation, they were able to release the siRNA via polymer disassembly that followed ONB detachment. This siRNA delivery proved effective in suppressing A549 tumor growth *in vivo*.[216]

Disassembly via Retro [2+2] Reaction. Lastly, design of photolytic disassembly is achievable using retro [2+2] cycloaddition. Alemayehu et al. designed DOX-loaded polymer micelles prepared by inter-polymer crosslinking via [2+2] cycloaddition of two complementary polymers, each tethered with adenine (A) or uracil (U).[217] Irradiation at 254 nm led to DOX release which was attributed to polymer micelle disassembly that occurred through polymer de-crosslinking by retro [2+2] reaction. The drug release was confirmed by the induction of cytotoxicity in cancer cells.

In summary, linker photolysis has played a growing role in the control of disassembly that enables payload release. It has shown promising applications for Nile red,[119, 206] DOX,[213, 217] camptothecin,[214] an MRI contrast agent,[205] and siRNA[216] using nanocarriers based on liposomes, polymer micelles and UCN as summarized in **Table 2**.

Table 2. Therapeutic release systems via nanocarrier disassembly or gating enabled by linker photolysis

Release Mode	Nano Delivery System	Design		Ref
		Payload	Linker (Light, nm)	
Disassembly	Polymer micelle	DOX	ONB	[207, 208]
	HA polymer micelle	DOX	ONB	[210]
	Polymer micelle-Aptamer Sgc8	DOX	ONB	[211]
	Polymer tubisome	DOX	ONB (365)	[209]
	UCN@Polymer micelle	DOX	ONB (980)	[212, 215]
	Crosslinked polymer micelle	DOX	[2+2] Addition (254)	[217]
	Polymer micelle	DOX	Coumarin (430)	[213]
	NP aggregate	Camptothecin	2-Nitroresorcinol (UV–vis)	[214]
	UCN@siRNA	siRNA	ONB (980)	[216]

	Liposome	Gd(II) complex	ONB (400)	[205]
	Liposome	Carboxyfluorescein	ONB (365)	[204]
	Polymer micelle	Nile red	ONB (365), BODIPY (470)	[119, 206]
Gating	$mSiO_2$@Polymer	-	ONB	[218]
	AuNS@$mSiO_2$	DOX	ONB (980)	[219]
	UCN@$mSiO_2$	Fluorescein	ONB (980)	[220]
	$mSiO_2$	Rhodamine	Ru-S (455)	[221]
	UCN@$mSiO_2$	DOX	Ru-S (977)	[222]

6. Therapeutic Release via Photolytic Gate Control

Linker photolysis plays a notable role in the control of gating mechanism for controlled drug release. Lai et al. reported fluorescein-loaded mesoporous silica nanoparticle (MSN) grafted with ONB-caged poly(*N*-isopropylacrylamide-co-acrylate) polymer on its porous surface. Under an ambient condition, its pores remained closed due to its randomly collapsed polymer brushes (**Figure 9A**).[218] However, under UV irradiation, they observed pore opening that allowed payload diffusion. This was attributed to the loss of ONB moieties, which made polymer brushes more water soluble and elongated to a preferred conformation for pore opening.

Hernández-Montoto et al. advanced this gating strategy for NIR control.[219] They designed $mSiO_2$-coated gold nanostar (AuNS@$mSiO_2$), which was then loaded with DOX prior to capping with a layer of photocleavable PEG derivatives on its silica shell (**Figure 9B**).[219] Irradiation at 808 nm resulted in DOX release and the induction of toxicity in HeLa cells, which was attributed to pore opening associated with polymer photolysis. NIR-controlled photolytic gating was also achieved using UCN@$mSiO_2$ capped with photocleavable polymers as reported by Xiang et al.[220] They showed this UCN system for fluorescein release by NIR irradiation.

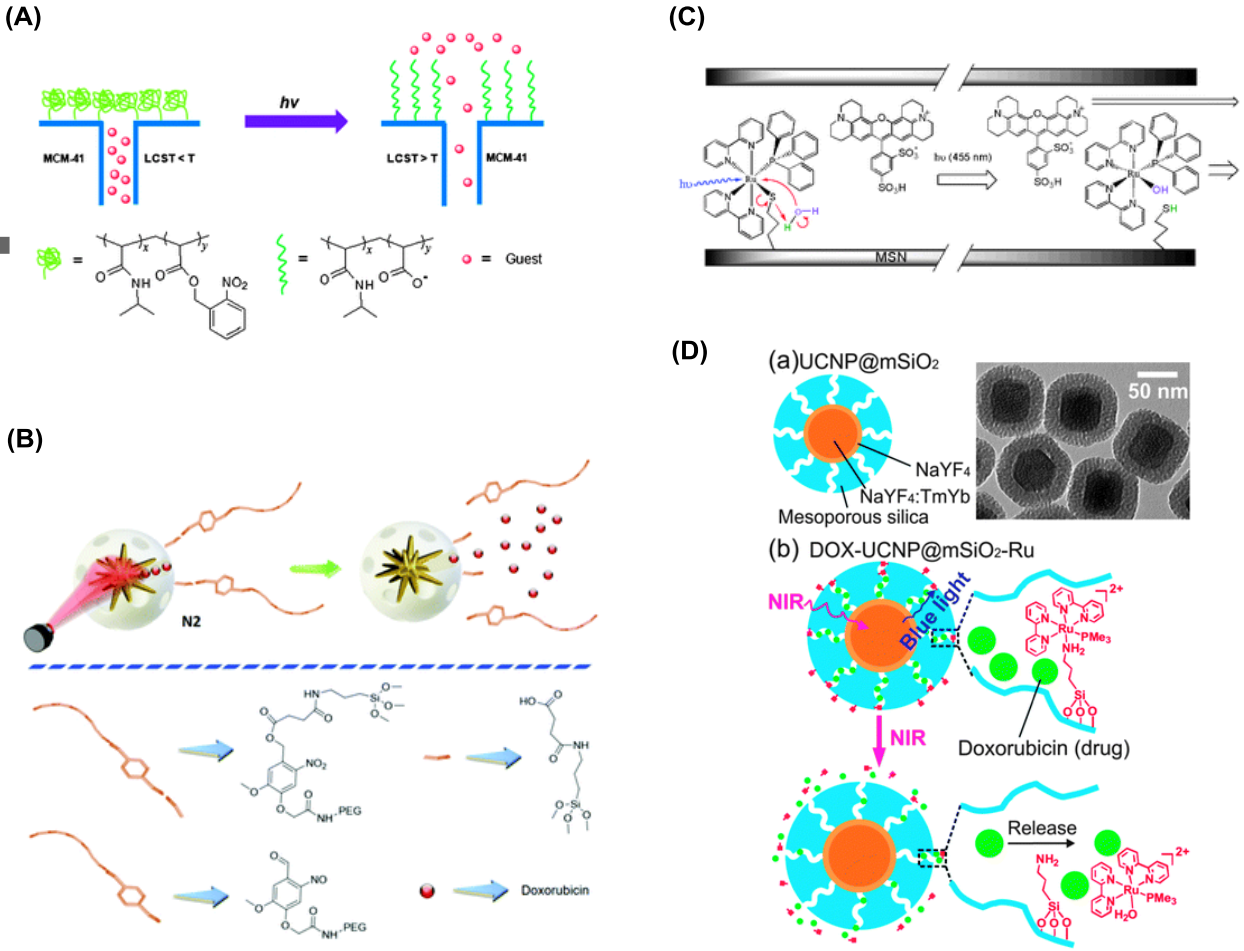

Figure 9. Photolytic gate control designed with mesoporous silica nanoparticles (MSN). (A) MSN coated with polymer brushes.[218] Reproduced with permission, Copyright 2010, Royal Society of Chemistry. (B) DOX-loaded AuNS@mSiO_2 nanoparticles capped with a photolabile PEG derivative.[219] Reproduced with permission, Copyright 2019, Royal Society of Chemistry. (C) MSN encapsulated with Dye Sr101 and functionalized with thiol-coordinated $Ru(bpy)_2(PPh_3)$ moieties inside the pores.[221] Reproduced with permission, Copyright 2011, Royal Society of Chemistry. (D) DOX-loaded UCN@mSiO_2 nanoparticles capped with a photocleavable Ru complex.[222] Reproduced with permission, Copyright 2015, Royal Society of Chemistry.

Another approach for a gate control in MSN involves an internal capping within its pore interior in lieu of on its surface. This was achieved using MSN functionalized internally with thiol-coordinated ruthenium-bipyridyl moieties (**Figure 9C**).[221] Visible irradiation at 455 nm of this MSN loaded with rhodamine enabled the dye release. This was attributed to its pore opening which occurred when its ruthenium capping complex dissociated by Ru-S photolysis. He et al. further advanced this gating strategy for NIR control using mesoporous silica coated UCN that displayed blue luminescence at 470 nm (**Figure 9D**).[222] They demonstrated DOX release by irradiation at 974 nm.

In summary, linker photolysis has been applied for a gate control using MSN,[218, 219] UCN[222] and their core-shell integration (**Table 2**). Despite only a few applications, it shows a promising potential in the design of gating systems for drug delivery.

7. Therapeutic Release via Photoisomerization

7.1. Gating via Photoisomerization

Azobenzene/Cyclodextrin Rotaxane. Azobenzene plays an active role in the control of gating by serving as a photoresponsive switch.[162, 223] Zhao et al. reported polymer vesicles designed to release entrapped drug molecules using this mechanism (**Figure 10A**).[163] They designed bacteria-like, rod-shaped vesicles which were prepared by the self-assembly of a host-guest polymer complex referred to as "rotaxane" made between β-cyclodextrin (β-CD) and an azobenzene derivative. UV irradiation of these vesicles entrapped with DOX led to the drug release by a gating mechanism. This release was attributed to cilia-like stretching motions that occurred in response to azobenzene decomplexation from its rotaxane when it isomerized to cis conformation.

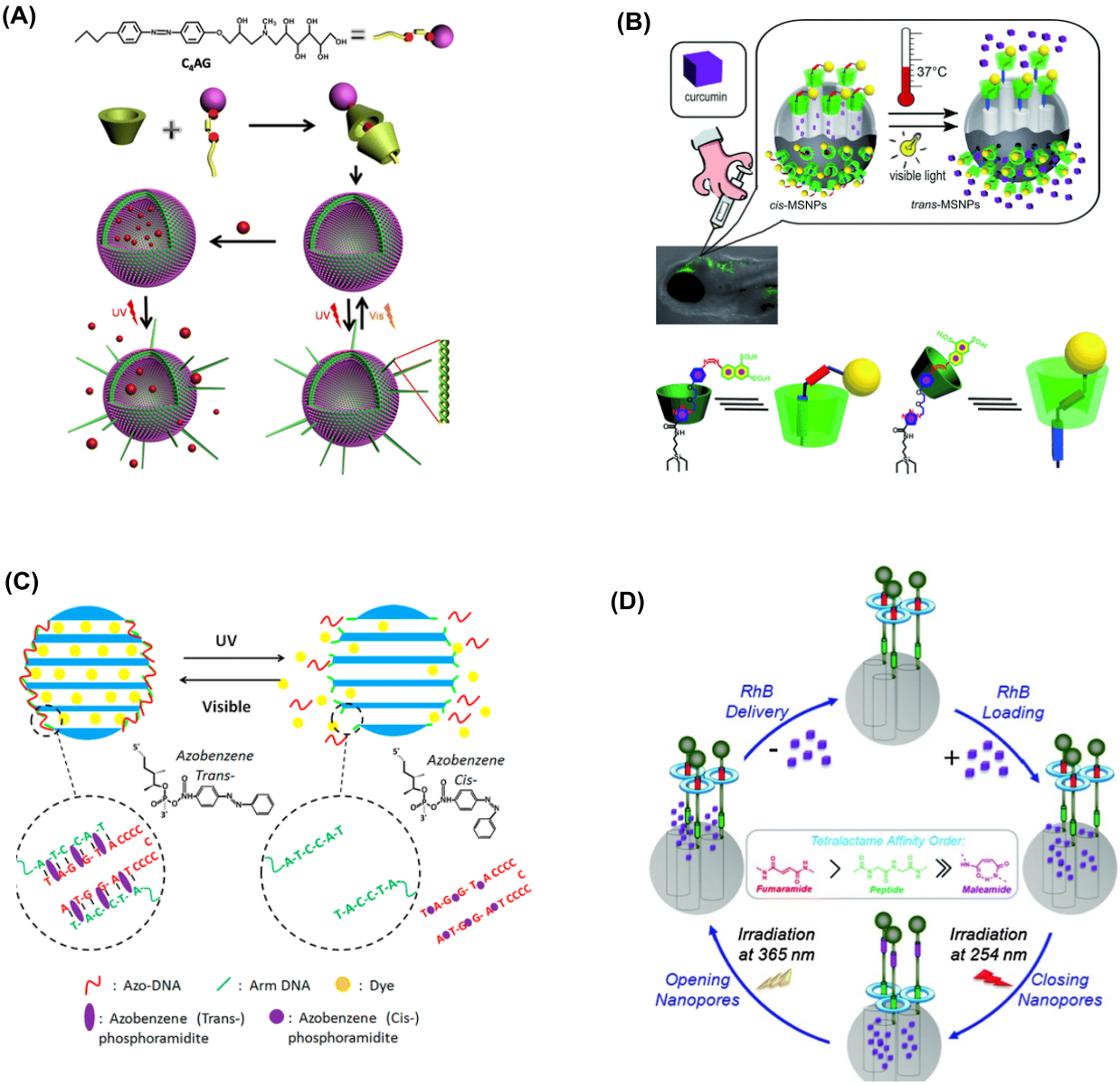

Figure 10. Gating control by photoisomerization. (A) Light-triggered gate opening for DOX release in bacteria-like vesicles.[163] Reproduced with permission, Copyright 2014, American Chemical Society. (B) Visible light-triggered gate opening for curcumin release in zebrafish larvae.[160] Reproduced with permission, Copyright 2012, The Wiley & Sons. (C) Gating control via dsDNA dehybridization triggered by azobenzene isomerization.[164] Reproduced with permission, Copyright 2012, American Chemical Society. (D) Isomerization-induced control of rotaxane (fumaramide-CD complex) shuttling between a proximal (closed) and distal (open) position.[165] Reproduced with permission, Copyright 2015, Royal Society of Chemistry.

Designing a gating mechanism using an azobenzene/CD rotaxane is also applicable in MSN which contains internal pores.[160, 224] Yan et al. generated gate keepers at its surface by capping with azobenzene/α-CD rotaxane shuttles (**Figure 10B**).[160] Such design made its pores either closed under UV light (cis, rotaxane decomplexed) or open under visible light (trans, rotaxane complexed). Using this delivery system, they successfully demonstrated curcumin release in zebrafish larvae under visible light irradiation. Wang et al. reported a MSN system similarly functionalized with azobenzene/β-CD complexes, which was effectively used for DOX release in porcine skin under red light (625 nm).[224] Lastly, Yuan et al. reported another type of gating mechanism for MSN by functionalization with a DNA strand hybridized with an azobenzene-containing complementary DNA strand (**Figure 10C**).[164] This particular design allowed a pore closing at DNA hybridization (trans, visible) due to steric blocking by dsDNA, which switched to an opening at dsDNA dehybridization (cis, UV). This delivery system was successfully demonstrated for DOX release following irradiation at 365 nm.

NIR-controlled isomerization is applicable in the design of gating mechanisms. Liu et al. reported DOX-loaded UCN@mSiO_2 which was then modified by capping with azobenzene residues at its pores (**Figure 11A**).[161] Its irradiation at 980 nm resulted in DOX release, which was attributed to pore opening by trans to cis isomerization at the pore entrance. This UCN-enabled NIR control was successfully applied in another delivery vehicle such as UCN-encapsulated azobenzene vesicles as reported by Yao et al. (**Figure 11B**). Irradiation at 980 nm of the vesicles co-loaded with DOX resulted in effective drug release.[120]

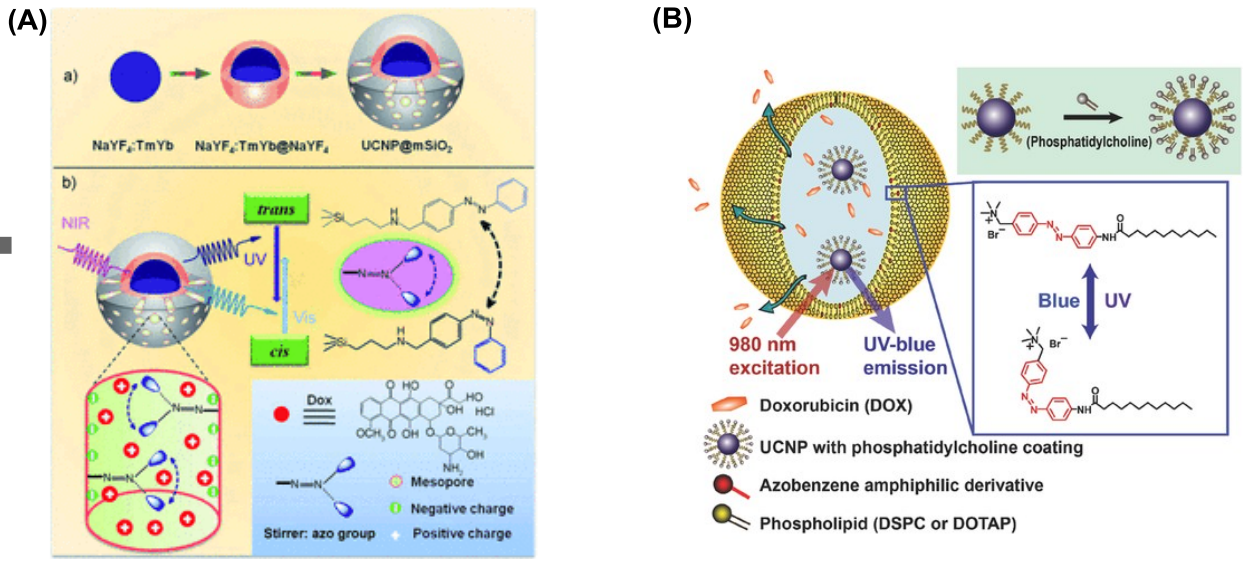

Figure 11. NIR-controlled gating systems designed with upconversion nanocrystal (UCN). (A) NIR-triggered release of DOX loaded in UCN@$mSiO_2$ grafted with azobenzene molecules in its mesoporous network by trans to cis photoisomerization.[161] Reproduced with permission, Copyright 2013, The Wiley & Sons. (B) A schematic illustration for azobenzene-incorporated vesicles encapsulated with DOX and UCN for NIR-controlled drug release.[120] Reproduced with permission, Copyright 2016, The Wiley & Sons.

Emerging Host-Guest Systems. In addition to CD, there are various types of host molecules that are effectively applied in gating systems. These include cucurbit[8]uril, a pumpkin-shaped hollow container, that is also able to form a rotaxane complex. Ma et al. reported MSN functionalized with trans-azobenzene peptide derivatives, each engaged in forming a rotaxane shuttle with cucurbit[8]uril.[225] Irradiation at 350 nm of this MSN loaded with DOX enabled DOX release due to its pore opening that occurred in response to rotaxane decomplexation.

Gate controls are also achieved using other photoisomerization systems based on coumarate,[226] fumaramide,[165] spiropyran[227] and a donor–acceptor Stenhouse adduct (DASA).[228] Like azobenzene, coumaric acid attached on the MSN surface allowed light-controlled release of naproxen, a non-steroidal anti-inflammatory drug, loaded in silica pores following irradiation at 254 nm.[226] Fumaramide plays a similar role as applied in the design of its rotaxane-guided gating system. Martinez-Cuezva et al. designed MSN attached with a fumaramide-containing peptide in complex with [2]rotaxane (**Figure 10D**).[165] This design allowed its pore opening at 365 nm (trans) by which its payload rhodamine B was released. Spiropyran engages in a gate control though it works differently by displaying different properties upon isomerization between its cyclic hydrophobic form at >450 nm and its open zwitterionic form at <420 nm. Wang et al. used such distinct property in the gate control of polymer vesicles made of a spiropyran-branched copolymer.[227] These vesicles remained tightly sealed at >450 nm, but developed porosity after irradiation at <420 nm, which was attributed to an increase in internal hydrophilicity due to isomerization to zwitterions. Lastly, a functional unit known as a donor-acceptor Stenhouse adduct (DASA)[228] offers an unique ability to undergo an intramolecular cycloaddition at 550 nm by which its physicochemical property is reversed from hydrophobicity to hydrophilicity. Such physicochemical alteration was used to control the

release of DOX or camptothecin loaded in DASA polymer NPs designed for FAR-targeted drug delivery.[228]

7.2. Disassembly via Photoisomerization

Azobenzene Micelle. Azobenzene photoisomerization constitutes a prominent principle in the function of disassembly systems. One such system involves liposomes assembled with azobenzene lipid molecules as reported by Liang et al.[229] They demonstrated its ability to engage in an on-off switch by light such that the liposome remained intact under visible light at 450 nm, but disassembled after irradiation at 365 nm. Namazi et al. effectively applied this concept for the light controlled release of erlotinib which was encapsulated in polymer micelles prepared with azobenzene-grafted dendrimer copolymer.[230]

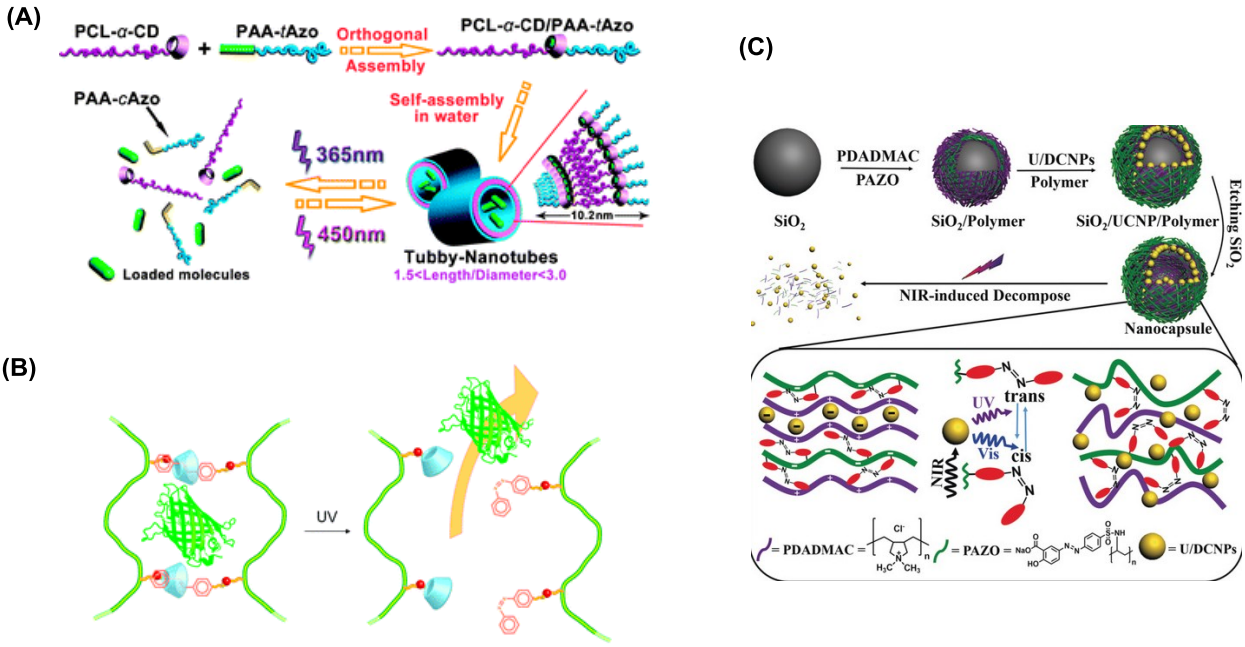

Figure 12. Release systems of photoisomerization-induced disassembly. (A) A schematic for photoresponsive disassembly by nanotubes made of PCL-α-CD and PAA-Azo.[231] Reproduced with permission, Copyright 2011, Royal Society of Chemistry. (B) Release of green fluorescent protein (GFP) from an azobenzene/β-CD hydrogel by UV isomerization.[232] Reproduced with permission, Copyright 2010, Royal Society of Chemistry. (C) DOX release by NIR-induced disassembly of hollow nanocapsule@up/downconversion NP.[233] Reproduced with permission, Copyright 2018, The Wiley & Sons.

Azobenzene isomerization is equally applied in azobenzene/CD complexes for disassembly control. Yan et al. demonstrated the disassembly of tube-shaped vesicles made of azobenzene poly(acrylate) and α-CD poly(caprolactone)[231] which occurred following irradiation at 365 nm (**Figure 12A**). They further applied this strategy for the controlled release of propranolol (α-blocker) encapsulated in the same vesicles.[234] Azobenzene isomerization normally occurs by absorption in a

UV or visible range, though it can also occur in a longer NIR region via energy transfer. Huang et al. reported such polymer micelle disassembly for DOX release in HeLa cells that occurred by two-photon absorption of the azobenzene polymer at 800 nm through its fluorescence resonance energy transfer.[235]

Besides small drug molecules, release by disassembly is applicable for larger siRNA. Li et al. designed positively charged NPs made of azobenzene/CD-HA complexes,[236] which was used for loading siRNA (GAPDH-homo). This siRNA release occurred through vesicle disassembly following irradiation at 365 nm, which was consistent with the induction of growth inhibition in cancer cells. In other similar applications, release by disassembly occurs as a result of changes in shape. This is illustrated by azobenzene/CD polymer vesicles which shifted their shape from soft vesicles to smaller compact NPs after UV irradiation.[237]

Donor–Acceptor Stenhouse Adduct (DASA) Polymer. Triggering polymer disassembly is achievable through the isomerization of the DASA moiety. Poelma et al. reported paclitaxel-loaded micelles containing DASA moieties localized in the inner layer.[238] Following exposure to visible light at 550 nm, these micelles showed disassembly, which was attributed to increased hydrophilicity associated with cyclized DASA moieties. This system was effectively used for paclitaxel delivery in MCF-7 breast cancer cells that occurred under visible light irradiation.

Hydrogel. Defined as a polymer network which is crosslinked covalently or non-covalently, hydrogel retains its shape with the help of such crosslinks. Peng et al. designed a hydrogel disassembly system using a non-covalent azobenzene/CD crosslinker as the photoswitch (**Figure 12B**).[232] They demonstrated an effective release of green fluorescent protein (GFP) which was pre-loaded by irradiation at 365 nm. Karcher et al. similarly applied this release strategy for ciprofloxacin which was encapsulated in an azobenzene-based photochromic hydrogel.[239] Its release occurred precisely when the hydrogel (trans) turned to a liquid form (cis) under green light (510 nm). This was consistent with the inhibition of *E. coli* growth under 523 nm light, which was in contrast with its normal growth observed under the dark condition.[239]

Metal-Organic Framework. Using an azobenzene switch is effectively applied in the control of physical stability in metal-organic framework (MOF). This is illustrated with azobenzenedicarboxylate which was incorporated within the lattice of UiO-type MOF as an organic ligand.[240] This MOF remained stable in the dark but showed degradation after irradiation at 340 nm. This disassembly strategy was effective in the controlled release of 5-FU loaded in the MOF.

Core-Shell UCN. Integration of UV–vis luminescent UCN and azobenzene systems offers a principal route for NIR-controlled disassembly. This is illustrated with azobenzene/CD-coated UCN which displayed polymer disassembly at 980 nm as reported by Möller et al.[241] Zhao et al. directed this strategy to drug delivery by designing DOX-loaded nanocapsule, in which DOX was co-encapsulated with UCN in its shell layer made of azobenzene polymers (**Figure 12C**).[233] Irradiation at 980 nm resulted in DOX release, which was verified with the induction of potent cytotoxicity in tumor cells.

In section summary, photoisomerization actively engages in the design of release systems controlled via either gating or disassembly. This strategy has been widely applied as evident with numerous delivery systems based on MSN, micelles, polymer micelles, hydrogel, MOF and UCN, and various types of payloads including DOX, paclitaxel, 5-FU, ciprofloxacin or GFP (**Table 3**).

Table 3. Therapeutic release via photoisomerization-induced gating and disassembly

Release Mode	Nano Delivery System	Design		Ref
		Payload	**Linker (Light, nm)**	
Gating	$mSiO_2$@Azo/CD	Curcumin	Azobenzene/CD (Vis)	[160]
	Supramolecular vesicle	DOX	Azobenezene/CD (UV)	[163]
	$mSiO_2$@Azo/CD	DOX	Azobenzene/CD (650)	[224]
	$mSiO_2$@Azo-dsDNA	DOX	Azobenzene (365)	[164]
	UCN@Azo	DOX	Azobenzene (980)	[161]
	UCN@Azoliposome	DOX	Azolipid (980)	[120]
	MSN@Azo/Cucurbituril	DOX	Azobenzene/Cucurbituril (350)	[225]
	MSN@Coumarate	Naproxen	Coumarate (254, 365)	[226]
	MSN@Fumaramide/Rotaxane	Rhodamine B	Fumaramide/Rotaxane (365)	[165]
	Polymer vesicle	DAPI	Spiropyran (420)	[227]
	Folate Polymer NP	DOX, Camptothecin	DASA (550)	[228]
Disassembly	Polymer micelle	Nile Red	Azobenzene (365)	[229]
	Polymer micelle	Erlotinib	Azobenzene (365)	[230]
	HA polymer NP	siRNA	Azobenzene/CD (365)	[236]
	Azo/CD polymer micelle	Rhodamine B	Azobenzene/CD (365)	[231]
	Azo/CD polymer micelle	(R/S)-Propranolol	Azobenzene/CD (UV)	[234]
	Azo/CD polymer micelle	DOX	Azobenzene/CD (800)	[235]
	Polymer micelle	Paclitaxel	DASA (550)	[238]
	Hydrogel	GFP	Azobenzene/CD (365)	[232]
	Hydrogel	Ciprofloxacin	Azobenzene (523)	[239]

	MOF@5-FU	5-FU	Azobenzene (340)	[240]
	UCN@DOX	DOX	Azobenzene/CD (980)	[233]

8. Therapeutic Release by Photothermal Activation

8.1. Photothermal Gating

Yagüe et al. explored this gating mechanism using ibuprofen-loaded MSN, which was coated with a porous layer of Au on its shell surface.[242] Its ibuprofen release occurred by NIR exposure at 808 nm, which was attributed to pore opening induced by heat production in Au. Marquez et al. advanced this strategy for naproxen delivery using a mesoporous nanomaterial co-loaded with AuNR. Its pores were sterically blocked by capping with a cucurbit[6]uril derivative via host-guest complexation.[243] Its drug release occurred in responsive to green light or NIR irradiation, which was absorbed for heat production by AuNR. Another example for photothermal gating involved isomerization-controlled rotaxane shuttling at the pore entrance. Li et al. reported mesoporous silica-coated AuNR, which was loaded with DOX prior to capping with cis-azobenzene/β-CD rotaxane in its shell layer.[244] This design allowed DOX release under visible irradiation at 543 nm, which was attributed to thermally-induced isomerization to trans-azobenzene due to AuNR photothermal heating. This delivery condition proved effective for *in vivo* DOX delivery in zebrafish embryo. Lastly, another approach for a gating control in pore-loaded MSN involves surface coating with a polymer layer encapsulated with AuNP as demonstrated for rhodamine B release.[245]

HAuNS,[246] a class of nano gold that shows interior cavity-tunable surface plasmon activation, has played an important role in controlled drug release via photothermal gating.[79] Li et al. designed PEG-coated HAuNS which was then loaded with DOX, and demonstrated its controlled DOX release by NIR irradiation at 808 nm.[77] This release was consistent with the induction of photocytotoxicity observed in cell studies using MDA-MB-231 cells.[77] They further developed this photothermal system for the co-delivery of DOX and combretastatin A-4 phosphate for treating hepatocellular carcinoma,[75] and expanded its applications to numerous anticancer therapeutics including paclitaxel,[247] cisplatin,[83] and siRNA.[84]

AuNC, another distinct class of nano gold, also offers capability for photothermal pore gating.[79] Yayz et al. reported DOX-loaded AuNC coated with thermo-sensitive polymer brushes on the surface by which DOX was sterically confined within its internal cavity without premature release.[78] Upon NIR irradiation at 790 nm, its localized heat production caused polymer brush shrinkage that triggered pore opening for DOX release. This release control was consistent with its light-controlled induction of potent cytotoxicity in breast cancer cells in vitro.[79]

Moreover, nanomaterials other than noble element NPs have shown potential utility for drug delivery via photothermal gating. These include Bi_2Se_3 nanosponge[248] and carbon dots,[249] which offer desired features including NIR absorbance, efficient photothermal conversion, or high loading capacity. Lv et al. employed carbon dots in the release control of mesoporous silica-coated UCN nanocapsule, which was co-loaded with DOX and ZnPc for ROS production.[249] Its payloads retained without diffusion until NIR stimulation at 980 nm when pore opening occurred due to heat generation from the activated carbon dot by UCN red luminescence. This nanocapsule proved highly efficacious

in inhibiting tumor growth *in vivo*, which was attributed to synergy by a combination of three therapeutic modalities that comprise of hyperthermia, DOX release, and $^1O_2$.

8.2. Photothermal Disassembly

Liposome Loaded with Photothermal NP. Liposomes constitute one of ideal systems applicable for photothermal disassembly because their membrane rupture is highly susceptible to a temperature elevation. An et al. designed berberine-loaded liposomes which contained AuNP embedded in its lipid bilayer,[250] and demonstrated the drug release in response to visible light irradiation. Geng et al. reported using black phosphorous QD as a photothermal agent embedded in the liposome membrane.[251] This DOX-loaded liposome proved effective in killing breast cancer cells by irradiation at 808 nm.

Polymer Micelle Loaded with NIR Dye. NIR absorbing dyes serve as a useful tool in the design of photothermal disassembly systems. These include cyanine-based dyes such as cypate[252] and indocyanine green.[253, 254] Li et al. designed cypate-encapsulated polymer micelles which were co-loaded with a Pt(IV) prodrug.[252] They showed NIR-induced hyperthermia, which led to its Pt(IV) prodrug release via micelle disassembly. These micelles showed a broad spectrum of cytotoxicity in various cancer cells including cisplatin resistant cells. Indocyanine green plays a similar role in the photothermal induction of drug release in polymer micelles as applied for DOX[253] and Pt agent.[254] Their design involved indocyanine green-encapsulated polymer liposomes co-loaded with DOX[253] or a cisplatin prodrug[254] and under 808 nm irradiation, demonstrated potent inhibition of tumor cell growth *in vitro* and *in vivo*. Such efficacy was attributed to the dual role of indocyanine dye in ROS production and localized hyperthermia responsible for drug release. Besides cyanine dyes, photothermal disassembly was validated using BODIPY for camptothecin delivery under NIR irradiation.[255]

Polymer Micelle Loaded with Photothermal NP. Photothermal systems for disassembly have been more actively studied using nano Au. Takahashi et al. reported AuNR loaded with plasmid DNA on its surface. They showed its DNA release by irradiation at 1064 nm.[256] Using AuNR for photothermal disassembly has further advanced through its surface functionalization with polymers for drug loading. This is effectively applied for DOX delivery using a number of polymers made of PEG-poly(ε-caprolactone),[257] poly(*N*-isopropylacrylamide),[258] and poly(dopamine) (PDA).[259] They showed that irradiation at 808 nm induced a phase transition in the polymer layer, by which DOX was released to kill cancer cells. Alternatively, AuNR is encapsulated in polymer micelles as reported by Song et al. in their design of PLGA micelles co-loaded with reduced graphene oxide (rGO) and DOX.[260] PDA also serves as an effective agent in inducing photothermal disassembly as applied for DOX delivery by Ding et al.[261] In its another application, Zhang et al. designed PDA-coated AuNR loaded with cisplatin in the PDA layer,[259] and further modified by conjugation with c(RGDyC), a targeting ligand for $\alpha_v\beta_3$ integrin tumor biomarker. They demonstrated an NIR-induced antitumor effect by hyperthermia and cisplatin release in $\alpha_v\beta_3$(+) tumors.

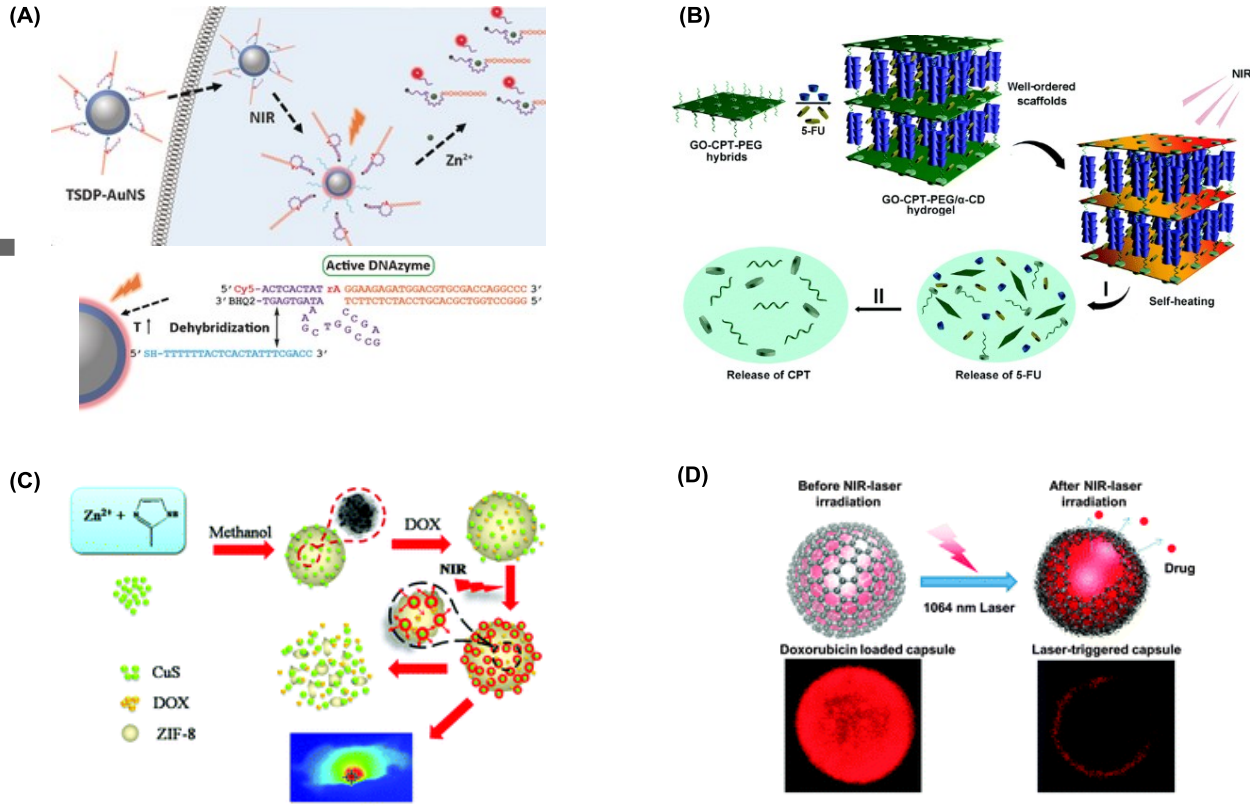

Figure 13. Therapeutic release by photothermal activation. (A) NIR-controlled photothermal release of DNAzyme conjugated to gold nanoshell (AuNS) for Zn ion detection in living cells.[262] Reproduced with permission, Copyright 2017, The Wiley & Sons. (B) GO and α-CD-embedded hydrogel applied for anticancer drug delivery via photothermal gel-sol transition by NIR light.[263] Reproduced with permission, Copyright 2016, Royal Society of Chemistry. (C) CuS-incorporated ZIF-8 MOF for NIR-triggered DOX delivery and photothermal therapy.[264] Reproduced with permission, Copyright 2016, Royal Society of Chemistry. (D) NIR-controlled photothermal rupture of GO microcapsules for DOX delivery.[265] Reproduced with permission, Copyright 2013, Royal Society of Chemistry.

Nano gold structured in non-rod shapes are effectively applied for photothermal disassembly that include Au nanoflower (AuNF),[266] gold nanosphere[267] and Au nanoshell (AuNS).[262] He et al. designed PEG-polystyrene micelle embedded with AuNF,[266] and showed its photothermal activation at 800 nm that enabled to release rhodamine B encapsulated in the polymer layer. Spherical nano gold was also effectively used in the delivery of siRNA oligonucleotides loaded on the surface of gold-coated polymer NP as reported by Jeong et al.[267] Irradiation at 808 nm led to siRNA release in HeLa cells by which its target GFP gene was effectively silenced. In another shape, Wang et al. reported AuNS loaded with DNAzyme precursor via complementary hybridization (**Figure 13A**).[262] Au hyperthermia occurred by irradiation at 808 nm, which enabled its payload release via DNA dehybridization.

Hydrogel Loaded with Photothermal Agent. Use of hydrogel for photothermal disassembly is illustrated with an indocyanine green dye-encapsulated nanogel which was co-encapsulated with

DOX.[268] This nanogel showed a phase transition after NIR irradiation, and its deformation to a sol form enabled to trigger DOX release and thus induced cytotoxicity in 4T1 cells. Photothermal hydrogels are more actively designed using noble element NPs made of Au[269] and Pt.[270] These include an agarose hydrogel loaded with polymer-coated AuNP, which was demonstrated for the photothermal release of bevacizumab, a biologic protein, for its potential ocular delivery.[269] Nano platinum loaded in a hydrogel was also effective for photothermal activation by NIR irradiation, which resulted in hydrogel degradation and release of bortezomib entrapped to kill PC-9 cancer cells.[270]

Besides, use of other photothermal agents such as GO[263] and black phosphorus QD[271] has proved effective in hydrogel-based release control. These include a GO-based hydrogel prepared via non-covalent crosslinking of drug-coated GO and α-CD (**Figure 13B**).[263] This hydrogel enabled co-delivery of two drugs, camptothecin and 5-FU, each loaded on the surface of GO by irradiation at 808 nm. Encapsulation of black phosphorus QD was also effective for photothermal hydrogel disassembly as validated by DOX release at 808 nm.[271] Using a conductive organic polymer constitute another approach for photothermal hydrogel disassembly. Sun et al. reported a DOX-loaded hydrogel prepared with thiophene-incorporated conductive polymer. This hydrogel showed ability for photothermal activation, DOX release and ROS production at 915 nm.[272] Its triple modes of action was consistent with the induction of high antitumor efficacy observed in tumor grafted mice.

Porous Nanomaterial Loaded with Photothermal NP. While using mesoporous silica nanomaterials has played a prominent role in the gating control, it is also being explored in the design of photothermal disassembly systems. Li et al. designed nano Au-encapsulated $mSiO_2$ which was then used for loading dsDNA oligonucleotides on its porous surface.[273] This nanomaterial enabled NIR-triggered DNA release through photothermal detachment, which was attributed to an elevated temperature on the surface by heat produced from nano Au. Besides nano Au, $mSiO_2$ disassembly allows integration with other photothermal agents such as iron oxide (Fe_3O_4) nanoparticle (IONP)[274] and perylene diimide.[275] Lu et al. reported a silica nanocapsule loaded with DOX and IONP in its hollow cavity.[274] The encapsulated IONP enabled heat production through magnetic field induction, which contributed to nanocapsule disassembly for drug release. Yang et al. reported a mesoporous organosilica nanocontainer loaded with SN38 and perylene diimide in its cavity.[275] NIR irradiation led to its shell deformation, which contributed to drug release in the tumor.

MOF-based nanocontainers also show growing potential in the design of photothermal disassembly systems. Wang et al. reported DOX-loaded ZIF-8 MOF, which was prepared by incorporating nano CuS as a photothermal agent into its lattice (**Figure 13C**).[264] Irradiation at 980 nm led to MOF disintegration, which was positively correlated with the induction of cytotoxicity in MCF-7 cells. Lastly, microscale capsules can serve as the delivery container for photothermal disassembly. Kurapati et al. reported dextran sulfate-doped microcapsules loaded with DOX and modified with GO sheet on the surface (**Figure 13D**).[265] Following irradiation at 1064 nm, these microcapsules ruptured due to photothermal heating by GO, which contributed to DOX release.

Photothermal Disassembly for Antibacterial Agent Release. Photothermal nanomaterials are effective in killing bacteria by NIR-induced hyperthermia as studied with nano Au,[276] nano Cu,[277] CuS[278] and rGO.[279] Such hyperthermia can engage in photothermal disassembly for drug release. This is illustrated with the photothermal delivery of vancomycin, a glycopeptide class of antibiotics effective for treating Gram (+) bacterial infections.[280, 281] Wang et al. reported that AuNP immobilized with vancomycin on its surface showed induction of a potent bactericidal activity against

drug-resistant bacteria at 808 nm.[282] This effect was attributed to multiple modes of action that comprise of cell wall-specific adsorption guided by vancomycin, AuNP hyperthermia and hyperthermia-induced vancomycin release. Chitosan also contributes in bacteria-targeted delivery due to its binding affinity to lipopolysaccharides and teichoic acids present in the bacterial cell wall.[283, 284] Thus the chitosan-immobilized AuNR[283, 285] was designed for the photothermal delivery of daptomycin.[283] This drug-loaded AuNR displayed ability for specific accumulation in an infection site, and following irradiation at 808 nm, it induced a potent bactericidal activity due to hyperthermia-induced drug release.[283] Using an antibody raised against a specific cell wall component constitutes another promising approach for bacteria-targeted delivery as reported by Meeker et al.[286] They designed Au nanocage immobilized with an anti-staphylococcal protein A antibody and demonstrated a dual capability for targeting and photothermal drug release as applied to various antibiotic agents including daptomycin, vancomycin or gentamycin.

Using polymer-based photothermal agents is effective in the control of antibacterial disassembly as investigated with PDA[284] and poly(pyrrole).[287] This involves a PDA/glycolchitosan hydrogel encapsulated with ciprofloxacin.[284] This chitosan-targeted hydrogel showed a potent antibacterial efficacy against *S. aureus* in a mouse infection model at 808 nm.[284] Poly(pyrrole) plays a similar role in photothermal disassembly as employed in a hollow microsphere co-encapsulated with vancomycin.[287] This drug-loaded microsphere showed a faster vancomycin release, which occurred at 808 nm due to hyperthermia-enhanced shell porosity, and it proved high bactericidal efficacy in abscesses.

In section summary, photothermal activation constitutes a core strategy that has been employed in various release systems via gating and disassembly. A variety of photothermal agents have been explored for this purpose that include NIR dyes,[252-254] nano Au,[70, 92, 288] HAuNS,[75, 79] [83, 84, 247] AuNC,[78, 79] carbon dots,[249] black phosphorous QD,[251] and conductive polymers,[284, 287] each responsive to Vis–NIR stimulation (500–1000 nm). Application of this photothermal strategy has resulted in promising results in the area of anticancer and antibacterial therapy as summarized in **Table 4**.

Table 4. Therapeutic release via photothermal activation

Release Mode	Nano Delivery System	Photothermal Agent (Light, nm)	Payload	Ref
Gating	AuNR@$mSiO_2$	Au (NIR)	Naproxen	[243]
	$mSiO_2$@Au	Au (808)	Ibuprofen	[242]
	AuNR@$mSiO_2$	Au (543)	DOX	[244]
	UCN@$mSiO_2$	Carbon dot (980)	DOX, ZnPc	[249]
	HAuNS	Au (808)	DOX, combretastatin A-4 phosphate, paclitaxel,	[75, 79] [83, 84, 247]

			cisplatin, siRNA	
	AuNC	Au (808)	DOX	[78, 79]
Disassembly	Liposome	AuNP (Vis)	Berberine	[250]
	Liposome	Black phosphorous (808)	DOX	[251]
	Polymer micelle	Cypate (NIR)	Pt (IV) prodrug	[252]
	Polymer micelle	Indocyanine (808)	Cisplatin	[254]
	Polymer micelle	Indocyanine (808)	DOX	[253]
	Polymer micelle	AuNR (808)	DOX	[257, 258]
	Polymer micelle	AuNR, GO (808)	DOX	[260]
	Polymer micelle	PDA (808)	DOX, NO	[261]
	Polymer micelle	BODIPY (NIR)	Camptothecin	[255]
	PDA-RGD	AuNR, PDA (NIR)	Cisplatin	[259]
	Polymer micelle	AuNF (800)	Rhodamine	[266]
	Polymer micelle	Au (808)	siRNA (GFP)	[267]
	AuNR@dsDNA	AuNR (1064)	Plasmid DNA	[256]
	AuNS@Oligo	Au (808)	DNAzyme	[262]
	Hydrogel	Indocyanine Green (NIR)	DOX	[268]
	Hydrogel	AuNP (NIR)	Bevacizumab	[269]
	Hydrogel	Pt@Dendrimer (NIR)	Bortezomib	[270]
	Hydrogel	GO (808)	Camptothecin, 5-FU	[263]
	Hydrogel	Black phosphorous (808)	DOX	[271]
	Hydrogel	Thiophene polymer (915)	DOX	[272]
	Hydrogel-Chitosan	Poly(dopamine) (808)	Ciprofloxacin	[284]

	Microsphere	Poly(pyrrole) (808)	Vancomycin	[287]
	Silica nanocapsule	Fe_3O_4 (NIR)	DOX	[274]
	Silica nanocapsule	AuNP (NIR)	Rhodamine	[245]
	$mSiO_2$@Au	Au (NIR)	dsDNA	[273]
	Organosilica NP	Perylene diimide (NIR)	SN38	[275]
	ZIF-8 MOF	CuS (980)	DOX	[264]
	$CacO_3$ microcapsule	GO (1064)	DOX	[265]
	AuNP@Vancomycin	Au (808)	Vancomycin	[282]
	AuNR@Chitosan	Au (808)	Daptomycin	[283, 285]
	Au nanocage@Antibody	Au (NIR)	Daptomycin, Vancomycin	[286]

9. Therapeutic Release via Photodynamic Activation

9.1. Photodynamic Delivery for Anticancer Therapeutics

Oxidative Linker Cleavage. ROS is associated with a high chemical reactivity that makes it engage in linker cleavage for payload release. The linkers known to be susceptible for ROS cleavage comprise of catechol,[289] bis(alkylthio)ethene,[159] thioether[290] and boronate.[291] They engage in ROS-mediated release as illustrated with nano TiO_2 chelated with 3,4-dihydroxybenzoic acid, which served as a linker for hemoglobin attachment.[289] This nano TiO_2 was able to release the protein in response to visible irradiation at >420 nm. Its release was attributed to Ti–catechol bond cleavage that occurred due to photoinduced electron transfer from TiO_2 or by phenol oxidation reaction with TiO_2-produced $^1O_2$. The ROS-mediated linker cleavage occurs more frequently via sulfide oxidation. Lee et al. employed $^1O_2$-sensitive bis(alkylthio)ethene linker for payload (naphthalene dye) conjugation to the surface of MSN which was pre-encapsulated with ZnPc within its pores (**Figure 14A**).[159] Visible irradiation at 525 nm led to the dye release, which was attributed to $^1O_2$-triggered linker fragmentation. Pei et al. applied this release approach for lipid vesicles loaded with a paclitaxel homodimer tethered through thioether along with tetraphenylchlorin photosensitizer.[290] Light irradiation enabled these vesicles to produce $^1O_2$ that contributed to paclitaxel monomer release. Lastly, another ROS-responsive release involved a catechol–boronate linkage which was used for attaching anticancer bortezomib to crosslinked poly(dopamine) polymers.[291] Irradiation at 635 nm enabled $^1O_2$ production which contributed to the drug release through oxidative cleavage at its boronate linkage.

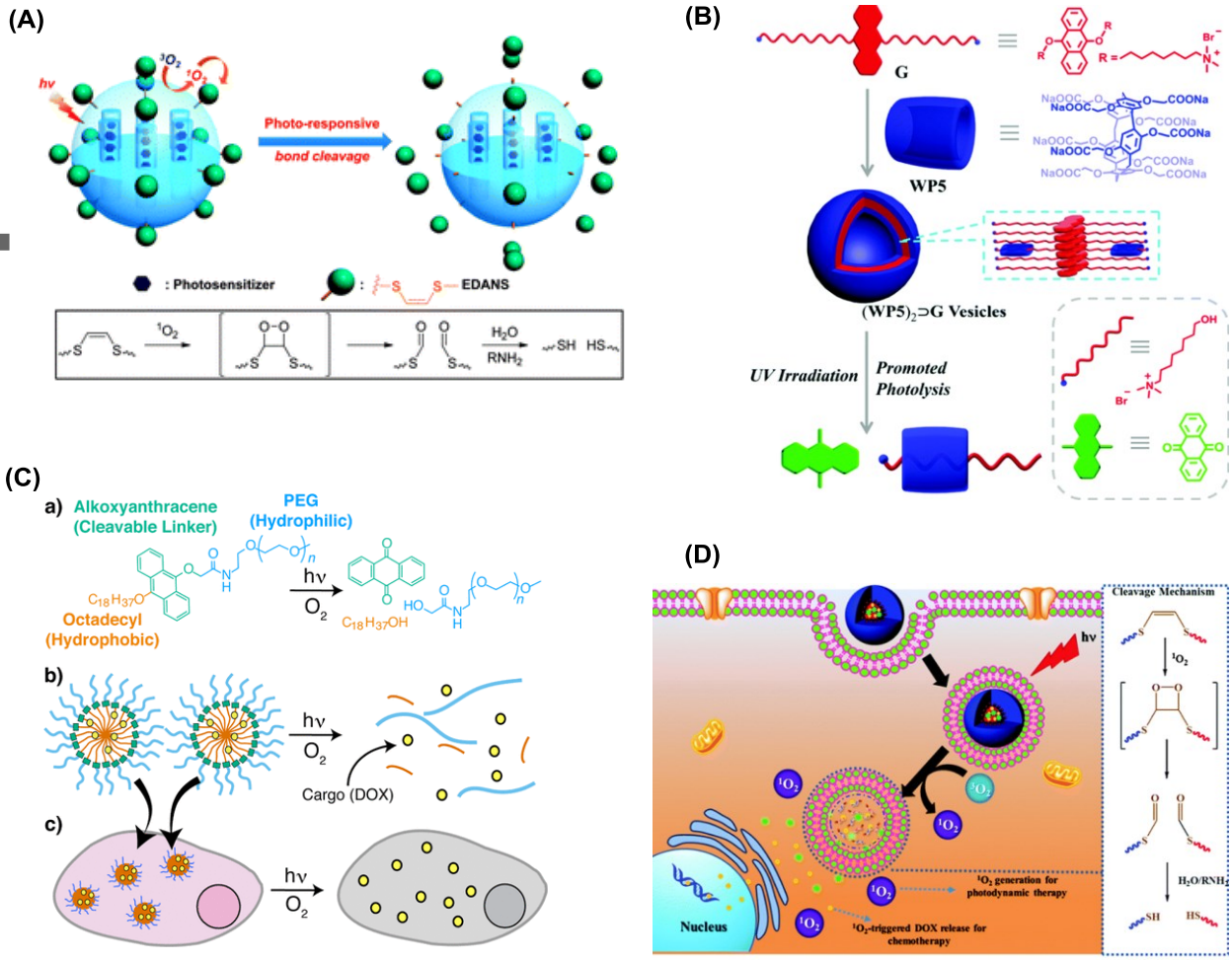

Figure 14. Therapeutic release systems by $^1O_2$-mediated photodynamic activation. (A) Gating control in MSN via bis(alkylthio)ethene linker fragmentation by $^1O_2$ produced by encapsulated ZnPc.[159] Reproduced with permission, Copyright 2013, Royal Society of Chemistry. (B) Disassembly of 9,10-dialkoxyanthracene-based supramolecular vesicles triggered by encapsulated eosin Y.[117] Reproduced with permission, Copyright 2016, Royal Society of Chemistry. (C) Disassembly of 9,10-dialkoxyanthracene-based polymer micelles designed for DOX release.[32] Reproduced with permission, Copyright 2019, American Chemical Society. (D) Disassembly of Ce6 and DOX co-loaded micelles via visible light-triggered $^1O_2$ production for chemo and photodynamic therapy.[115] Reproduced with permission, Copyright 2015, Royal Society of Chemistry.

Oxidative Disassembly. Due to its short half-life, ROS restricts the scope of its oxidative fragmentation to nearby molecules and objects at a close proximity. These include nanocontainers that engage in its production such as PS-encapsulated liposomes[292] and polymer micelles.[32, 117] Wang et al. demonstrated this approach using tetraphenylporphyrin PS-loaded liposomes incorporated with 7-dehydrocholesterol, an ROS-reactive cholesterol precursor.[292] Irradiation at 420 nm produced $^1O_2$ which contributed to vesicle fragmentation and release of cytotoxic endoperoxides derived from its reactions with 7-dehydrocholesterol. In another system, ROS-

mediated disassembly occurred in polymer micelles composed of 9,10-dialkoxyanthracene-based amphiphilic molecules as reported by Guo et al. (**Figure 14B**).[117] Irradiation at 525 nm of these micelles which were encapsulated with eosin Y and anticancer mitoxantrone resulted in the drug release via disassembly. Brega et al. further defined the role of the alkoxyanthracene linkage in the disassembly of DOX-loaded polymer micelles (**Figure 14C**).[32]

A drug linkage based on sulfur[115, 116, 293] or selenium[294] displays sufficient ROS reactivity for facile oxidation. This is illustrated with thioether polymer micelles loaded with PS such as chlorin e6 (Ce6) [115, 116] and PPIX,[293] each applied in a delivery system for DOX[115, 116] or SN38.[293] Their irradiation at visible light (660 or 635 nm) resulted in drug release through self-fragmentation, as illustrated by thioether reaction with $^1O_2$ produced from Ce6 (**Figure 14D**).[115] Like sulfur in the chalogen family, selenium is also reactive to $^1O_2$, and applicable in ROS-mediated disassembly. Pan et al. designed porphyrin-loaded micelles made of di-selenide lipids.[294] These micelles showed degradation under visible irradiation at 400 nm, leading to the release of selenium byproducts which accounted for the induction of cytotoxicity in A549 cancer cells.

NIR Responsive Oxidative Disassembly. NIR irradiation is applicable in ROS production for photodynamic disassembly. Ji et al. explored this approach using an NIR-responsive indocyanine dye which has ability for producing singlet oxygen.[295] They prepared $\alpha_v\beta_3$ integrin-targeted polymer NP conjugated with camptothecin through the indocyanine. Following its irradiation at 660 nm, it showed a decrease in particle size due to its oxidative fragmentation, which contributed to drug release.

9.2. Photodynamic Delivery for Antibacterial Therapeutics

Non-targeted ROS Disassembly. ROS confers a broad spectrum of cytotoxicity against Gram(+) and Gram(−) pathogens due to its general ability for inducing membrane ruptures in bacterial pathogens.[296-298] Several types of PS molecules have proven effective in ROS production for antibacterial efficacy. These comprise of toluidine blue,[299] curcumin,[300] RB,[64, 86] PPIX,[98, 142] and ZnPc.[301] Despite such critical function, these PS molecules have poor solubility and tend to aggregate in water. Therefore, PS delivery using a nanocarrier should be beneficial as it allows to reduce their aggregation and induce more bacterial uptake than free PS. These benefits are illustrated by ROS-mediated disassembly of toluidine blue encapsulated in lipid NP,[299] RB conjugated to an exopolysaccharide nanocarrier,[302] or curcumin encapsulated in poly(lactic acid) NP.[300] Visible irradiation of these PS-loaded nanocarriers resulted in induction of potent bactericidal activity against *E. coli* or *S. aureus*.

Bacteria-targeted ROS Disassembly. Targeted ROS delivery to bacterial cells is achieved using a system with a targeting capability through its specific recognition and adherence on the cell surface. This is illustrated with poly(fluorine-benzothiadiazole) conductive polymer conjugated with a targeting ligand such as vancomycin for Gram(+) cells or PMB for Gram(−) cells.[303] In this system, the polymer backbone itself serves as PS for ROS production.[303] This polymer showed a potent bactericidal activity against bacterial cells *S. aureus* and *P. aeruginosa*, which was induced only under white light irradiation. This bacteria-targeted delivery was also achieved using an antimicrobial peptide (YVLWKRKRKFCFI) which has a high affinity to lipopolysaccharides. Thus, PPIX conjugated to this peptide showed a greater antibacterial activity against Gram(−) pathogens compared to PPIX alone.[304]

ROS Disassembly by Upconversion Luminescence. PS integration in UCN enables NIR-triggered ROS production and disassembly.[64, 86, 305-307] This approach involves UCN coated with a polymer layer made of poly(ethyleneimine),[308] poly(vinylpyrrolidone)[301] or *N*-octyl chitosan,[309] and loaded PS such as curcumin[308] or ZnPc[301, 309] in its polymer shell layer. NIR irradiation at 980 nm led to $^1O_2$ production, which was attributed to PS excitation and release by UCN luminescence (432 nm). Such ROS delivery accounted for potent antibacterial activity observed against multidrug-resistant bacterial pathogens *in vitro* and *in vivo* infection models.

Min et al. reported another approach for PS loading using UCN@mSiO_2 for RB encapsulation in its porous shell layer.[64, 86] At 980 nm irradiation, the RB-loaded UCN core emitted luminescence at 540 nm, which was effectively transferred for RB activation for ROS production and disassembly. This accounted for a potent antibacterial activity against MRSA and extended spectrum beta-lactamase-producing *E. coli*. In a continuing work, they designed a hollow yolk-shell UCN loaded with two PS types, RB embedded in its porous silica shell and hematoporphyrin methyl ether encapsulated in its yolk cavity.[64] Its luminescence enabled $^1O_2$ production through UCN-loaded PS activation, which led to effective killing of bacteria including antibiotic-resistant MRSA and lactamase-producing *E. coli*. This ROS disassembly system has further advanced to release an antibacterial agent as reported by Xu et al.[310] They designed Au/TiO_2-coated UCN which was then loaded with ampicillin in its shell layer. Its NIR excitation resulted in both ROS production and drug release which enabled to kill ampicillin-resistant bacteria strains.

In section summary, photodynamic activation involves ROS production catalyzed by photosensitizers or photoactive NPs. It constitutes another core strategy that plays a critical role in PDT and drug delivery.[28, 34] Its applications have been explored in various ways in which payload release could be induced via linker oxidation, oxidative gating, or disassembly. Photodynamic activation has made a significant impact on expanding the scope in anticancer and antibacterial delivery systems as summarized in **Table 5**.

Table 5. Therapeutic release via photodynamic activation

Release Mode	Delivery System (ROS reactive spacer)	Photoactivation Species (Light, nm)	Payload (ROS reactive linker)	Ref
Linker Cleavage	nano TiO_2	TiO_2 (420)	Hemoglobin (Dihydroxybenzoate)	[289]
	MSN (Alkylthioethene)	ZnPc (525)	Naphthalene dye	[159]
	Liposome	Tetraphenylchlorin	Paclitaxel (Thioether)	[290]
	Crosslinked polymer	Poly(dopamine) (635)	Bortezomib (Catechol–boronate)	[291]
Disassembly	Liposome (Dehydrocholesterol)	Tetraphenylporphyrin (420)	Dehydrocholesterol endoperoxide	[292]
	Polymer micelle (Alkoxyanthracene)	Eosin Y (525)	Mitoxantrone	[117]

	Polymer micelle (Alkoxyanthracene)	Anthracene (365)	DOX	[32]
	Polymer micelle (Thioether)	Ce6 (660)	DOX	[115]
	Polymer micelle (Propylene sulfide)	Chlorin e6 (670)	DOX	[116]
	Polymer micelle	PPIX (635)	SN38 (Thioether)	[293]
	Polymer micelle	Porphyrin (400)	Se (Di-selenide)	[294]
	Polymer micelle	Poly(fluorine-benzothiadiazole) (Vis)	Vancomycin, PMB	[303]
	RGD-Targeted polymer micelle	Indocyanine (660)	Camptothecin	[295]
	UCN@PEI	Curcumin (432; 980)	Curcumin	[308]
	UCN@mSiO$_2$	UCN (980); RB (540)	RB	[64, 86]
	UCN Yolk-Shell	UCN (980); RB, hematoporphyrin (540)	RB, hematoporphyrin	[64]
	UCN@Au/TiO$_2$	UCN (980); TiO$_2$ (NIR)	Ampicillin	[310]
	UCN@Poly(vinylpyrrolidone)	UCN (980); ZnPc	ZnPc	[301]
	UCN@Chitosan	UCN (980); ZnPc	ZnPc	[309]

10. Conclusions and Perspectives

Photoactivation allows therapeutic delivery to occur in an actively controlled manner within spatially well-defined cells and tissues only. It opens a novel route for a non-invasive, spatiotemporal control of drug activation.[11] This strategy has been applied in numerous therapeutic areas including cancers and infectious diseases, and it has made a significant impact on rapid advances in the field of delivery applications as reviewed here and elsewhere.[11, 13, 15, 42] However, despite such promising results and potential, its further development faces numerous technical issues and challenges that pertain to intrinsic light properties, its synthetic methods and its integration with an active targeting strategy among others. These aspects are addressed briefly with a focus on light limitations, drug conjugation methods, multivalent ligand design,[5, 8] and potential in clinical translation.

Light Limitation. Lights used in photoactivation strategies comprise of UV, Vis and NIR, each offering a different set of properties in phototoxicity, molecular absorptivity, tissue scattering and penetration.[311] Identifying an optimal light is critical in the successful application of photoactivation systems. Irradiation at short wavelength UV (UVC) is reported to cause DNA damages and considered cytotoxic.[312] However, irradiation in longer UV (medium, long wavelength), visible and

NIR range is generally well tolerable or non-toxic in mammalian cells[23, 169, 172] Light absorptivity varies to a significant extent dependent on photocleavable linker types, PS molecules and photoactive NPs used. Long wavelength UV light better enables linker photolysis for drug release[11] than visible light which shows only limited effectiveness via one or two-photon absorption.[11, 124, 127] However, visible light better fits in photodynamic activation because of its stronger absorption by most PS molecules or NPs.[70, 92, 313] It also shows lower light scattering than UV as the extent of light scattering varies inversely proportional to the square of light wavelength.[314] Both UV and visible light shows lower degree of penetration with 100 μm (350–400 nm) and 150–750 μm (450–700 nm)[315, 316] compared to NIR light that penetrates as deep as 1200–2200 μm (800–1200 nm).[316] However, despite its high tissue penetrability,[317-319] NIR irradiation carries a much lower energy, and its direct use for photoactivation is limited only to a few NPs including UCNs (808 nm, 980 nm).[86, 98, 104, 110, 142, 320, 321] UCNs offer needed ability for UV–vis upconversion luminescence by NIR excitation,[89, 101, 102, 104-106, 320] and they have shown growing opportunities in the development of NIR-triggered release systems.[89, 104, 320]

Synthetic Method. Drug conjugation methods developed for photoactivation strategies largely rely on covalent drug-nanocarrier conjugation through a photocleavable linker. Numerous types of drug molecules have been successfully applied for such conjugation through amide,[19, 81] carbamate,[169] ester,[126, 140] triazole via azide-alkyne click chemistry,[170] amine via *N*-alkylation,[172] and gold-thiol chemisorption.[140] However, despite such broad applicability, most of existing methods are still challenging to use because they require a multi-step, divergent process. Recently, this has drawn growing attention as illustrated with new synthetic approaches. Wong et al. addressed this issue by developing a TNB linker[126] which provides important benefits such as synthetic convenience (one step), multi-gram synthesis, and dual caging arms.[169] They validated its synthetic convenience and capability in the photocontrolled delivery of DOX conjugated in PAMAM dendrimer. Dcona et al. employed a non-covalent approach in lieu of a stable covalent bond.[171] They demonstrated the feasibility of using electrostatic complexation in the loading of ONB-caged DOX on the UCN surface.[171] Lastly, conjugation via azide-alkyne click chemistry[170] offers a unique benefit by providing an orthogonal approach that can occur under biological conditions even in the presence of interfering functional moieties such as amines and carboxylic acids.[170, 171, 182]

Active Targeting Strategy. The precision and efficiency in drug delivery can be greatly improved by combining the photoactivated strategy with the active targeting strategy. The latter is achieved by conjugating a nanocarrier with a targeting ligand, aptamer or antibody to a tumor or bacterial biomarker.[5, 7, 8] Of these, the multivalent ligand approach has proven effective in improving targeting specificity in a range of delivery systems.[5, 7, 8] However, this ligand targeted approach has been applied only to a limited extent in a few photoactivation systems. As reviewed here, these include ligand conjugation with folate,[23, 24, 83, 142, 169, 182, 228] cyclic RGD[41, 259] anti-EGFR antibody,[74] or aptamer[76, 211] in tumor-targeted systems, and ligand conjugation with polymyxin,[172, 303] chitosan,[283] an amphiphilic peptide[304] or antibody[286] in bacteria-targeted systems. Integration of the two strategies, active ligand targeting and photoactivation delivery, remains unexplored in most other biomarkers in cancers. Besides FAR[9, 322, 323] and $\alpha_v\beta_3$ integrin receptor,[324-326] each reported here, there are other promising biomarkers applicable such as prostate-specific membrane antigen receptor,[327] Her2,[328] riboflavin receptor,[329, 330] and transferrin receptor.[10] Given recent advances in new synthetic methods on ligand conjugation, it would be increasingly feasible to integrate these two complementary strategies in a single delivery system. Their integration would offer greater potential for improved safety and efficacy than either strategy alone.

Prospect in Clinical Translation. Photoactivated nanotherapeutic agents developed for clinical therapies are mostly at an early stage[46, 331] except verteporfin liposome (Visudyne®), the PDT prototype approved for age-related macular degeneration and further evaluated for locally advanced pancreatic cancer (phase 2).[331, 332] Their future development can be considerably facilitated using insights from developed nanotherapeutics and light therapies practiced in clinics. First, numerous types of nanotherapeutic formulations have been approved or advanced to clinical stages, in particular, in cancers.[333] These include PEGylated liposome encapsulated with DOX (Doxil®),[334] heat-sensitive liposome loaded with DOX (ThermoDox®),[335] PLGA nanoparticles encapsulated with leuprolide (Eligard®),[336] albumin nanoparticles bound with paclitaxel (Abraxane®),[337] polyglutamate conjugated with paclitaxel (Opaxio®),[338] and liposomes encapsulated with mifamurtide (Mepact®),[339] vincristine (Marqibo®),[340] or irinotecan (Onivyde®).[341] However, in spite of such success, the progression rates of nanotherapeutic candidates toward regulatory approval show significant drops at the efficacy stage as supported with phase 2 (48%) and phase 3 (14%) compared to phase 1 (94%).[333] This is clearly indicative of poor or lack of efficacy rather than toxicity, which could be attributable to targeting and release control issues. Therefore, it would be possible to improve outcomes in efficacy through actively controlled photoactivation in targeted tissues only.

Second, light therapies find more opportunities in topical and superficial applications than systemic ones. This is illustrated with nanoemulsion-based 5-aminolevulinic acid (BF-200),[342] a topical agent being investigated for treating superficial basal cell carcinomas such as actinic keratosis (phase 3) with laser irradiation at 632 nm.[343] Besides, recent advances in fiber optics technology enable to induce photoactivation in deeper tissues. For example, verteporfin was photoactivated for PDT within solid pancreatic tumors by light delivered through a diffusing optical catheter placed through a needle into the tumor tissue (phase 2).[332] In summary, clinical prospect of photoactivated nanotherapeutics is growing conceivably in a range of therapeutic indications from anticancer treatments to antimicrobial procedures.

Acknowledgement. The author acknowledges support for cited works in part by the British Council and Department for Business Innovation & Skills through the Global Innovation Initiative (GII 207).

Conflicts of Interest. The author declares no competing financial interest.

Keywords: Therapeutic Release, Linker Photolysis, Photoiosmerization, Photothermal Activation, Photodynamic Reaction, Upconversion Luminescence

Abbreviations

AgNP	Ag (Silver) Nanoparticle
AuNC	Au (Gold) Nanocage
AuNF	Au Nanoflower
AuNP	Au Nanoparticle
AuNR	Au Nanorod
AuNS	Au Nanoshell
BODIPY	Boron-Dipyrromethene
CD	Cyclodextrin
CO	Carbon Monoxide
DAPI	4′,6-Diamidino-2-phenylindole
DASA	Donor–Acceptor Stenhouse Adduct

DOX	Doxorubicin
FA	Folic Acid
FAR	Folic Acid Receptor
5-FU	5-Fluorouracil
G5	Generation 5
GFP	Green Fluorescent Protein
GO	Graphene Oxide
HA	Hyaluronic Acid
HAuNS	Hollow Au Nanosphere
IONP	Iron Oxide (Fe_3O_4) Nanoparticle
MRI	Magnetic Resonance Imaging
$mSiO_2$	Mesoporous Silica Oxide
MOF	Metal-Organic Framework
MRSA	Methicillin-Resistant *S. aureus*
MSN	Mesoporous Silica Nanoparticle
MTX	Methotrexate
NIR	Near Infrared
NO	Nitrogen Oxide
NP	Nanoparticle
ONB	*Ortho*-Nitrobenzene
PAMAM	Poly(amidoamine)
PDA	Poly(dopamine)
PDT	Photodynamic Therapy
PEG	Polyetheleneglycol
PLGA	Poly(Lactic-co-Glycolic Acid)
PMB	Polymyxin B
PPIX	Protoporphyrin IX
PS	Photosensitizer
PTT	Photothermal Therapy
QD	Quantum Dot
RB	Rose Bengal
rGO	Reduced Graphene Oxide
ROS	Reactive Oxygen Species
TNB	Thioacetal *ortho*-Nitrobenzene
UCN	Upconversion Nanocrystal
UVA	Long Wavelength UV
UV–Vis	Ultraviolet Visible
ZnPc	Zinc Phthalocyanine

References

[1] Y. Lu, P. S. Low, *Adv. Drug Delivery Rev.* **2002**, *54*, 675–693.

[2] A. K. Patri, J. F. Kukowska-Latallo, J. R. Baker Jr, *Adv. Drug Delivery Rev.* **2005**, *57*, 2203–2214.

[3] N. Kamaly, Z. Xiao, P. M. Valencia, A. F. Radovic-Moreno, O. C. Farokhzad, *Chem. Soc. Rev.* **2012**, *41*, 2971–3010.

[4] H. Maeda, *Adv. Enzyme Regul.* **2001**, *41*, 189–207.

[5] M. Mammen, S. K. Choi, G. M. Whitesides, *Angew. Chem., Int. Ed.* **1998**, *37*, 2754–2794.

[6] P. S. Low, W. A. Henne, D. D. Doorneweerd, *Acc. Chem. Res.* **2008**, *41*, 120–129.

[7] S. Bhatia, L. C. Camacho, R. Haag, *J. Am. Chem. Soc.* **2016**, *138*, 8654–8666.

[8] L. L. Kiessling, J. E. Gestwicki, L. E. Strong, *Angew. Chem., Int. Ed.* **2006**, *45*, 2348–2368.

[9] P. S. Low, S. A. Kularatne, *Curr. Opin. Chem. Biol.* **2009**, *13*, 256–262.

[10] Z. M. Qian, H. Li, H. Sun, K. Ho, *Pharmacol. Rev.* **2002**, *54*, 561–587.

[11] P. T. Wong, S. K. Choi, *Chem. Rev. (Washington, DC, U. S.)* **2015**, *115*, 3388–3432.

[12] J. Zhuang, M. R. Gordon, J. Ventura, L. Li, S. Thayumanavan, *Chem. Soc. Rev.* **2013**, *42*, 7421–7435.

[13] R. Tong, D. S. Kohane, *Wiley Interdiscip. Rev.: Nanomed. Nanobiotechnol.* **2012**, *4*, 638–662.

[14] N. Fomina, J. Sankaranarayanan, A. Almutairi, *Adv. Drug Delivery Rev.* **2012**, *64*, 1005–1020.

[15] C. Englert, I. Nischang, C. Bader, P. Borchers, J. Alex, M. Pröhl, M. Hentschel, M. Hartlieb, A. Traeger, G. Pohnert, S. Schubert, M. Gottschaldt, U. S. Schubert, *Angew. Chem., Int. Ed.* **2018**, *57*, 2479–2482.

[16] Y. Liu, P. Bhattarai, Z. Dai, X. Chen, *Chem. Soc. Rev.* **2019**, *48*, 2053–2108.

[17] C. Brieke, F. Rohrbach, A. Gottschalk, G. Mayer, A. Heckel, *Angew. Chem., Int. Ed.* **2012**, *51*, 8446–8476.

[18] P. Rai, S. Mallidi, X. Zheng, R. Rahmanzadeh, Y. Mir, S. Elrington, A. Khurshid, T. Hasan, *Adv. Drug Delivery Rev.* **2010**, *62*, 1094–1124.

[19] J. P. Celli, B. Q. Spring, I. Rizvi, C. L. Evans, K. S. Samkoe, S. Verma, B. W. Pogue, T. Hasan, *Chem. Rev. (Washington, DC, U. S.)* **2010**, *110*, 2795–2838.

[20] J. H. Kaplan, B. Forbush, J. F. Hoffman, *Biochemistry* **1978**, *17*, 1929–1935.

[21] A. P. Billington, K. M. Walstrom, D. Ramesh, A. P. Guzikowski, B. K. Carpenter, G. P. Hess, *Biochemistry* **1992**, *31*, 5500–5507.

[22] P. Klán, T. Šolomek, C. G. Bochet, A. Blanc, R. Givens, M. Rubina, V. Popik, A. Kostikov, J. Wirz, *Chem. Rev. (Washington, DC, U. S.)* **2013**, *113*, 119–191.

[23] S. K. Choi, T. Thomas, M. Li, A. Kotlyar, A. Desai, J. R. Baker Jr, *Chem. Commun. (Cambridge, U. K.)* **2010**, *46*, 2632–2634.

[24] S. K. Choi, T. P. Thomas, M.-H. Li, A. Desai, A. Kotlyar, J. R. Baker, *Photochem. Photobiol. Sci.* **2012**, *11*, 653–660.

[25] M. M. Lerch, M. J. Hansen, G. M. van Dam, W. Szymanski, B. L. Feringa, *Angew. Chem., Int. Ed.* **2016**, *55*, 10978–10999.

[26] M. Wegener, M. J. Hansen, A. J. M. Driessen, W. Szymanski, B. L. Feringa, *J. Am. Chem. Soc.* **2017**, *139*, 17979–17986.

[27] Y. Huang, R. Dong, X. Zhu, D. Yan, *Soft Matter* **2014**, *10*, 6121–6138.

[28] W. Wu, X. Shao, J. Zhao, M. Wu, *Adv. Sci. (Weinheim, Ger.)* **2017**, *4*, 1700113.

[29] S. K. Choi, *NanoImpact* **2016**, *3-4*, 81–89.

[30] Q. Mu, G. Jiang, L. Chen, H. Zhou, D. Fourches, A. Tropsha, B. Yan, *Chem. Rev. (Washington, DC, U. S.)* **2014**, *114*, 7740–7781.

[31] C. C. Winterbourn, *Nat. Chem. Biol.* **2008**, *4*, 278–286.

[32] V. Brega, F. Scaletti, X. Zhang, L.-S. Wang, P. Li, Q. Xu, V. M. Rotello, S. W. Thomas, *ACS Appl. Mater. Interfaces* **2019**, *11*, 2814–2820.

[33] N. Nishiyama, Y. Morimoto, W.-D. Jang, K. Kataoka, *Adv. Drug Delivery Rev.* **2009**, *61*, 327–338.

[34] S. S. Lucky, K. C. Soo, Y. Zhang, *Chem. Rev. (Washington, DC, U. S.)* **2015**, *115*, 1990–2042.

[35] A. Moussaron, Z. Youssef, A. Ben-Mihoub, R. Vanderesse, C. Frochot, S. Acherar, in *Photonanotechnology for Therapeutics and Imaging* (Ed.: S. K. Choi), Elsevier, **2020**, pp. 105–146.

[36] L. Vigderman, E. R. Zubarev, *Adv. Drug Delivery Rev.* **2013**, *65*, 663–676.

[37] Y. Chen, C. Tan, H. Zhang, L. Wang, *Chem. Soc. Rev.* **2015**, *44*, 2681–2701.

[38] Y. Shi, M. Liu, F. Deng, G. Zeng, Q. Wan, X. Zhang, Y. Wei, *J. Mater. Chem. B* **2017**, *5*, 194–206.

[39] X. Wu, C.-M. Dong, in *Photonanotechnology for Therapeutics and Imaging* (Ed.: S. K. Choi), Elsevier, **2020**, pp. 83–104.

[40] C. Zhang, D. Li, X. Shi, in *Photonanotechnology for Therapeutics and Imaging* (Ed.: S. K. Choi), Elsevier, **2020**, pp. 23–43.

[41] W. Lu, M. P. Melancon, C. Xiong, Q. Huang, A. Elliott, S. Song, R. Zhang, L. G. Flores, J. G. Gelovani, L. V. Wang, G. Ku, R. J. Stafford, C. Li, *Cancer Res.* **2011**, *71*, 6116–6121.

[42] J. M. Silva, E. Silva, R. L. Reis, *J. Controlled Release* **2019**, *298*, 154–176.

[43] T. Dvir, M. R. Banghart, B. P. Timko, R. Langer, D. S. Kohane, *Nano Lett.* **2010**, *10*, 250–254.

[44] B. P. Timko, T. Dvir, D. S. Kohane, *Adv. Mater.* **2010**, *22*, 4925–4943.

[45] Q. Liu, C. Zhan, D. S. Kohane, *Bioconjugate Chem.* **2017**, *28*, 98–104.

[46] M. Karimi, P. Sahandi Zangabad, S. Baghaee-Ravari, M. Ghazadeh, H. Mirshekari, M. R. Hamblin, *J. Am. Chem. Soc.* **2017**, *139*, 4584–4610.

[47] M. J. Geisow, W. H. Evans, *Exp. Cell Res.* **1984**, *150*, 36–46.

[48] P. Chan, J. Lovrić, J. Warwicker, *PROTEOMICS* **2006**, *6*, 3494–3501.

[49] M. J. Geisow, *Exp. Cell Res.* **1984**, *150*, 29–35.

[50] R. P. Feazell, N. Nakayama-Ratchford, H. Dai, S. J. Lippard, *J. Am. Chem. Soc.* **2007**, *129*, 8438–8439.

[51] G. M. Dubowchik, M. A. Walker, *Pharmacol. Therap.* **1999**, *83*, 67–123.

[52] B. Huang, S. Tang, A. Desai, X.-m. Cheng, A. Kotlyar, A. V. D. Spek, T. P. Thomas, J. R. Baker Jr, *Bioorg. Med. Chem. Lett.* **2009**, *19*, 5016–5020.

[53] E. Gullotti, Y. Yeo, *Mol. Pharmaceutics* **2009**, *6*, 1041–1051.

[54] L. M. Kaminskas, B. D. Kelly, V. M. McLeod, G. Sberna, B. J. Boyd, D. J. Owen, C. J. H. Porter, *Mol. Pharmaceutics* **2011**, *8*, 338–349.

[55] L. M. Kaminskas, B. D. Kelly, V. M. McLeod, B. J. Boyd, G. Y. Krippner, E. D. Williams, C. J. H. Porter, *Mol. Pharmaceutics* **2009**, *6*, 1190–1204.

[56] A. Homma, H. Sato, A. Okamachi, T. Emura, T. Ishizawa, T. Kato, T. Matsuura, S. Sato, T. Tamura, Y. Higuchi, T. Watanabe, H. Kitamura, K. Asanuma, T. Yamazaki, M. Ikemi, H. Kitagawa, T. Morikawa, H. Ikeya, K. Maeda, K. Takahashi, K. Nohmi, N. Izutani, M. Kanda, R. Suzuki, *Bioorg. Med. Chem.* **2009**, *17*, 4647–4656.

[57] S. Dhar, Z. Liu, J. r. Thomale, H. Dai, S. J. Lippard, *J. Am. Chem. Soc.* **2008**, *130*, 11467–11476.

[58] D. P. Naughton, *Adv. Drug Delivery Rev.* **2001**, *53*, 229–233.

[59] H. H. W. Chen, I.-S. Song, A. Hossain, M.-K. Choi, Y. Yamane, Z. D. Liang, J. Lu, L. Y.-H. Wu, Z. H. Siddik, L. W. J. Klomp, N. Savaraj, M. T. Kuo, *Mol. Pharmacol.* **2008**, *74*, 697–704.

[60] I. Ojima, *Acc. Chem. Res.* **2008**, *41*, 108–119.

[61] J. M. Chan, L. Zhang, R. Tong, D. Ghosh, W. Gao, G. Liao, K. P. Yuet, D. Gray, J.-W. Rhee, J. Cheng, G. Golomb, P. Libby, R. Langer, O. C. Farokhzad, *Proc. Natl. Acad. Sci. U. S. A.* **2010**, *107*, 2213–2218.

[62] X. Xue, Y. Zhao, L. Dai, X. Zhang, X. Hao, C. Zhang, S. Huo, J. Liu, C. Liu, A. Kumar, W.-Q. Chen, G. Zou, X.-J. Liang, *Adv. Mater. (Weinheim, Ger.)* **2014**, *26*, 712–717.

[63] V. G. Deepagan, D. G. You, W. Um, H. Ko, S. Kwon, K. Y. Choi, G.-R. Yi, J. Y. Lee, D. S. Lee, K. Kim, I. C. Kwon, J. H. Park, *Nano Lett.* **2016**, *16*, 6257–6264.

[64] F. Xu, M. Hu, C. Liu, S. K. Choi, *Biomater. Sci.* **2017**, *5*, 678–685.

[65] J.-F. Gohy, Y. Zhao, *Chem. Soc. Rev.* **2013**, *42*, 7117–7129.

[66] L. Cheng, C. Wang, L. Feng, K. Yang, Z. Liu, *Chem. Rev. (Washington, DC, U. S.)* **2014**, *114*, 10869–10939.

[67] V. Biju, *Chem. Soc. Rev.* **2014**, *43*, 744–764.

[68] N. L. Rosi, C. A. Mirkin, *Chem. Rev. (Washington, DC, U. S.)* **2005**, *105*, 1547–1562.

[69] Y. Xia, W. Li, C. M. Cobley, J. Chen, X. Xia, Q. Zhang, M. Yang, E. C. Cho, P. K. Brown, *Acc. Chem. Res.* **2011**, *44*, 914–924.

[70] M.-C. Daniel, D. Astruc, *Chem. Rev. (Washington, DC, U. S.)* **2004**, *104*, 293–346.

[71] H. Chen, L. Shao, Q. Li, J. Wang, *Chem. Soc. Rev.* **2013**, *42*, 2679–2724.

[72] H. Cai, K. Li, J. Li, S. Wen, Q. Chen, M. Shen, L. Zheng, G. Zhang, X. Shi, *Small* **2015**, *11*, 4584–4593.

[73] D. Li, S. Wen, W. Sun, J. Zhang, D. Jin, C. Peng, M. Shen, X. Shi, *ACS Appl. Bio Mater.* **2018**, *1*, 221–225.

[74] G. Ku, Q. Huang, X. Wen, J. Ye, D. Piwnica-Worms, C. Li, *ACS Omega* **2018**, *3*, 5888–5895.

[75] J. Li, M. Zhou, F. Liu, C. Xiong, W. Wang, Q. Cao, X. Wen, J. D. Robertson, X. Ji, Y. A. Wang, S. Gupta, C. Li, *Radiology* **2016**, *281*, 427–435.

[76] N. Zhao, J. You, Z. Zeng, C. Li, Y. Zu, *Small* **2013**, *9*, 3477–3484.

[77] J. You, G. Zhang, C. Li, *ACS Nano* **2010**, *4*, 1033–1041.

[78] M. S. Yavuz, Y. Cheng, J. Chen, C. M. Cobley, Q. Zhang, M. Rycenga, J. Xie, C. Kim, K. H. Song, A. G. Schwartz, L. V. Wang, Y. Xia, *Nat. Mater.* **2009**, *8*, 935–939.

[79] C. M. Cobley, L. Au, J. Chen, Y. Xia, *Expert Opin. Drug Delivery* **2010**, *7*, 577–587.

[80] N. S. Abadeer, C. J. Murphy, *J. Phys. Chem. C* **2016**, *120*, 4691–4716.

[81] M. A. Mackey, M. R. K. Ali, L. A. Austin, R. D. Near, M. A. El-Sayed, *J. Phys. Chem. B* **2014**, *118*, 1319–1326.

[82] L. Au, D. Zheng, F. Zhou, Z.-Y. Li, X. Li, Y. Xia, *ACS Nano* **2008**, *2*, 1645–1652.

[83] C. Xiong, W. Lu, M. Zhou, X. Wen, C. Li, *Cancer Nanotechnol.* **2018**, *9*, 10.1186/s12645-12018-10041-12649.

[84] W. Lu, G. Zhang, R. Zhang, L. G. Flores, Q. Huang, J. G. Gelovani, C. Li, *Cancer Res.* **2010**, *70*, 3177–3188.

[85] W. Li, J. Yang, L. Luo, M. Jiang, B. Qin, H. Yin, C. Zhu, X. Yuan, J. Zhang, Z. Luo, Y. Du, Q. Li, Y. Lou, Y. Qiu, J. You, *Nat. Commun.* **2019**, *10*, 3349.

[86] F. Xu, Y. Zhao, M. Hu, p. zhang, N. Kong, r. Liu, C. Liu, S. K. Choi, *Chem. Commun. (Cambridge, U. K.)* **2018**, *54*, 9525–9528.

[87] M. Dahl, Y. Liu, Y. Yin, *Chem. Rev. (Washington, DC, U. S.)* **2014**, *114*, 9853–9889.

[88] J. M. Anglada, M. Martins-Costa, J. S. Francisco, M. F. Ruiz-López, *Acc. Chem. Res.* **2015**, *48*, 575–583.

[89] G. Chen, H. Qiu, P. N. Prasad, X. Chen, *Chem. Rev. (Washington, DC, U. S.)* **2014**, *114*, 5161–5214.

[90] R. Justin, S. Roman, D. Chen, K. Tao, X. Geng, R. T. Grant, S. MacNeil, K. Sun, B. Chen, *RSC Advances* **2015**, *5*, 51934–51946.

[91] S. Barua, X. Geng, B. Chen, in *Photonanotechnology for Therapeutics and Imaging* (Ed.: S. K. Choi), Elsevier, **2020**, pp. 45–81.

[92] D. Eder, *Chem. Rev. (Washington, DC, U. S.)* **2010**, *110*, 1348–1385.

[93] Q. Mu, D. L. Broughton, B. Yan, *Nano Lett.* **2009**, *9*, 4370–4375.

[94] J. Zhou, Y. Yang, C.-y. Zhang, *Chem. Rev. (Washington, DC, U. S.)* **2015**, *115*, 11669–11717.

[95] T. Daimon, Y. Nosaka, *J. Phys. Chem. C* **2007**, *111*, 4420–4424.

[96] M. Buchalska, P. Labuz, L. Bujak, G. Szewczyk, T. Sarna, S. Mackowski, W. Macyk, *Dalton Trans.* **2013**, *42*, 9468–9475.

[97] A. Amirshaghaghi, L. Yan, J. Miller, Y. Daniel, J. M. Stein, T. M. Busch, Z. Cheng, A. Tsourkas, *Sci. Rep.* **2019**, *9*, 2613.

[98] D. Chen, R. Tao, K. Tao, B. Chen, S. K. Choi, Q. Tian, Y. Xu, G. Zhou, K. Sun, *Small* **2017**, *13*, 1602053.

[99] B. Zhao, P. J. Bilski, Y.-Y. He, L. Feng, C. F. Chignell, *Photochem. Photobiol.* **2008**, *84*, 1215–1223.

[100] S. Heer, K. Kömpe, H. U. Güdel, M. Haase, *Adv. Mater. (Weinheim, Ger.)* **2004**, *16*, 2102–2105.

[101] X. Liu, C.-H. Yan, J. A. Capobianco, *Chem. Soc. Rev.* **2015**, *44*, 1299–1301.

[102] M. Haase, H. Schäfer, *Angew. Chem., Int. Ed.* **2011**, *50*, 5808–5829.

[103] O. S. Wolfbeis, *Chem. Soc. Rev.* **2015**, *44*, 4743–4768.

[104] N. M. Idris, M. K. G. Jayakumar, A. Bansal, Y. Zhang, *Chem. Soc. Rev.* **2015**, *44*, 1449–1478.

[105] F. Wang, X. Liu, *Chem. Soc. Rev.* **2009**, *38*, 976–989.

[106] K. Tao, K. Sun, in *Photonanotechnology for Therapeutics and Imaging* (Ed.: S. K. Choi), Elsevier, **2020**, pp. 147–176.

[107] A. Alabugin, *Photochem. Photobiol.* **2019**, *95*, 722–732.

[108] M. Hu, W. Liu, in *Photonanotechnology for Therapeutics and Imaging* (Ed.: S. K. Choi), Elsevier, **2020**, pp. 205–241.

[109] J. Jin, Y.-J. Gu, C. W.-Y. Man, J. Cheng, Z. Xu, Y. Zhang, H. Wang, V. H.-Y. Lee, S. H. Cheng, W.-T. Wong, *ACS Nano* **2011**, *5*, 7838–7847.

[110] Q. Tian, K. Tao, W. Li, K. Sun, *J. Phys. Chem. C* **2011**, *115*, 22886–22892.

[111] J. Vuilleumier, G. Gaulier, R. De Matos, Y. Mugnier, G. Campargue, J.-P. Wolf, L. Bonacina, S. Gerber-Lemaire, *Helv. Chim. Acta* **2020**, *103*, e1900251.

[112] D. Staedler, T. Magouroux, R. Hadji, C. Joulaud, J. Extermann, S. Schwung, S. Passemard, C. Kasparian, G. Clarke, M. Gerrmann, R. Le Dantec, Y. Mugnier, D. Rytz, D. Ciepielewski, C. Galez, S. Gerber-Lemaire, L. Juillerat-Jeanneret, L. Bonacina, J.-P. Wolf, *ACS Nano* **2012**, *6*, 2542–2549.

[113] M. J. Hansen, W. A. Velema, M. M. Lerch, W. Szymanski, B. L. Feringa, *Chem. Soc. Rev.* **2015**, *44*, 3358–3377.

[114] M. Bio, G. Nkepang, Y. You, *Chem. Commun. (Cambridge, U. K.)* **2012**, *48*, 6517-6519.

[115] G. Saravanakumar, J. Lee, J. Kim, W. J. Kim, *Chem. Commun. (Cambridge, U. K.)* **2015**, *51*, 9995–9998.

[116] K. Kim, C.-S. Lee, K. Na, *Chem. Commun. (Cambridge, U. K.)* **2016**, *52*, 2839–2842.

[117] S. Guo, X. Liu, C. Yao, C. Lu, Q. Chen, X.-Y. Hu, L. Wang, *Chem. Commun. (Cambridge, U. K.)* **2016**, *52*, 10751–10754.

[118] Z. Liu, Q. Lin, Q. Huang, H. Liu, C. Bao, W. Zhang, X. Zhong, L. Zhu, *Chem. Commun. (Cambridge, U. K.)* **2011**, *47*, 1482–1484.

[119] N. G. Patil, N. B. Basutkar, A. V. Ambade, *Chem. Commun. (Cambridge, U. K.)* **2015**, *51*, 17708–17711.

[120] C. Yao, P. Wang, X. Li, X. Hu, J. Hou, L. Wang, F. Zhang, *Adv. Mater. (Weinheim, Ger.)* **2016**, *28*, 9341–9348.

[121] G. Mayer, A. Heckel, *Angew. Chem., Int. Ed.* **2006**, *45*, 4900–4921.

[122] M. Goard, G. Aakalu, O. D. Fedoryak, C. Quinonez, J. St. Julien, S. J. Poteet, E. M. Schuman, T. M. Dore, *Chem. Biol. (Oxford, U. K.)* **2005**, *12*, 685–693.

[123] P. Neveu, I. Aujard, C. Benbrahim, T. Le Saux, J.-F. Allemand, S. Vriz, D. Bensimon, L. Jullien, *Angew. Chem., Int. Ed.* **2008**, *47*, 3744–3746.

[124] A. Momotake, N. Lindegger, E. Niggli, R. J. Barsotti, G. C. R. Ellis-Davies, *Nat. Methods* **2006**, *3*, 35–40.

[125] I. Aujard, C. Benbrahim, M. Gouget, O. Ruel, J.-B. Baudin, P. Neveu, L. Jullien, *Chem. - Eur. J.* **2006**, *12*, 6865–6879.

[126] P. T. Wong, S. Tang, J. Cannon, J. Mukherjee, D. Isham, K. Gam, M. Payne, S. A. Yanik, J. R. Baker, S. K. Choi, *ChemBioChem* **2017**, *18*, 126–135.

[127] T. Furuta, S. S. H. Wang, J. L. Dantzker, T. M. Dore, W. J. Bybee, E. M. Callaway, W. Denk, R. Y. Tsien, *Proc. Natl. Acad. Sci. U. S. A.* **1999**, *96*, 1193–1200.

[128] S. Tang, J. Cannon, K. Yang, M. F. Krummel, J. R. Baker, S. K. Choi, *J. Org. Chem.* **2020**, *85*, 2945–2955.

[129] A. P. Gorka, R. R. Nani, J. Zhu, S. Mackem, M. J. Schnermann, *J. Am. Chem. Soc.* **2014**, *136*, 14153–14159.

[130] R. R. Nani, A. P. Gorka, T. Nagaya, T. Yamamoto, J. Ivanic, H. Kobayashi, M. J. Schnermann, *ACS Cent. Sci.* **2017**, *3*, 329–337.

[131] E. Janett, Y. Bernardinelli, D. Müller, C. G. Bochet, *Bioconjugate Chem.* **2015**, *26*, 2408–2418.

[132] R. Johnsson, J. G. Lackey, J. J. Bogojeski, M. J. Damha, *Bioorg. Med. Chem. Lett.* **2011**, *21*, 3721–3725.

[133] S. Kantevari, S. Passlick, H.-B. Kwon, M. T. Richers, B. L. Sabatini, G. C. R. Ellis-Davies, *ChemBioChem* **2016**, *17*, 953–961.

[134] R. J. T. Mikkelsen, K. E. Grier, K. T. Mortensen, T. E. Nielsen, K. Qvortrup, *ACS Comb. Sci.* **2018**, *20*, 377–399.

[135] F. M. Rossi, M. Margulis, C.-M. Tang, J. P. Y. Kao, *J. Biol. Chem.* **1997**, *272*, 32933–32939.

[136] F. M. Rossi, J. P. Y. Kao, *J. Biol. Chem.* **1997**, *272*, 3266–3271.

[137] L. Niu, K. R. Gee, K. Schaper, G. P. Hess, *Biochemistry* **1996**, *35*, 2030–2036.

[138] S. K. Choi, M. Verma, J. Silpe, R. E. Moody, K. Tang, J. J. Hanson, J. R. Baker Jr, *Bioorg. Med. Chem.* **2012**, *20*, 1281–1290.

[139] M. A. Inlay, V. Choe, S. Bharathi, N. B. Fernhoff, J. R. Baker, I. L. Weissman, S. K. Choi, *Chem. Commun. (Cambridge, U. K.)* **2013**, *49*, 4971–4973.

[140] S. S. Agasti, A. Chompoosor, C.-C. You, P. Ghosh, C. K. Kim, V. M. Rotello, *J. Am. Chem. Soc.* **2009**, *131*, 5728–5729.

[141] P. T. Wong, E. W. Roberts, S. Tang, J. Mukherjee, J. Cannon, A. J. Nip, K. Corbin, M. F. Krummel, S. K. Choi, *ACS Chem. Biol.* **2017**, *12*, 1001–1010.

[142] P. T. Wong, D. Chen, S. Tang, S. Yanik, M. Payne, J. Mukherjee, A. Coulter, K. Tang, K. Tao, K. Sun, J. R. Baker Jr, S. K. Choi, *Small* **2015**, *11*, 6078–6090.

[143] M. Gaplovsky, Y. V. Il'ichev, Y. Kamdzhilov, S. V. Kombarova, M. Mac, M. A. Schworer, J. Wirz, *Photochem. Photobiol. Sci.* **2005**, *4*, 33–42.

[144] Y. V. Il'ichev, M. A. Schwörer, J. Wirz, *J. Am. Chem. Soc.* **2004**, *126*, 4581–4595.

[145] M. Wilcox, R. W. Viola, K. W. Johnson, A. P. Billington, B. K. Carpenter, J. A. McCray, A. P. Guzikowski, G. P. Hess, *J. Org. Chem.* **1990**, *55*, 1585–1589.

[146] R. K. Paradise, D. A. Lauffenburger, K. J. Van Vliet, *PLoS One* **2011**, *6*, e15746.

[147] S. K. Choi, in *Photonanotechnology for Therapeutics and Imaging* (Ed.: S. K. Choi), Elsevier, **2020**, pp. 243–275.

[148] Y. M. Li, J. Shi, R. Cai, X. Chen, Z. F. Luo, Q. X. Guo, *J. Photochem. Photobiol., A* **2010**, *211*, 129–134.

[149] T. Narumi, K. Miyata, A. Nii, K. Sato, N. Mase, T. Furuta, *Org. Lett.* **2018**, *20*, 4178–4182.

[150] A.-L. K. Hennig, D. Deodato, N. Asad, C. Herbivo, T. M. Dore, *J. Org. Chem.* **2020**, *85*, 726–744.

[151] N. Asad, D. Deodato, X. Lan, M. B. Widegren, D. L. Phillips, L. Du, T. M. Dore, *J. Am. Chem. Soc.* **2017**, *139*, 12591–12600.

[152] Y. Venkatesh, S. Nandi, M. Shee, B. Saha, A. Anoop, N. D. P. Singh, *Eur. J. Org. Chem.* **2017**, *2017*, 6121–6130.

[153] Y. Venkatesh, Y. Rajesh, S. Karthik, A. C. Chetan, M. Mandal, A. Jana, N. D. P. Singh, *J. Org. Chem.* **2016**, *81*, 11168–11175.

[154] R. G. Wylie, M. S. Shoichet, *J. Mater. Chem.* **2008**, *18*, 2716–2721.

[155] C. Bao, G. Fan, Q. Lin, B. Li, S. Cheng, Q. Huang, L. Zhu, *Org. Lett.* **2011**, *14*, 572–575.

[156] K. R. Gee, L. Niu, K. Schaper, V. Jayaraman, G. P. Hess, *Biochemistry* **1999**, *38*, 3140–3147.

[157] J. W. Walker, J. A. McCray, G. P. Hess, *Biochemistry* **1986**, *25*, 1799–1805.

[158] K. Mitra, C. E. Lyons, M. C. T. Hartman, *Angew. Chem., Int. Ed.* **2018**, *57*, 10263–10267.

[159] J. Lee, J. Park, K. Singha, W. J. Kim, *Chem. Commun. (Cambridge, U. K.)* **2013**, *49*, 1545–1547.

[160] H. Yan, C. Teh, S. Sreejith, L. Zhu, A. Kwok, W. Fang, X. Ma, K. T. Nguyen, V. Korzh, Y. Zhao, *Angew. Chem., Int. Ed.* **2012**, *51*, 8373–8377.

[161] J. Liu, W. Bu, L. Pan, J. Shi, *Angew. Chem., Int. Ed.* **2013**, *52*, 4375–4379.

[162] R. J. Mart, R. K. Allemann, *Chem. Commun. (Cambridge, U. K.)* **2016**, *52*, 12262–12277.

[163] Q. Zhao, Y. Wang, Y. Yan, J. Huang, *ACS Nano* **2014**, *8*, 11341–11349.

[164] Q. Yuan, Y. Zhang, T. Chen, D. Lu, Z. Zhao, X. Zhang, Z. Li, C.-H. Yan, W. Tan, *ACS Nano* **2012**, *6*, 6337–6344.

[165] A. Martinez-Cuezva, S. Valero-Moya, M. Alajarin, J. Berna, *Chem. Commun. (Cambridge, U. K.)* **2015**, *51*, 14501–14504.

[166] J. R. Schnell, H. J. Dyson, P. E. Wright, *Annu. Rev. Biophys. Biomol. Struct.* **2004**, *33*, 119–140.

[167] M. H. N. Tattersall, B. Brown, E. Frei, *Nature* **1975**, *253*, 198–200.

[168] D. Farquhar, R. A. Newman, J. E. Zuckerman, B. S. Andersson, *J. Med. Chem.* **1991**, *34*, 561–564.

[169] P. T. Wong, S. Tang, J. Cannon, D. Chen, R. Sun, J. Lee, J. Phan, K. Tao, K. Sun, B. Chen, J. R. Baker, S. K. Choi, *Bioconjugate Chem.* **2017**, *28*, 3016–3028.

[170] J. A. Johnson, Y. Y. Lu, A. O. Burts, Y.-H. Lim, M. G. Finn, J. T. Koberstein, N. J. Turro, D. A. Tirrell, R. H. Grubbs, *J. Am. Chem. Soc.* **2011**, *133*, 559–566.

[171] M. M. Dcona, Q. Yu, J. A. Capobianco, M. C. T. Hartman, *Chem. Commun. (Cambridge, U. K.)* **2015**, *51*, 8477–8479.

[172] P. Wong, S. Tang, J. Mukherjee, K. Tang, K. Gam, D. Isham, C. Murat, R. Sun, J. R. Baker, S. K. Choi, *Chem. Commun. (Cambridge, U. K.)* **2016**, *52*, 10357–10360.

[173] J. Xiang, X. Tong, F. Shi, Q. Yan, B. Yu, Y. Zhao, *J. Mater. Chem. B* **2018**, *6*, 3531–3540.

[174] Y. Dai, H. Xiao, J. Liu, Q. Yuan, P. a. Ma, D. Yang, C. Li, Z. Cheng, Z. Hou, P. Yang, J. Lin, *J. Am. Chem. Soc.* **2013**, *135*, 18920–18929.

[175] S. Li, R. Liu, X. Jiang, Y. Qiu, X. Song, G. Huang, N. Fu, L. Lin, J. Song, X. Chen, H. Yang, *ACS Nano* **2019**, *13*, 2103–2113.

[176] Q. Jin, F. Mitschang, S. Agarwal, *Biomacromolecules* **2011**, *12*, 3684–3691.

[177] M. Noguchi, M. Skwarczynski, H. Prakash, S. Hirota, T. Kimura, Y. Hayashi, Y. Kiso, *Bioorg. Med. Chem.* **2008**, *16*, 5389–5397.

[178] M. Skwarczynski, M. Noguchi, S. Hirota, Y. Sohma, T. Kimura, Y. Hayashi, Y. Kiso, *Bioorg. Med. Chem. Lett.* **2006**, *16*, 4492–4496.

[179] A. Z. Suzuki, R. Sekine, S. Takeda, R. Aikawa, Y. Shiraishi, T. Hamaguchi, H. Okuno, H. Tamamura, T. Furuta, *Chem. Commun. (Cambridge, U. K.)* **2018**, *55*, 451–454.

[180] R. A. Gropeanu, H. Baumann, S. Ritz, V. Mailänder, T. Surrey, A. del Campo, *PLoS One* **2012**, *7*, e43657.

[181] C. Xu, H. Li, K. Zhang, D. W. Binzel, H. Yin, W. Chiu, P. Guo, *Nano Res.* **2019**, *12*, 41–48.

[182] X. Hu, J. Tian, T. Liu, G. Zhang, S. Liu, *Macromolecules* **2013**, *46*, 6243–6256.

[183] G. Yu, W. Yu, Z. Mao, C. Gao, F. Huang, *Small* **2015**, *11*, 919–925.

[184] L. Huang, Y. Zhao, H. Zhang, K. Huang, J. Yang, G. Han, *Angew. Chem., Int. Ed.* **2017**, *56*, 14400–14404.

[185] X. Li, J. Mu, F. Liu, E. W. P. Tan, B. Khezri, R. D. Webster, E. K. L. Yeow, B. Xing, *Bioconjugate Chem.* **2015**, *26*, 955–961.

[186] H. Song, W. Li, R. Qi, L. Yan, X. Jing, M. Zheng, H. Xiao, *Chem. Commun. (Cambridge, U. K.)* **2015**, *51*, 11493–11495.

[187] H. Song, X. Kang, J. Sun, X. Jing, Z. Wang, L. Yan, R. Qi, M. Zheng, *Chem. Commun. (Cambridge, U. K.)* **2016**, *52*, 2281–2283.

[188] M. LeBel, *Pharmacotherapy* **1988**, *8*, 3–30.

[189] Y. Shi, V. X. Truong, K. Kulkarni, Y. Qu, G. P. Simon, R. L. Boyd, P. Perlmutter, T. Lithgow, J. S. Forsythe, *J. Mater. Chem. B* **2015**, *3*, 8771–8774.

[190] P. T. Wong, S. Tang, K. Tang, A. Coulter, J. Mukherjee, K. Gam, J. R. Baker, S. K. Choi, *J. Mater. Chem. B* **2015**, *3*, 1149–1156.

[191] G. Han, C.-C. You, B.-j. Kim, R. S. Turingan, N. S. Forbes, C. T. Martin, V. M. Rotello, *Angew. Chem., Int. Ed.* **2006**, *45*, 3165–3169.

[192] P. K. Brown, A. T. Qureshi, A. N. Moll, D. J. Hayes, W. T. Monroe, *ACS Nano* **2013**, *7*, 2948–2959.

[193] Y. Pan, J. Yang, X. Luan, X. Liu, X. Li, J. Yang, T. Huang, L. Sun, Y. Wang, Y. Lin, Y. Song, *Sci. Adv.* **2019**, *5*, eaav7199.

[194] M. K. G. Jayakumar, A. Bansal, K. Huang, R. Yao, B. N. Li, Y. Zhang, *ACS Nano* **2014**, *8*, 4848–4858.

[195] A. Fraix, N. Kandoth, I. Manet, V. Cardile, A. C. E. Graziano, R. Gref, S. Sortino, *Chem. Commun. (Cambridge, U. K.)* **2013**, *49*, 4459–4461.

[196] C. Fowley, A. P. McHale, B. McCaughan, A. Fraix, S. Sortino, J. F. Callan, *Chem. Commun. (Cambridge, U. K.)* **2015**, *51*, 81–84.

[197] H.-J. Xiang, L. An, W.-W. Tang, S.-P. Yang, J.-G. Liu, *Chem. Commun. (Cambridge, U. K.)* **2015**, *51*, 2555–2558.

[198] M. Guo, H.-J. Xiang, Y. Wang, Q.-L. Zhang, L. An, S.-P. Yang, Y. Ma, Y. Wang, J.-G. Liu, *Chem. Commun. (Cambridge, U. K.)* **2017**, *53*, 3253–3256.

[199] A. E. Pierri, P.-J. Huang, J. V. Garcia, J. G. Stanfill, M. Chui, G. Wu, N. Zheng, P. C. Ford, *Chem. Commun. (Cambridge, U. K.)* **2015**, *51*, 2072–2075.

[200] W. Chen, M. Chen, Q. Zang, L. Wang, F. Tang, Y. Han, C. Yang, L. Deng, Y.-N. Liu, *Chem. Commun. (Cambridge, U. K.)* **2015**, *51*, 9193–9196.

[201] W. Chen, D. Ni, Z. T. Rosenkrans, T. Cao, W. Cai, *Adv. Sci. (Weinheim, Ger.)* **2019**, *6*, 1901724.

[202] C. Alvarez-Lorenzo, L. Bromberg, A. Concheiro, *Photochem. Photobiol.* **2009**, *85*, 848–860.

[203] F. Huang, W.-C. Liao, Y. S. Sohn, R. Nechushtai, C.-H. Lu, I. Willner, *J. Am. Chem. Soc.* **2016**, *138*, 8936–8945.

[204] B. Chandra, S. Mallik, D. K. Srivastava, *Chem. Commun. (Cambridge, U. K.)* **2005**, 3021–3023.

[205] F. Reeßing, M. C. A. Stuart, D. F. Samplonius, R. A. J. O. Dierckx, B. L. Feringa, W. Helfrich, W. Szymanski, *Chem. Commun. (Cambridge, U. K.)* **2019**, *55*, 10784–10787.

[206] H. Wu, J. Dong, C. Li, Y. Liu, N. Feng, L. Xu, X. Zhan, H. Yang, G. Wang, *Chem. Commun. (Cambridge, U. K.)* **2013**, *49*, 3516–3518.

[207] X. Zhao, M. Qi, S. Liang, K. Tian, T. Zhou, X. Jia, J. Li, P. Liu, *ACS Appl. Mater. Interfaces* **2016**, *8*, 22127–22134.

[208] Y. Li, Y. Qian, T. Liu, G. Zhang, S. Liu, *Biomacromolecules* **2012**, *13*, 3877–3886.

[209] J. Yang, J.-I. Song, Q. Song, J. Y. Rho, E. D. H. Mansfield, S. C. L. Hall, M. Sambrook, F. Huang, S. Perrier, *Angew. Chem., Int. Ed.* **2020**, *59*, 8860–8863.

[210] F. Sun, P. Zhang, Y. Liu, C. Lu, Y. Qiu, H. Mu, J. Duan, *Carbohydr. Polym.* **2019**, *206*, 309–318.

[211] L. Yang, H. Sun, Y. Liu, W. Hou, Y. Yang, R. Cai, C. Cui, P. Zhang, X. Pan, X. Li, L. Li, B. S. Sumerlin, W. Tan, *Angew. Chem., Int. Ed.* **2018**, *57*, 17048–17052.

[212] B. Yan, J.-C. Boyer, N. R. Branda, Y. Zhao, *J. Am. Chem. Soc.* **2011**, *133*, 19714–19717.

[213] Z. Sun, G. Liu, J. Hu, S. Liu, *Biomacromolecules* **2018**, *19*, 2071–2081.

[214] G. Pasparakis, T. Manouras, M. Vamvakaki, P. Argitis, *Nat. Commun.* **2014**, *5*, 3623.

[215] Y. Zhang, G. Lu, Y. Yu, H. Zhang, J. Gao, Z. Sun, Y. Lu, H. Zou, *ACS Appl. Bio Mater.* **2019**, *2*, 495–503.

[216] H. Zhao, W. Hu, H. Ma, R. Jiang, Y. Tang, Y. Ji, X. Lu, B. Hou, W. Deng, W. Huang, Q. Fan, *Adv. Funct. Mater.* **2017**, *27*, 1702592.

[217] Y. Abebe Alemayehu, B. Tewabe Gebeyehu, C.-C. Cheng, *Biomacromolecules* **2019**, *20*, 4535–4545.

[218] J. Lai, X. Mu, Y. Xu, X. Wu, C. Wu, C. Li, J. Chen, Y. Zhao, *Chem. Commun. (Cambridge, U. K.)* **2010**, *46*, 7370–7372.

[219] A. Hernández-Montoto, M. Gorbe, A. Llopis-Lorente, J. M. Terrés, R. Montes, R. Cao-Milán, B. Díaz de Greñu, M. Alfonso, M. Orzaez, M. D. Marcos, R. Martínez-Máñez, F. Sancenón, *Chem. Commun. (Cambridge, U. K.)* **2019**, *55*, 9039–9042.

[220] J. Xiang, F. Ge, B. Yu, Q. Yan, F. Shi, Y. Zhao, *ACS Appl. Mater. Interfaces* **2018**, *10*, 20790–20800.

[221] N. Ž. Knežević, B. G. Trewyn, V. S. Y. Lin, *Chem. Commun. (Cambridge, U. K.)* **2011**, *47*, 2817–2819.

[222] S. He, K. Krippes, S. Ritz, Z. Chen, A. Best, H.-J. Butt, V. Mailänder, S. Wu, *Chem. Commun. (Cambridge, U. K.)* **2015**, *51*, 431–434.

[223] S. Alberti, G. J. A. A. Soler-Illia, O. Azzaroni, *Chem. Commun. (Cambridge, U. K.)* **2015**, *51*, 6050–6075.

[224] D. Wang, S. Wu, *Langmuir* **2016**, *32*, 632–636.

[225] N. Ma, W.-J. Wang, S. Chen, X.-S. Wang, X.-Q. Wang, S.-B. Wang, J.-Y. Zhu, S.-X. Cheng, X.-Z. Zhang, *Chem. Commun. (Cambridge, U. K.)* **2015**, *51*, 12970–12973.

[226] E. Beňová, V. Zeleňák, D. Halamová, M. Almáši, V. Petrul'ová, M. Psotka, A. Zeleňáková, M. Bačkor, V. Hornebecq, *J. Mater. Chem. B* **2017**, *5*, 817–825.

[227] X. Wang, J. Hu, G. Liu, J. Tian, H. Wang, M. Gong, S. Liu, *J. Am. Chem. Soc.* **2015**, *137*, 15262–15275.

[228] T. Senthilkumar, L. Zhou, Q. Gu, L. Liu, F. Lv, S. Wang, *Angew. Chem., Int. Ed.* **2018**, *57*, 13114–13119.

[229] X. Liang, X. Yue, Z. Dai, J.-i. Kikuchi, *Chem. Commun. (Cambridge, U. K.)* **2011**, *47*, 4751–4753.

[230] H. Namazi, S. Jafarirad, *J. Pharm. Pharm. Sci.* **2011**, *14*, 162–180.

[231] Q. Yan, Y. Xin, R. Zhou, Y. Yin, J. Yuan, *Chem. Commun. (Cambridge, U. K.)* **2011**, *47*, 9594–9596.

[232] K. Peng, I. Tomatsu, A. Kros, *Chem. Commun. (Cambridge, U. K.)* **2010**, *46*, 4094–4096.

[233] T. Zhao, P. Wang, Q. Li, A. A. Al-Khalaf, W. N. Hozzein, F. Zhang, X. Li, D. Zhao, *Angew. Chem., Int. Ed.* **2018**, *57*, 2611–2615.

[234] T. Yan, F. Li, S. Qi, J. Tian, R. Tian, J. Hou, Q. Luo, Z. Dong, J. Xu, J. Liu, *Chem. Commun. (Cambridge, U. K.)* **2020**, *56*, 149–152.

[235] Y. Huang, L. Shen, D. Guo, W. Yasen, Y. Wu, Y. Su, D. Chen, F. Qiu, D. Yan, X. Zhu, *Chem. Commun. (Cambridge, U. K.)* **2019**, *55*, 6735–6738.

[236] F.-Q. Li, Q.-L. Yu, Y.-H. Liu, H.-J. Yu, Y. Chen, Y. Liu, *Chem. Commun. (Cambridge, U. K.)* **2020**, *56*, 3907–3910.

[237] H. Zhang, X. Fan, R. Suo, H. Li, Z. Yang, W. Zhang, Y. Bai, H. Yao, W. Tian, *Chem. Commun. (Cambridge, U. K.)* **2015**, *51*, 15366–15369.

[238] S. O. Poelma, S. S. Oh, S. Helmy, A. S. Knight, G. L. Burnett, H. T. Soh, C. J. Hawker, J. Read de Alaniz, *Chem. Commun. (Cambridge, U. K.)* **2016**, *52*, 10525–10528.

[239] J. Karcher, Z. L. Pianowski, *Chem. - Eur. J.* **2018**, *24*, 11605–11610.

[240] K. Roth Stefaniak, C. C. Epley, J. J. Novak, M. L. McAndrew, H. D. Cornell, J. Zhu, D. K. McDaniel, J. L. Davis, I. C. Allen, A. J. Morris, T. Z. Grove, *Chem. Commun. (Cambridge, U. K.)* **2018**, *54*, 7617–7620.

[241] N. Möller, T. Hellwig, L. Stricker, S. Engel, C. Fallnich, B. J. Ravoo, *Chem. Commun. (Cambridge, U. K.)* **2017**, *53*, 240–243.

[242] C. Yagüe, M. Arruebo, J. Santamaria, *Chem. Commun. (Cambridge, U. K.)* **2010**, *46*, 7513–7515.

[243] D. T. Marquez, J. C. Scaiano, *Langmuir* **2016**, *32*, 13764–13770.

[244] M. Li, H. Yan, C. Teh, V. Korzh, Y. Zhao, *Chem. Commun. (Cambridge, U. K.)* **2014**, *50*, 9745–9748.

[245] D. Paramelle, S. Gorelik, Y. Liu, J. Kumar, *Chem. Commun. (Cambridge, U. K.)* **2016**, *52*, 9897–9900.

[246] H.-P. Liang, L.-J. Wan, C.-L. Bai, L. Jiang, *J. Phys. Chem. B* **2005**, *109*, 7795–7800.

[247] J. You, R. Shao, X. Wei, S. Gupta, C. Li, *Small* **2010**, *6*, 1022–1031.

[248] Z. Li, J. Liu, Y. Hu, K. A. Howard, Z. Li, X. Fan, M. Chang, Y. Sun, F. Besenbacher, C. Chen, M. Yu, *ACS Nano* **2016**, *10*, 9646–9658.

[249] R. Lv, P. Yang, F. He, S. Gai, C. Li, Y. Dai, G. Yang, J. Lin, *ACS Nano* **2015**, *9*, 1630–1647.

[250] X. An, F. Zhang, Y. Zhu, W. Shen, *Chem. Commun. (Cambridge, U. K.)* **2010**, *46*, 7202–7204.

[251] S. Geng, L. Wu, H. Cui, W. Tan, T. Chen, P. K. Chu, X.-F. Yu, *Chem. Commun. (Cambridge, U. K.)* **2018**, *54*, 6060–6063.

[252] Y. Li, Y. Deng, X. Tian, H. Ke, M. Guo, A. Zhu, T. Yang, Z. Guo, Z. Ge, X. Yang, H. Chen, *ACS Nano* **2015**, *9*, 9626–9637.

[253] M. Zheng, C. Yue, Y. Ma, P. Gong, P. Zhao, C. Zheng, Z. Sheng, P. Zhang, Z. Wang, L. Cai, *ACS Nano* **2013**, *7*, 2056–2067.

[254] W. Wang, G. Liang, W. Zhang, D. Xing, X. Hu, *Chem. Mater.* **2018**, *30*, 3486–3498.

[255] B. Shi, N. Ren, L. Gu, G. Xu, R. Wang, T. Zhu, Y. Zhu, C. Fan, C. Zhao, H. Tian, *Angew. Chem., Int. Ed.* **2019**, *58*, 16826–16830.

[256] H. Takahashi, Y. Niidome, S. Yamada, *Chem. Commun. (Cambridge, U. K.)* **2005**, 2247–2249.

[257] Y. Zhong, C. Wang, L. Cheng, F. Meng, Z. Zhong, Z. Liu, *Biomacromolecules* **2013**, *14*, 2411–2419.

[258] Z. Zhang, J. Wang, X. Nie, T. Wen, Y. Ji, X. Wu, Y. Zhao, C. Chen, *J. Am. Chem. Soc.* **2014**, *136*, 7317–7326.

[259] L. Zhang, H. Su, J. Cai, D. Cheng, Y. Ma, J. Zhang, C. Zhou, S. Liu, H. Shi, Y. Zhang, C. Zhang, *ACS Nano* **2016**, *10*, 10404–10417.

[260] J. Song, X. Yang, O. Jacobson, L. Lin, P. Huang, G. Niu, Q. Ma, X. Chen, *ACS Nano* **2015**, *9*, 9199–9209.

[261] Y. Ding, C. Du, J. Qian, C.-M. Dong, *Nano Lett.* **2019**, *19*, 4362–4370.

[262] W. Wang, N. S. R. Satyavolu, Z. Wu, J.-R. Zhang, J.-J. Zhu, Y. Lu, *Angew. Chem., Int. Ed.* **2017**, *56*, 6798–6802.

[263] W. Ha, X.-B. Zhao, K. Jiang, Y. Kang, J. Chen, B.-J. Li, Y.-P. Shi, *Chem. Commun. (Cambridge, U. K.)* **2016**, *52*, 14384–14387.

[264] Z. Wang, X. Tang, X. Wang, D. Yang, C. Yang, Y. Lou, J. Chen, N. He, *Chem. Commun. (Cambridge, U. K.)* **2016**, *52*, 12210–12213.

[265] R. Kurapati, A. M. Raichur, *Chem. Commun. (Cambridge, U. K.)* **2013**, *49*, 734–736.

[266] J. He, P. Zhang, T. Babu, Y. Liu, J. Gong, Z. Nie, *Chem. Commun. (Cambridge, U. K.)* **2013**, *49*, 576–578.

[267] E. H. Jeong, J. H. Ryu, H. Jeong, B. Jang, H. Y. Lee, S. Hong, H. Lee, H. Lee, *Chem. Commun. (Cambridge, U. K.)* **2014**, *50*, 13388–13390.

[268] L. Yu, A. Dong, R. Guo, M. Yang, L. Deng, J. Zhang, *ACS Biomater. Sci. Eng.* **2018**, *4*, 2424–2434.

[269] J. S. Basuki, F. Qie, X. Mulet, R. Suryadinata, A. V. Vashi, Y. Y. Peng, L. Li, X. Hao, T. Tan, T. C. Hughes, *Angew. Chem., Int. Ed.* **2017**, *56*, 966–971.

[270] X. Wang, C. Wang, Q. Zhang, Y. Cheng, *Chem. Commun. (Cambridge, U. K.)* **2016**, *52*, 978–981.

[271] M. Qiu, D. Wang, W. Liang, L. Liu, Y. Zhang, X. Chen, D. K. Sang, C. Xing, Z. Li, B. Dong, F. Xing, D. Fan, S. Bao, H. Zhang, Y. Cao, *Proc. Natl. Acad. Sci. U. S. A* **2018**, *115*, 501–506.

[272] P. Sun, T. Huang, X. Wang, G. Wang, Z. Liu, G. Chen, Q. Fan, *Biomacromolecules* **2020**, *21*, 556–565.

[273] W.-P. Li, P.-Y. Liao, C.-H. Su, C.-S. Yeh, *J. Am. Chem. Soc.* **2014**, *136*, 10062–10075.

[274] F. Lu, A. Popa, S. Zhou, J.-J. Zhu, A. C. S. Samia, *Chem. Commun. (Cambridge, U. K.)* **2013**, *49*, 11436–11438.

[275] Z. Yang, W. Fan, J. Zou, W. Tang, L. Li, L. He, Z. Shen, Z. Wang, O. Jacobson, M. A. Aronova, P. Rong, J. Song, W. Wang, X. Chen, *J. Am. Chem. Soc.* **2019**, *141*, 14687–14698.

[276] N. N. Mahmoud, A. M. Alkilany, E. A. Khalil, A. G. Al-Bakri, *Sci. Rep.* **2018**, *8*, 6881.

[277] B. Tao, C. Lin, Y. Deng, Z. Yuan, X. Shen, M. Chen, Y. He, Z. Peng, Y. Hu, K. Cai, *J. Mater. Chem. B* **2019**, *7*, 2534–2548.

[278] Y. Zhao, Q. Cai, W. Qi, Y. Jia, T. Xiong, Z. Fan, S. Liu, J. Yang, N. Li, B. Chang, *ChemistrySelect* **2018**, *3*, 9510–9516.

[279] M.-C. Wu, A. R. Deokar, J.-H. Liao, P.-Y. Shih, Y.-C. Ling, *ACS Nano* **2013**, *7*, 1281–1290.

[280] P.-A. Ashford, S. P. Bew, *Chem. Soc. Rev.* **2012**, *41*, 957–978.

[281] S. Bowden, C. Joseph, S. Tang, J. Cannon, E. Francis, M. Zhou, J. R. Baker, S. K. Choi, *Biochemistry* **2018**, *57*, 2723–2732.

[282] S.-G. Wang, Y.-C. Chen, Y.-C. Chen, *Nanomedicine (London, U. K.)* **2018**, *13*, 1405–1416.

[283] D. He, T. Yang, W. Qian, C. Qi, L. Mao, X. Yu, H. Zhu, G. Luo, J. Deng, *Appl. Mater. Today* **2018**, *12*, 415–429.

[284] G. Gao, Y.-W. Jiang, H.-R. Jia, F.-G. Wu, *Biomaterials* **2019**, *188*, 83–95.

[285] M. Liu, D. He, T. Yang, W. Liu, L. Mao, Y. Zhu, J. Wu, G. Luo, J. Deng, *J. Nanobiotechnol.* **2018**, *16*, 1–20.

[286] D. G. Meeker, T. Wang, W. N. Harrington, V. P. Zharov, S. A. Johnson, S. V. Jenkins, S. E. Oyibo, C. M. Walker, W. B. Mills, M. E. Shirtliff, K. E. Beenken, J. Chen, M. S. Smeltzer, *Int. J. Hyperthermia* **2018**, *34*, 209–219.

[287] W.-L. Chiang, T.-T. Lin, R. Sureshbabu, W.-T. Chia, H.-C. Hsiao, H.-Y. Liu, C.-M. Yang, H.-W. Sung, *J. Controlled Release* **2015**, *199*, 53–62.

[288] X. Li, L. Xing, K. Zheng, P. Wei, L. Du, M. Shen, X. Shi, *ACS Appl. Mater. Interfaces* **2017**, *9*, 5817–5827.

[289] L. Luo, Y. Guo, J. Yang, Y. Liu, S. Chu, F. Kong, Y. Wang, Z. Zou, *Chem. Commun. (Cambridge, U. K.)* **2011**, *47*, 11243–11245.

[290] Q. Pei, X. Hu, X. Zheng, S. Liu, Y. Li, X. Jing, Z. Xie, *ACS Nano* **2018**, *12*, 1630–1641.

[291] H. Li, Y. Zhao, Y. Jia, C. Qu, J. Li, *Chem. Commun. (Cambridge, U. K.)* **2019**, *55*, 15057–15060.

[292] Y. Wang, N. Tian, C. Li, Y. Hou, X. Wang, Q. Zhou, *Chem. Commun. (Cambridge, U. K.)* **2019**, *55*, 14081–14084.

[293] Y. Li, S. Wang, Y. Huang, Y. Chen, W. Wu, Y. Liu, J. Zhang, Y. Feng, X. Jiang, M. Gou, *Chem. Commun. (Cambridge, U. K.)* **2019**, *55*, 13128–13131.

[294] H. Pan, S. Wang, Y. Xue, H. Cao, W. Zhang, *Chem. Commun. (Cambridge, U. K.)* **2016**, *52*, 14208–14211.

[295] C. Ji, Q. Gao, X. Dong, W. Yin, Z. Gu, Z. Gan, Y. Zhao, M. Yin, *Angew. Chem., Int. Ed.* **2018**, *57*, 11384–11388.

[296] M. R. Hamblin, *Photochem. Photobiol.* **2012**, *88*, 496–498.

[297] S. Perni, P. Prokopovich, J. Pratten, I. P. Parkin, M. Wilson, *Photochem. Photobiol. Sci.* **2011**, *10*, 712–720.

[298] R. Yin, T. Agrawal, U. Khan, G. K. Gupta, V. Rai, Y.-Y. Huang, M. R. Hamblin, *Nanomedicine (London, U. K.)* **2015**, *10*, 2379–2404.

[299] B. Rout, C.-H. Liu, W.-C. Wu, *Sci. Rep.* **2017**, *7*, 7892.

[300] J. K. Trigo Gutierrez, G. C. Zanatta, A. L. M. Ortega, M. I. C. Balastegui, P. V. Sanitá, A. C. Pavarina, P. A. Barbugli, E. G. d. O. Mima, *PLoS One* **2017**, *12*, e0187418.

[301] Y. Zhang, P. Huang, D. Wang, J. Chen, W. Liu, P. Hu, M. Huang, X. Chen, Z. Chen, *Nanoscale* **2018**, *10*, 15485–15495.

[302] C. Li, F. Lin, W. Sun, F.-G. Wu, H. Yang, R. Lv, Y.-X. Zhu, H.-R. Jia, C. Wang, G. Gao, Z. Chen, *ACS Appl. Mater. Interfaces* **2018**, *10*, 16715–16722.

[303] Y. Wan, L. Zheng, Y. Sun, D. Zhang, *J. Mater. Chem. B* **2014**, *2*, 4818–4825.

[304] F. Liu, A. Soh Yan Ni, Y. Lim, H. Mohanram, S. Bhattacharjya, B. Xing, *Bioconjugate Chem.* **2012**, *23*, 1639–1647.

[305] S. Cui, D. Yin, Y. Chen, Y. Di, H. Chen, Y. Ma, S. Achilefu, Y. Gu, *ACS Nano* **2012**, *7*, 676–688.

[306] N. M. Idris, M. K. Gnanasammandhan, J. Zhang, P. C. Ho, R. Mahendran, Y. Zhang, *Nat. Med. (N. Y., NY, U. S.)* **2012**, *18*, 1580–1585.

[307] M. R. Hamblin, T. Hasan, *Photochem. Photobiol. Sci.* **2004**, *3*, 436–450.

[308] Y. Ye, Y. Li, F. Fang, *Int. J. Nanomed.* **2014**, *9*, 5157–5165.

[309] S. Li, S. Cui, D. Yin, Q. Zhu, Y. Ma, Z. Qian, Y. Gu, *Nanoscale* **2017**, *9*, 3912–3924.

[310] J. Xu, N. Liu, D. Wu, Z. Gao, Y.-Y. Song, P. Schmuki, *ACS Nano* **2020**, *14*, 337–346.

[311] S. K. Choi, in *Photonanotechnology for Therapeutics and Imaging* (Ed.: S. K. Choi), Elsevier, **2020**, pp. 1–21.

[312] A. Gupta, P. Avci, T. Dai, Y.-Y. Huang, M. R. Hamblin, *Advances in Wound Care* **2013**, *2*, 422–437.

[313] Y.-H. Hsin, C.-F. Chen, S. Huang, T.-S. Shih, P.-S. Lai, P. J. Chueh, *Toxicol. Lett.* **2008**, *179*, 130–139.

[314] L. J. Steven, *Phys. Med. Biol.* **2013**, *58*, R37.

[315] G. M. Hale, M. R. Querry, *Appl. Opt.* **1973**, *12*, 555–563.

[316] R. R. Anderson, J. A. Parrish, *J. Invest. Dermatol.* **1981**, *77*, 13–19.

[317] J. V. Frangioni, *Curr. Opin. Chem. Biol.* **2003**, *7*, 626–634.

[318] R. Weissleder, *Nat. Biotechnol.* **2001**, *19*, 316.

[319] A. M. Smith, M. C. Mancini, S. Nie, *Nat. Nanotechnol.* **2009**, *4*, 710–711.

[320] J.-N. Liu, W.-B. Bu, J.-L. Shi, *Acc. Chem. Res.* **2015**, *48*, 1797–1805.

[321] F. Ai, Q. Ju, X. Zhang, X. Chen, F. Wang, G. Zhu, *Sci. Rep.* **2015**, *5*, 10785.

[322] A. R. Hilgenbrink, P. S. Low, *J. Pharm. Sci.* **2005**, *94*, 2135–2146.

[323] R. J. Lee, P. S. Low, *Biochim. Biophys. Acta, Biomembr.* **1995**, *1233*, 134–144.

[324] X. Montet, M. Funovics, K. Montet-Abou, R. Weissleder, L. Josephson, *J. Med. Chem.* **2006**, *49*, 6087–6093.

[325] R. Shukla, T. P. Thomas, J. Peters, A. Kotlyar, A. Myc, J. R. Baker Jr, *Chem. Commun. (Cambridge, U. K.)* **2005**, 5739–5741.

[326] K. Temming, M. Lacombe, R. Q. J. Schaapveld, L. Orfi, G. Kéri, K. Poelstra, G. Molema, R. J. Kok, *ChemMedChem* **2006**, *1*, 1200–1203.

[327] Y. Chen, C. A. Foss, Y. Byun, S. Nimmagadda, M. Pullambhatla, J. J. Fox, M. Castanares, S. E. Lupold, J. W. Babich, R. C. Mease, M. G. Pomper, *J. Med. Chem.* **2008**, *51*, 7933–7943.

[328] R. Shukla, T. P. Thomas, A. M. Desai, A. Kotlyar, S. J. Park, J. R. Baker Jr, *Nanotechnology* **2008**, *19*, 295102.

[329] T. P. Thomas, S. K. Choi, M.-H. Li, A. Kotlyar, J. R. Baker Jr, *Bioorg. Med. Chem. Lett.* **2010**, *20*, 5191–5194.

[330] A. Plantinga, A. Witte, M.-H. Li, A. Harmon, S. K. Choi, M. M. Banaszak Holl, B. G. Orr, J. R. Baker Jr, K. Sinniah, *ACS Med. Chem. Lett.* **2011**, *2*, 363–367.

[331] G. Obaid, M. Broekgaarden, A.-L. Bulin, H.-C. Huang, J. Kuriakose, J. Liu, T. Hasan, *Nanoscale* **2016**, *8*, 12471–12503.

[332] M. T. Huggett, M. Jermyn, A. Gillams, R. Illing, S. Mosse, M. Novelli, E. Kent, S. G. Bown, T. Hasan, B. W. Pogue, S. P. Pereira, *Br. J. Cancer* **2014**, *110*, 1698–1704.

[333] H. He, L. Liu, E. E. Morin, M. Liu, A. Schwendeman, *Acc. Chem. Res.* **2019**, *52*, 2445–2461.

[334] O. Lyass, B. Uziely, R. Ben-Yosef, D. Tzemach, N. I. Heshing, M. Lotem, G. Brufman, A. Gabizon, *Cancer* **2000**, *89*, 1037–1047.

[335] M. Dunne, B. Epp-Ducharme, A. M. Sofias, M. Regenold, D. N. Dubins, C. Allen, *J. Controlled Release* **2019**, *308*, 197–208.

[336] O. Sartor, *Urology* **2003**, *61*, 25–31.

[337] A. Sparreboom, C. D. Scripture, V. Trieu, P. J. Williams, T. De, A. Yang, B. Beals, W. D. Figg, M. Hawkins, N. Desai, *Clin. Cancer Res.* **2005**, *11*, 4136–4143.

[338] C. Li, *Adv. Drug Delivery Rev.* **2002**, *54*, 695–713.

[339] K. Venkatakrishnan, Y. Liu, D. Noe, J. Mertz, M. Bargfrede, T. Marbury, K. Farbakhsh, C. Oliva, A. Milton, *Br. J. Clin. Pharmacol.* **2014**, *77*, 998–1010.

[340] J. A. Silverman, S. R. Deitcher, *Cancer Chemother Pharmacol* **2013**, *71*, 555–564.

[341] H. Zhang, *OncoTargets Ther.* **2016**, *9*, 3001–3007.

[342] T. Maisch, F. Santarelli, S. Schreml, P. Babilas, R.-M. Szeimies, *Exp. Dermatol.* **2010**, *19*, e302–e305.

[343] H. S. de Bruijn, S. Brooks, A. van der Ploeg-van den Heuvel, T. L. M. ten Hagen, E. R. M. de Haas, D. J. Robinson, *PLoS One* **2016**, *11*, e0148850.

Table of Contents Graphic

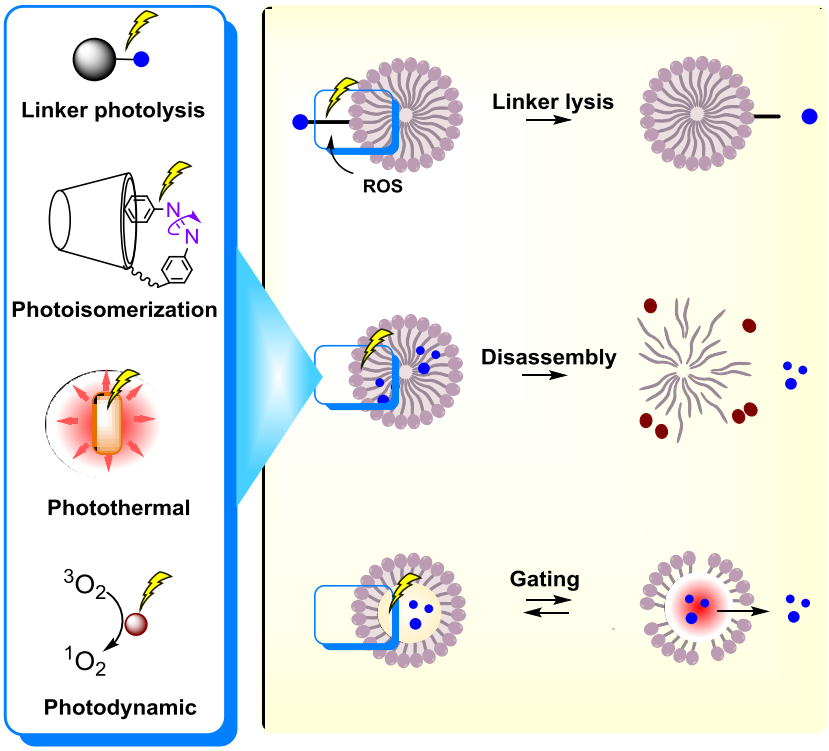

Photoactivation constitutes one of major release mechanisms applied in delivery systems. Its strategies consist primarily of linker photolysis, photoisomerization, photothermal activation, or photodynamic reaction. Recently, their applications have made a significant impact on the advancement of nanotherapeutic delivery systems in various disease areas. This article addresses recent achievements and challenges in the development of photoactivation release systems.

Author Biography

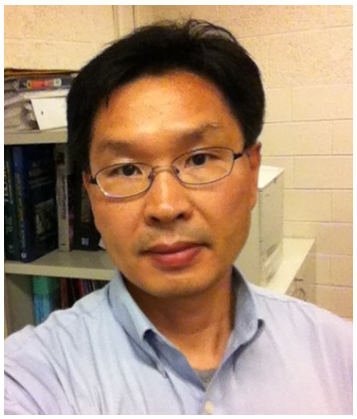

Seok Ki Choi, PhD is Associate Professor in research track at the Michigan Nanotechnology Institute for Medicine and Biological Sciences, University of Michigan Medical School, United States. He earned BS and MS at Seoul National University and PhD (1994) in Chemistry at Columbia, New York. After his postdoctoral training at Harvard and a career at Theravance Biopharma, California, he has performed biologic nanotechnology research at Michigan with a focus on multivalent ligand targeting, and photoactivated nanomedicine.